# Universitá degli Studi di Ferrara

DOTTORATO DI RICERCA IN

FISICA

CICLO XXVI

COORDINATORE Prof. Vincenzo Guidi

# Spin Tracking Studies for EDM Search in Storage Rings

Settore Scientifico Disciplinare FIS/04


**Dottorando**

Dott. Andrea Pesce

**Tutore**

Prof. Paolo Lenisa


Anni 2011/2013

*To my parents*

# Abstract

This thesis is part of the research project finalized to the measurements of the Electric Dipole Moment (EDM) of charged particles in a storage ring. The measurements presented here concern the feasibility tests performed at the COoler SYnchrotron (COSY), located at the Forschungszentrum-Jülich (Germany).

The Standard Model *CP* violation source is not strong enough to explain the matter-antimatter asymmetry of the universe. The observation of a non-zero EDM aligned along the spin axis of a fundamental particle, nucleus or atomic system would be a signal of *CP* violation beyond the Standard Model and, therefore, of new physics.

For a neutral system, the usual method for detecting the EDM $\vec{d}$ consists of the application of an electric field $\vec{E}$ and the measure of the energy shift $\vec{d} \cdot \vec{E}$. This procedure cannot be applied to charged particles, since they would be accelerated by the electric field and then lost. The use of a storage ring opens the EDM search to charged, polarized particles. The basic idea is to align the beam polarization along the momentum, and keep the beam circulating while interacting with the radial electric field always present in the particle frame. The EDM signal would then be detected as a polarization precession starting from the horizontal plane and rotating towards the vertical direction.

One of the most serious issues to be dealt with in such an experiment is the limited horizontal polarization lifetime, called Spin Coherence Time, that is the time that takes to the particle spins for spreading around in the ring plane. This characteristic time of the system defines the observation time available to detect the EDM signal. The goal for the proposed deuteron EDM experiment is to achieve an EDM sensitivity of $10^{-29}\ e \cdot cm$, which requires a SCT of at least 1000 $s$.

The development and design of such a high precision experiment demands a powerful tracking code that allows to track both the position and the spin of the particles circulating in the storage ring. The code I used to perform the simulations presented in this work is COSY

INFINITY, created by Prof. Martin Berz at the Michigan State University.

The purpose of this thesis is to benchmark the COSY INFINITY code against the feasibility studies for the deuteron EDM experiment performed at the COSY storage ring. The comparison of the simulations to the measurements represented a unique possibility of testing the COSY INFINITY code with actual data. The presented results demonstrate that COSY INFINITY correctly computes the beam and spin dynamics of a charged particles beam in a storage ring. The dependence of the spin coherence time on betatron and synchrotron oscillations is qualitatively reproduced, as well as its dependence on the strength of the sextupole magnets implemented in the simulated lattice. It has been confirmed that, with the right choice of sextupole strength, it is possible to simultaneously compensate for the vertical and horizontal beam emittance effects and, therefore, lengthen the SCT.

# Riassunto

Questa tesi è parte del progetto di ricerca finalizzato alla misura del momento di dipolo elettrico (EDM) di particelle cariche in un anello di accumulazione. Le misure qui presentate riguardano i test di fattibilità svolti al COoler SYnchrotron (COSY), situato al Forschungszentrum-Jülich (Germania).

La sorgente di violazione di *CP* del Modello Standard non è sufficientemente grande per spiegare l'asimmetria materia-antimateria dell' universo. La scoperta di un EDM non nullo, allineato con l'asse di spin di una particella fondmentale, nucleo o sistema atomico, sarebbe un segnale di violazione di *CP* oltre il Modello Standard e, quindi, di nuova fisica.

Per un sistema neutro, il metodo di solito utilizzato per rilevare un EDM $\vec{d}$ consiste nell'appicare un campo elettrico $\vec{E}$ e misurare la variazione di energia $\vec{d} \cdot \vec{E}$. Questa procedura non può essere applicata a particelle cariche, poichè queste sarebbero accelerate dal campo elettrico e, quindi, perse. L'utilizzo di un anello di accumulazione apre alla ricerca di EDM per particelle cariche e polarizzate. L'idea è quella di allineare la polarizzazione del fascio con il momento, e mantenere il fascio in circolazione nell'anello mentre interagisce con il campo elettrico radiale che è sempre presente nel sistema di riferimento delle particelle. Il segnale EDM sarebbe quindi rilevato come una precessione della polarizzazione che parte dal piano orizzontale e ruota verso la direzione verticale.

Uno dei problemi più complessi da affrontare in un esperimento di questo tipo è la limitata vita media della polarizzazione orizzontale, chiamata tempo di coerenza di spin (SCT), che rappresenta il tempo che impiegano gli spin delle particelle del fascio per andare fuori fase nel piano orizzontale. Questo tempo caratteristico del sistema definisce il tempo di misura disponibile per rilevare il segnale EDM. L'obiettivo dell'esperimento proposto per la misura del momento di dipolo elettrico del deuterone è quello di raggiungere una sensitività di $10^{-29}\ e \cdot cm$, che richiede uno SCT di almeno 1000 $s$.

Lo sviluppo e la progettazione di un esperimento di tale precisione richiede l'utilizzo di

un potente codice di tracciamento che sia in grado di tracciare sia la posizione che lo spin delle particelle che circolano nell'anello di accumulazione. Il codice che ho usato per effettuare le simulazioni presentate in questo elaborato è COSY INFINITY, realizzato dal Prof. Martin Berz alla Michigan State University.

Lo scopo di questa tesi è confrontare le simulazioni eseguite con il codice COSY INFINITY con i risultati degli studi di fattibilità dell'esperimento EDM del deuterone, svolti a COSY. Tale confronto rappresenta una possibilità unica di testare il codice con dati sperimentali. I risultati presentati dimostrano che COSY INFINITY calcola correttamente la dinamica di fascio e di spin per un fascio di particelle cariche in un anello di accumulazione. La dipendenza del tempo di coerenza di spin dalle oscillazioni di sincrotrone e betatrone è qualitativamente riprodotta, così come lo è la sua dipendenza dall'intensità dei sestupoli implementati nel codice. É stato confermato che, per un valore opportuno di intensità dei sestupoli, è possibile compensare simultaneamente gli effetti dell'emittanza verticale e orizzontale del fascio e, quindi, allungare lo SCT.

# Contents

# Introduction

This work is included in the research project aimed to measure the Electric Dipole Moment (EDM) of charged particles in a storage ring. The measurements presented here concern the feasibility tests performed at the COoler SYnchrotron (COSY) ring, located at the Forschungszentrum-Jülich (Germany).

The discovery of a non-zero EDM aligned with the spin of fundamental particles would contribute to solving the matter-antimatter asymmetry (also known as baryon asymmetry) of our universe, which represents one of the mysteries of contemporary physics. The Big Bang Theory assumes that an equal amount of matter and antimatter was present at the origin of the universe. According to Sakharov's conditions, this symmetry must have been broken by mechanisms violating charge conjugation simmetry $C$ and the combined charge-parity simmetry $CP$, taking place outside of thermal equilibrium. Although the Standard Model of particle physics contains sources of $CP$ violation, coming from the electroweak theory (K-meson and B-meson decays) and (in principle) the quantum chromodynamics, they are not large enough to explain the size of the current baryon asymmetry. What is needed is the observation of new $CP$-violating processes.

The EDM is a measure of the permanent separation between positive and negative electrical charge that lies along the particle's spin axis. The action of the time reversal operator $T$, which inverts the time coordinate, inverts the spin vector leaving the EDM unchanged. Under a parity transformation $P$, which inverts the spacial coordinates, the spin direction remains the same whie the EDM is reversed. Neither of the two operator keeps the system in its original configuration, meaning that an EDM along the particle's spin axis violates both parity and time reversal symmetries. Assuming the $CPT$ theorem to be valid, a violation of $T$ represents a violation of $CP$, concluding that EDM indeed violates $CP$.

The theoretical predictions coming from the CKM mixing in the Standard Model (for the neutron $d_n^{CKM} \sim 10^{-32}\ e \cdot cm$) are several orders of magnitude below the current EDM ex-

perimental limits ($|d_n| \sim 10^{-26}\ e \cdot cm$). Models beyond the Standard Model, on the contrary, foresee EDMs within the experimental boundaries. The measurement of a non-vanishing EDM at the sensitivity of present or planned experiments would clearly prove the existence of new sources of *CP* violation beyond the Standard Model.

In 1950, pursuing the suggestion that the strong interactions, whose theory was still unknown at the time, may violate the parity simmetry, Purcell and Ramsey actually performed the first EDM experiment by searching for a *P*-violating up-down asymmetry in neutron scattering from spin zero nuclei. After that, EDM searches intensified and the level of experimental precision has increased steadily ever since, getting to include also heavy atoms and molecules. For a neutral system, the usual method for detecting the EDM $\vec{d}$ consists of the application of an electric field $\vec{E}$ and the measure of the energy shift $\vec{d} \cdot \vec{E}$. Unfortunately, this method cannot be applied to charged particles, since they would be accelerated by the electric field and then lost.

In order to solve this issue, charged particles EDM experiments in storage rings have recently been proposed. The basic idea is to inject in the ring a horizontally polarized charged particle beam (particle spins aligned along the momentum) and keep it circulating while interacting with the radial electric field always present in the particle frame. The EDM signal would then be detected as a polarization precession starting from the horizontal plane and rotating towards the vertical direction.

The success of this kind of experiment depends on the fulfillment of two fundamental conditions. First, the polarization precession in the horizontal plane, due to the anomalous magnetic moment of the particle, has to be frozen, so that the particle spins will always be aligned with the momentum during the motion and the beam will be longitudinally polarized. Second, it is necessary to provide a long horizontal polarization lifetime which defines the observation time available to detect the EDM signal.

The realization of a storage ring EDM experiment requires a perfect knowledge of beam and spin dynamics for the stored particles. In particular, the understanding of spin dynamics is essential for providing a long horizontal polarization lifetime. In a storage ring, the stable spin direction is the vertical one, orthogonal to the ring plane. Therefore, as soon as a spin vector is not aligned with the stable axis, it will start precessing around it with a frequency proportional to the relativistic factor $\gamma$ and the local magnetic field. The number of spin precessions around the stable spin axis per number of revolutions around the ring is called the *spin-tune*. Because of the momentum dispersion among the particles in the beam, the spin vectors will precess with diffent frequencies, going out of phase in the horizontal plane

and making the polarization vanish. The time that takes to the spins for spreading around in the ring plane is the horizontal polarization lifetime, called *spin coherence time*, and defines the observation time available to measure the EDM signal. The goal for the deuteron EDM experiment is to achieve an EDM sensitivity of $10^{-29}\ e \cdot cm$, which requires a spin coherence time of at least 1000 $s$, along with the capability of measuring microradians of polarization rotation.

The development and design of such a high precision experiment demands a powerful tracking code that allows to track both the position and the spin of the particles circulating in the storage ring. The code I used to perform the simulations presented in this work is COSY INFINITY, created by Prof. Martin Berz at the Michigan State University. Besides tracking particles during their motion, this code offers the possibility to track the particle spins by making use of differential algebraic techniques to calculate Taylor coefficients that define the spin transfer matrix of the system.

The purpose of this thesis is to benchmark the COSY INFINITY code against the feasibility studies for the deuteron EDM experiment performed at the COSY storage ring in Jülich. In these tests, the precession of the horizontal polarization as a function of time was measured, and the effects of the transverse beam size on the spin coherence time were studied. Also the contribution of sextupoles field to the horizontal polarization lifetime was investigated.

In order to probe the COSY INFINITY code, a lattice as close as possible to the real COSY ring was implemented. Making use of the code output coming from the spin tracking procedure, executed on a deuteron having momentum of 0.97 $GeV/c$, I developed a method to calculate the spin invariant axis and, consequently, the spin tune of the reference particle. The change in the spin tune due to either a position or a momentum offset of a particle with respect to the reference trajectory was then evaluated by selectively setting a certain value of $\Delta x$, $\Delta y$ and $\Delta p/p$. The *spin-tune spread* was determined and the associated spin coherence time was calculated. In this way, I was able to evaluate the influence of the betatron oscillations and the beam momentum spread to the horizontal polarization lifetime. Afterwards, the effect of synchrotron oscillations on the spin coherence time was studied by adding an RF cavity, that bunches the beam. Eventually, I investigated the possibility of lengthening the polarization lifetime by correcting emittance effects using sextupole magnets.

The thesis is divided in seven chapters:

- *Chapter 1* yields a theoretical overview of the EDM as a probe of new physics, in-

cluding the experimental results achieved so far. The proposed method for the measurement of a charged particle EDM in a storage ring is presented.

- *Chapter 2* provides the basic elements of beam dynamics in a storage ring, that are necessary to understand the simulations and the measurements presented in the thesis.

- *Chapter 3* describes the COSY storage ring, where the feaibility tests have been performed. It defines the polarization of a spin-1 particle like the deuteron, and shows how it can be measured.

- *Chapter 4* illustrates the characteristics of the COSY INFINITY code. The COSYScript language is defined, together with a basic structure of a program. It is described how beam physics was implemented; the optical elements composing the simulated lattice are introduced.

- *Chapter 5* shows the results of the COSY INFINITY simulations about the betatron and synchrotron oscillations effects on the spin coherence time, including their corrections by using sextupole magnets.

- *Chapter 6* gives a description of the measurements performed at the COSY ring in which I was involved during my stay at the Forschungszentrum-Jülich. These measurements were fundamental to compare the results emerging from the COSY INFINITY simulations with data from a real machine. They included the direct measurement of the horizontal polarization as a function of time, involving the emittance effects and their corrections with sextupole magnets.

# Chapter 1

# The Electric Dipole Moment as a sensitive probe of *CP* violation

## 1.1 Baryons-antibaryons asymmetry

One of the mysteries of contemporary physics comes from astronomical observation. We are living in a matter-dominated universe with basically no evidence for antimatter. This fact is represented in the baryon to photon ratio, calculated as the ratio between the number density of baryons $n_b$ and the number density of photons $n_\gamma$. The last measurement of this quantity, also known as baryon asymmetry parameter, is from PLANCK [1], and its value is [1, 2]:

$$\eta = \frac{n_b}{n_\gamma} = (6.08 \pm 0.14) \times 10^{-10} \tag{1.1}$$

The Standard Model prediction for the number of baryons and antibaryons is rather small:

$$\frac{n_b}{n_\gamma} = \frac{n_{\bar{b}}}{n_\gamma} \sim 10^{-18} \tag{1.2}$$

that is more than 8 orders of magnitude smaller than the observed value (see Eq. 1.1). This number does not justify the matter content of the universe coming from primordial nucleosynthesis [3]. The process responsible for this asymmetry of the universe, that started from a symmetric configuration, is known as baryogenesis.

In 1967 A. D. Sakharov formulated the three conditions necessary to allow a uni-

verse, containing initially an equal amount of matter and antimatter, to evolve into a matter-dominated universe [4], which we see today. These conditions are reported in the following:

1. **Baryon number B violation**. If every interaction conserves $B = n_b - n_{\bar{b}}$ individually, then it will always be conserved globally. Therefore must exist at least an elementary process that violates the baryon number, allowing the baryogenesis to bring the universe from a $B = 0$ condition to a $B > 0$ condition.

2. ***C* and CP symmetries violation**. Simple baryon number violation is not enough to explain matter-antimatter asymmetry if *C* and *CP* are symmetries of the universe. It is indeed possible to demonstrate that, if *C* and *CP* are not violated, the processes generating a baryon excess would occur at the same rate of the processes generating an antibaryon excess. In this conditions, the baryon asymmetry would preserve its initial value $\eta = 0$.

3. **Interactions outside of thermal equilibrium**. At thermal equilibrium, the Boltzmann distribution dictates that there should be equal amounts of matter and antimatter. Other reactions would then turn any baryon asymmetry back into even number of baryons and antibaryons. Therefore, any baryogenesis must happen under conditions outside from thermal equilibrium.

Remarkably, over the years it was realized that the Standard Model contains all three ingredients. Baryon number fails to be conserved through a combination of non-perturbative thermal processes in the $SU(2)$ space and an anomaly in the baryon current, fact that fulfills the first condition. This allows for fluctuations of baryon number in the early universe at $T \gtrsim 100\ GeV$, while a combination of the second and third conditions provides a preferred direction for these fluctuations, which can favor baryons over antibaryons. Despite that, the resulting baryon asymmetry falls several orders of magnitude short of the baryon asymmetry that is observed experimentally (see Eq. 1.1). In particular, the *SM* contributions to *CP* violation are not strong enough to explain the baryogenesis.

The impossibility of having successful baryogenesis within the *SM* is a very strong motivation for searching new sources of *CP* violation. In this chapter it will be presented how this research is connected to the possible existence of an electric dipole moment (EDM) aligned to the particles spin axis.

## 1.2 *CP* violation in the Standard Model and beyond

In the Standard Model of particle physics there are two distinct sources of *CP* violation:

- in the electroweak theory, the phase $\delta$ in the CKM (Cabibbo-Kobayashi-Maskawa) quark mixing matrix;
- in quantum chromodynamics (QCD), the $\theta_{QCD}$ parameter.

*CP* violation was first observed in 1964 in the system of neutral Kaons [5], when it was found that weak charged current interactions can violate strangeness and lead to $K^0 - \bar{K}^0$ mixing. A later confirmation came from the studies performed on the neutral B-mesons system [6]. Both these results can be explained through the so called Kobayashi-Maskawa mechanism, which links *CP* violation to the single physical phase $\delta$ in the unitary mixing matrix $V$ (the CKM matrix) describing transitions between the three generations of quarks. Besides the *CP*-violationg phase, the CKM matrix involves also three quark-flavor mixing angles. The smallness of *CP* violation is not due to the smallness of $\delta$, but rather to the fact that observable violations require that all three quark families contribute to the relevant transition amplitude, and then they are suppressed by small mixing angles. Although the Kobayashi-Maskawa mechanism explains the *CP* violation in the electroweak interactions, it fails in providing a *CP* violation source big enough to explain the baryogenesis, meaning that the Standard Model cannot explain the matter-antimatter asymmetry of our universe.

Quantum chromodynamics allows in principle the introduction in the Lagrangian of a dimension-four term, known as $\theta$-term, with a dimensionless coefficient $\theta_{QCD}$ which, if nonzero, would signify the violation of both parity $P$ and time reversal $T$ simmetries. Assuming the *CPT* theorem to be valid, this leads to *CP* violation. If $\theta_{QCD} \sim O(1)$, the neutron would have a non-zero EDM. The lack of experimental evidence of $P$ and $T$ conservation in strong interactions led Purcell and Ramsey to the first pioneering experiment [7, 8] aimed to the search of neutron EDM. It is nowadays known that $\theta_{QCD}$ is tuned to zero, or at least cancels, to better than one part in $10^9$. This tuning represents the *strong CP problem* of the Standard Model, which has been present since the early days of QCD.

As it has been already pointed out, the Standard Model fails to explains the baryon-antibaryon asymmetry of our universe. Furthermore, it neither provides an explanation for why only the electroweak part $SU(2) \times U(1)$ is chiral (parity-violating), nor for the *gauge hierarchy problem*, that reguards the fact that the masses of the known particles are orders of

magnitude smaller than the Planck mass ($\sim 10^{19}\ GeV/c$), representing the energy at which the four forces - electromagnetic, weak, strong and gravitational - would be unified. Gravity is not even included in the Standard Model. For these reasons, many extensions of the SM have been conceived, all of them including additional scalar fields that allow new sources of *CP* violation.

Among these new models, SuperSymmetry (SUSY) is one of the first which was developed, and it is motivated by the desire to give an explanation for the *gauge hierarchy problem*. SUSY attempts to avoid this problem in a natural way by linking physics at the weak scale to physics at the Planck scale. In order to achieve that, all SUSY models introduce, for each fermion (lepton or quark), a supersymmetric bosonic partner (slepton, squark), while for each Standard Model gauge boson, a supersymmetric fermionic partner called *gaugino*. The hypothetical new particles and their interactions yield new *CP*-violating phases in addition to SM phase $\delta$, and provide a measurable electric dipole moment of fundamental particles. For this reason, and, more in general, because of the strong suppression of EDMs that are induced only by the Kobayashi-Maskawa phase, combined with the prospects for improving the experimental sensitivity, EDM searches are placed at the forefront in probing *CP*-violating physics beyond the SM.

## 1.3 The EDM as a probe of new physics

The EDM of a fundamental particle is a measure of the permanent separation of positive and negative electrical charges within the particle volume. It is aligned to the particle spin vector because all the components perpendicular to that direction have null average. Because of this alignment, EDM violates both time reversal $T$ and parity $P$ symmetries, as it is illustrated in Fig. (1.1). In fact, the action of the time reversal operator, that inverts the time coordinate, would cause an inversion of the spin vector leaving the EDM vector untouched. On the contrary, the action of the parity operator, that inverts the spatial coordinates, would reverse the EDM vector without changing the spin direction. Since any *CPT* invariant interaction that violates one between time reversal and *CP* symmetries must violate the other, it is possible to conclude that EDM violates *CP*.

Despite this close relation through *CPT* theorem, $T$ and *CP* are different symmetries with different physical consequences, so possible $T$-violating observables open a new window on Standard Model tests and new physics searches.

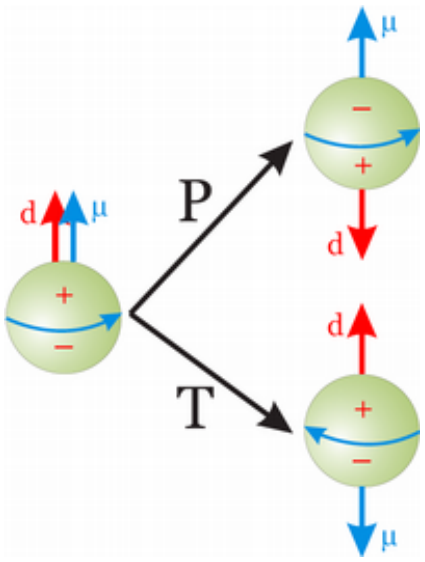


Figure 1.1: *The picture shows the effect of the separate application of parity* P *and time reversal* T *operators to a particle with an EDM* $\vec{d}$ *parallel to its spin* $\vec{\mu}$*. The application of* P *reverses the EDM leaving the spin unchanged, while a* T *operation changes the direction of the spin without affecting the EDM. The conclusion is that EDM violates both* P *and* T *symmetries.*

The predicted EDM effects due to the CKM mixing in the Standard Model are extremely small. The quark EDMs are only generated at the three-loop level, and are expected to be:

$$d_q^{CKM} \sim 10^{-34}\ e \cdot cm \tag{1.3}$$

while the electron ones only receive contributions from four-loop diagrams, at least for massless neutrinos, and should be [9]:

$$d_e^{CKM} \lesssim 10^{-38}\ e \cdot cm \tag{1.4}$$

The contributions of the quark EDMs to the neutron one are expected to be negligible, with the largest CKM contribution from a two-loop diagram involving a gluon penguin being:

$$d_n^{CKM} \sim 10^{-32}\ e \cdot cm \tag{1.5}$$

A major complication comes from the strong *CP* violation term $\theta_{QCD}$ in the QCD Lagrangian, which contributes to the proton and neutron EDMs [10] as:

$$|d_n^{\theta}| = |d_p^{\theta}| \sim (4.5 \times 10^{-15}\ e \cdot cm)\theta_{QCD} \tag{1.6}$$

Since the recent upper bound on the neutron EDM is $d_n < 2.9 \times 10^{-26} e \cdot cm$ [11] (see next section for further details), for the strong *CP*-violating phase is therefore required $\theta_{QCD} \lesssim 10^{-11}$. The unnaturally smallness of this value leads to the *strong CP problem*, already mentioned in the previous section.

A significant EDM in hadrons can rise from quark electromagnetic EDMs ($d_u$ and $d_d$) and from color (chromo) EDMs contributions. Both *CP*-violating sources have to be considered beyond the SM. To give an example, in SUSY the EDM coming from these processes is generated in a loop containing a supersymmetric particle. According to the supersymmetric models, as it is reported in the 2008 AGS proposal "Search for a permanent electric dipole moment of the deuteron nucleus at the $10^{-29}$ $e \cdot cm$ level" [12], neutron, proton and deuteron EDMs are defined as:

$$d_n = 1.4(d_d - 0.25 d_u) + 0.83e(d_u^c + d_d^c) - 0.27e(d_u^c - d_d^c) \quad (1.7)$$

$$d_p = 1.4(d_d - 0.25 d_u) + 0.83e(d_u^c + d_d^c) + 0.27e(d_u^c - d_d^c) \quad (1.8)$$

$$d_D = 1.4(d_d + d_u) + 0.2e(d_u^c + d_d^c) - 6e(d_u^c - d_d^c) \quad (1.9)$$

Comparing $d_n$ with $d_D$ in Eqs. (1.7) and (1.9) illustrates how $d_D$, if measured, would be about 20 times more sensitive to the isovector component $e(d_u^c - d_d^c)$ than $d_n$.

Because the SM contributions are expected to be small, EDMs are an excellent place to search for the effects of new physics. These typically have new *CP*-violating phases and allow EDMs at one-loop level, leading to values already excluded or within reach of future EDM experiments. The picture in Fig. (1.2) shows the comparison between the theoretical predictions from SM and beyond for EDM of fundamental particles and the actual experimental limits. Since the SM expected values are much smaller than the current experimental sensitivity, every non-zero EDM found between these limits and the SM predictions would be a strong sign of new physics pointing to a new *CP* violation source.

### 1.3.1 The search for EDM

The first search for an EDM is due to the Purcell and Ramsey idea, in 1950, to use EDMs of particles as high-precision probes of symmetry properties of the strong interactions. Remarkably, it precedes not only the discovery of *CP* violation in K mesons, but also the discovery of parity violation in weak interactions. The main motivation behind the initial idea was the suggestion that the theory of strong interactions, still unknown at the time, may

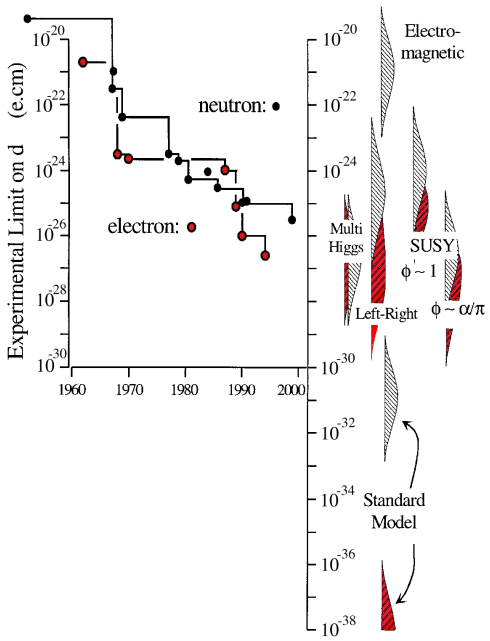


Figure 1.2: *The picture shows, on the left side, the actual experimental limits for electron (red) and neutron (black) EDMs. On the right side, the predictions of SM and models beyond it, such SUSY, are shown.*

violate the parity simmetry. It was only 25 years later that the introduction of QCD as the theory of strong interactions led to the possibility of $P$ and $CP$ violation by the $\theta$-term. In their work Purcell and Ramsey analyzed the existing experimental data on neutron scattering from spin zero nuclei, coming to the conclusion $|d_n| < 3 \times 10^{18}\ e \cdot cm$ [7].

The general strategy used in almost all EDM searches is to place a neutral particle (or atom, or molecule) of interest in an electric $\vec{E}$ and magnetic $\vec{B}$ field, parallel to each other. If the system under investigation has a non-zero EDM, the usual Zeeman effect is modified by an electric field-dependent term, giving the following interaction energy:

$$H = \hbar\omega = -\vec{\mu} \cdot \vec{B} - \vec{d} \cdot \vec{E} \tag{1.10}$$

where $\hbar$ is the reduced Planck constant, $\omega$ is the spin precession angular velocity, $\vec{\mu}$ is the magnetic dipole moment, and $\vec{d}$ is the electric dipole moment. The spin precession frequency in the case with the $\vec{E}$ field parallel to the $\vec{B}$ field ($\omega_1$) is compared to the one in the case with

anti-parallel fields ($\omega_2$):

$$\hbar\omega_1 = 2\mu B + 2dE \tag{1.11}$$

$$\hbar\omega_2 = 2\mu B - 2dE \tag{1.12}$$

The EDM is then determined by subtracting these two frequencies in order to cancel the magnetic term:

$$d = \frac{\hbar(\omega_1 - \omega_2)}{4E} \tag{1.13}$$

Following the discovery of *CP* violation in the mixing of neutral kaons, the EDM searches intensified, and the level of experimental precision has improved steadily ever since. Indeed, following significant progress througout the past decade, the EDMs of neutron [11] and of several heavy atoms and molecules [13, 14, 15] have been measured to vanish to remarkably high precision. These searches can be classified into three main categories, corresponding to the three classes of observable EDMs which currently provide the best constraints in term of *CP*-odd sources: the EDMs of paramagnetic atoms and molecules, that are systems with one unpaired electron and are therefore primarily sensitive to the electron EDM ; the EDMs of diamagnetic atoms, connected to the nucleus and its constituents EDMs; and the EDMs of hadrons, nucleons (N) in particular. Each of these categories probes EDMs induced by different physical processes. The atomic EDMs are complementary to the neutron and electron ones because they receive contributions not only from the EDMs of their constituents, but also from the *CP*-violating $e^- N$ or $\pi N$ interactions. Examples of EDMs values representing bounds on *CP*-violating parameters for these three categories are the atomic EDMs of thallium and mercury and the one of the neutron, whose values are listed in Tab. (1.1). These bounds have been used to constrain many beyond the

| Category | EDM | Current Limit |
|---|---|---|
| Paramagnetic | $^{205}Tl$ | $\lvert d_{Tl}\rvert < 9 \times 10^{-25}\ e \cdot cm$ [13] |
| Diamagnetic | $^{199}Hg$ | $\lvert d_{Hg}\rvert < 3.1 \times 10^{-29}\ e \cdot cm$ [16] |
| Nucleon | n | $\lvert d_n\rvert < 2.9 \times 10^{-26}\ e \cdot cm$ [11] |

Table 1.1: *Current upper limits of three representative categories of EDMs.*

Standard Model scenarios, and provide indirect charged particle EDMs limits. In particular, from a recent measurement performed on the polar molecule thorium monoxide (ThO), was derived the electron EDM limit [17]:

$$|d_e| < 8.7 \times 10^{-29}\ e \cdot cm \tag{1.14}$$

while from mercury was derived the proton one [16]:

$$|d_p| < 7.9 \times 10^{-25}\ e \cdot cm \tag{1.15}$$

All nuclear EDM searches carried out to this point have used nuclei that are part of an electrically neutral atomic or molecular system. This enables large electric fields, fundamental in EDM experiments, to be applied without accelerating the particle out of the apparatus.

A rough estimation, on dimensional grounds, of the scale of new physics probed by current EDM experiments was discussed in [18] :

$$d_i \approx \frac{m_i}{\Lambda^2} e \sin\phi \tag{1.16}$$

where $m_i$ is the quark or lepton mass, $\sin\phi$ is the result of *CP*-violating phase, and $\Lambda$ is the new physics energy scale. For a quark mass $m_q \sim 10\ MeV$ and $\sin\phi$ of order $1/2$, one finds:

$$|d_p| \sim |d_D| \sim 10^{-22} \left(\frac{1\ TeV}{\Lambda}\right)^2\ e \cdot cm \tag{1.17}$$

Therefore, for $|d_p| \sim |d_D| \sim 10^{-29}\ e \cdot cm$ sensitivity it would be possible to probe an energy scale $\Lambda \sim 3000\ TeV$, that is far beyond any present or future accelerators achievable energy. Making the same kind of considerations for a SUSY model with supersymmetric partners mass $M_{SUSY} \leq 1\ TeV$, if neither proton or deuteron EDM at a sensitivity level of $10^{-29}\ e \cdot cm$ were observed, $\sin\phi$ would have to be very small, thus $\sin\phi \leq 10^{-5}$ [12]. It is then clear how, although no EDM has been measured yet, the current generation of experiments defines important constraints on the theories beyond the Standard Model. In order to refine these bounds and eventually measure the EDM of fundamental particles, it is necessary to improve the experimental techniques and continue to perform such searches on different systems, so that it will be possible to understand where the new physics is generated.

## 1.4 EDM experiments in storage rings

The basic idea leading to Eq. (1.13) is not valid for charged particles, such as the electron, the proton and the deuteron, since they would be lost in an electric field. In order to solve this issue, the new generation of experiments probing charged particles EDMs require the use of a storage ring. In such kind of accelerators, a particle beam can be kept in circular motion up to many hours.

For a particle at rest, an EDM would couple only to the electric field while the magnetic dipole moment couples only to the magnetic field. The particle spin precesses according to:

$$\frac{d\vec{S}}{dt} = \mu\hat{S}\times\vec{B} + d\hat{S}\times\vec{E} \tag{1.18}$$

where $\mu$ is the particle magnetic dipole moment, $d$ is its electric dipole moment, and $\vec{S} = s\hat{S}$ is

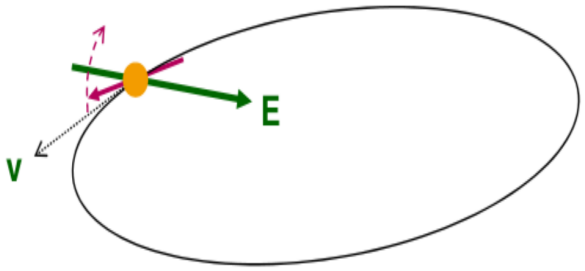


Figure 1.3: *The picture shows a particle with velocity $\vec{v}$ circulating in a storage ring. The purple arrow represents the particle spin vector that, at the injection, is aligned with the velocity. Because of the interaction between the EDM and the inward electric field $\vec{E}$ in the particle rest frame, the spin starts precessing in the vertical plane, that is orthogonal to the plane of the ring.*

the spin vector, with $S$ the spin quantum number. A relativistic particle in a storage ring feels both magnetic and electric fields in its rest frame, thus its spin precession will be modified by the presence of an EDM. Therefore, after injecting a longitudinally polarized beam in the storage ring, it is possible to detect the EDM signal by observing the increase of the vertical polarization due to the interaction with the inward radial electric field that is present in the particle rest frame. This process is sketched in Fig. (1.3).

Nevertheless, the EDM signal is very difficult to see. The problem is that this signal is very small compared to the spin precession relative to the momentum in the ring plane due to the anomalous magnetic moment, whose angular frequency is given by the Thomas-BMT equation [19, 20]:

$$\vec{\omega}_G = \vec{\omega}_S - \vec{\omega}_C = -\frac{q}{m}\left\{G\vec{B} - \left[G - \left(\frac{m}{p}\right)^2\right]\frac{\vec{\beta}\times\vec{E}}{c}\right\} \tag{1.19}$$

where it is assumed $\vec{\beta}\cdot\vec{B} = \vec{\beta}\cdot\vec{E} = 0$, and $\vec{\omega}_S$ is the spin precession in the horizontal plane, $\vec{\omega}_C$ is the particle cyclotron angular frequency ,$G = (g-2)/2$ is the particle anomalous magnetic

moment, while $q$, $m$ and $p$ are respectively the particle electric charge, mass, and momentum. A solution to this issue is given by the so called *frozen spin* method (see Fig. 1.4),

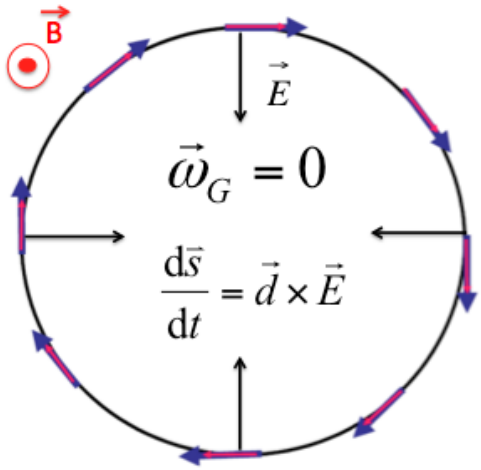


Figure 1.4: *The sketch shows a top view of an ideal EDM experiment in storage ring. The spin (purple) and momentum (blue) vectors are kept aligned for the duration of the storage, so that the in-plane precession angular frequency $\omega_G$ is cancelled. If the EDM $\vec{d}$ is not zero, the particle spin will precess out of plane due to the radial electric field [21].*

whose idea is to employ the proper combination of radial electric field and vertical magnetic field to cancel the spin precession due to the particle magnetic moment (see Eq. 1.19), with the net effect being a large amplification of the EDM signal. The horizontal spin precession can be frozen using different methods, depending on the sign of the anomalous magnetic moment.

Protons have a positive anomalous magnetic moment, $G_p = 1.79$, and therefore, according to Eq. (1.19), it is possible to get $\vec{\omega}_G = 0$ in a pure electrostatic ring ($\vec{B} = 0$) under the condition:

$$\left[ G - \left( \frac{m}{p} \right)^2 \right] = 0 \quad \Longrightarrow \quad p = \frac{m}{\sqrt{G}} = 0.701 \; GeV/c \tag{1.20}$$

which represents the so called *magic momentum*.

Deuterons have instead a negative anomalous magnetic moment, $G_D = -0.14$, and therefore there is no *magic momentum* that cancels $\vec{\omega}_G$. A combination of vertical magnetic and outward radial electric field is then needed to achieve the same result, being the additional

electric field defined as:

$$\frac{\beta}{c}\left[\left(\frac{m}{p}\right)^2 - G\right]E = GB \quad \Longrightarrow \quad E = \frac{GBc\beta\gamma^2}{1 - G\beta^2\gamma^2} \tag{1.21}$$

Charged particle EDM experiments in storage rings have recently been proposed, including a search for the deuteron EDM with a sensitivity of $10^{-29}\ e \cdot cm$ [12]. Also a proposal for a proton EDM experiment at BNL (Brookhaven National Laboratory) [21] with the same sensitivity has been submitted. The storage ring method is a good solution because a proton or deuteron beam can be held in circular motion by exploiting the Lorentz force. If the spin of the particles is kept aligned to the momentum, then the EDM signal would arise from the interaction between the spin itself and a radial electric field.

In order to perform such a precision measurement, it is fundamental that the beam horizontal polarization lifetime (see next section) is large enough for the EDM signal to accumulate up to a measurable value. Differences in the spin precession rate can occur due to particle misplacements or momentum spread within the beam, making the particle spins decohere by spreading in the horizontal plane. The works presented in this thesis concerns simulations of these depolarizing effects, performed using the COSY INFINITY code (see Chap. 4), in order to support the feasibility studies that have been taking place at the COoler SYnchrotron (COSY) facility for the last few years.

### 1.4.1 Spin Coherence Time

In a storage ring the stable direction for the polarization is the vertical one because the magnetic fields are vertical and do not influence spin vectors along this direction. The projection of the polarization onto the vertical axis is then not affected by decoherence effects.

Let us now consider a particle beam polarized in one direction in the horizontal plane. At injection all particles spin vectors are aligned and they start precessing in phase. After a characteristic time of the system, called *Spin Coherence Time* (SCT), the spins go out of phase due to momentum spread of the particles in the beam, causing the vanishing of the horizontal polarization (see Fig. 1.5). The spin coherence time is then the horizontal polarization lifetime, thus the time during which the particles spins precess coherently about the axis $\hat{n}$ while maintaining a fraction of the initial polarization. In an EDM experiment where the particles spins must be aligned along the momentum, the spin coherence time represents the time available to measure the EDM signal.

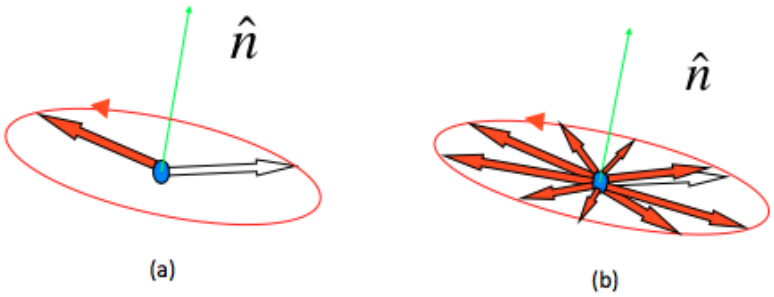


Figure 1.5: *Fig. (a) shows that the spin vectors are aligned at the injection and they start precessing in phase; Fig. (b) shows how, after a characteristic time of the system defined as spin coherence time, the spin vectors are all out of phase in the horizontal plane causing the depolarization of the beam.*

The expected EDM signal can be estimated from:

$$\frac{d\vec{S}}{dt} = \vec{d} \times \vec{E} \Rightarrow \frac{1}{2}\hbar\omega = dE \Rightarrow \frac{d\theta}{dt} = \frac{2dE}{\hbar} \tag{1.22}$$

whose solution is given by:

$$\theta(t) = \theta_0 + \frac{2dE}{\hbar}t \tag{1.23}$$

where $d$ is the electric dipole moment, that is orthogonal to the radial electric field E, $\hbar$ is the reduced Planck constant, ant $\theta$ is the vertical spin precession angle. If we take an EDM of $d = 10^{-29}\ e \cdot cm$ as the goal of the experiment, and an electric field close to the maximum available value $E \approx 10\ MV/m$, we obtain:

$$\theta(t) \approx \left(\frac{10^{-9}\ rad}{s}\right) t \tag{1.24}$$

Considering the minimal detectable precession angle to be $\theta_{min} \approx 10^{-6}\ rad$, the result leads to an estimation of the time requested for such a signal to buildup:

$$\tau_{SC} = \frac{\theta_{min}}{10^{-9}\ \frac{rad}{s}} \approx 10^3\ s \tag{1.25}$$

This number points out that, in order to be able to measure an EDM signal of the order of $10^{-29}\ e \cdot cm$, it is necessary that the spins of the stored particles stay aligned (coherent) for at least $\tau_{SC} \approx 10^3\ s$. This characteristic time of the system is the spin coherence time.

# Chapter 2

# Elements of particle accelerator physics

The aim of this chapter is to present a brief introduction to the beam dynamics in a storage ring, in both longitudinal and transverse directions, in the perspective of the search of the electric dipole moment. Emphasis will be given to the aspects of the beam dynamics involved in the studies that will be presented in the following chapters of this work.

It has to be pointed out that it is possible to treat the so called transverse degrees of freedom for the particle motion independently of the longitudinal one. In fact, the frequency of longitudinal oscillations is generally rather smaller than that of transverse oscillations, meaning that, to a reasonable approximation, they are decoupled [22].

## 2.1 The transverse motion

In a synchrotron storage ring, charged particles are kept circulating by dipole magnets providing a closed orbit. In order to guarantee a stable transverse motion along this orbit, quadrupole magnets, providing linear restoring forces, are used. The two transverse degrees of freedom, thus the vertical and the radial directions, can be treated independently [22].

### 2.1.1 Strong focusing

A quadrupole magnet cannot provide a restoring force in both transverse degrees of freedom simultaneously. If it has a focusing effect in the radial direction, it will have a defocusing effect in the vertical direction, and vice versa. In fact, the condition $\vec{\nabla} \times \vec{B} = 0$ leads to $\partial B_y/\partial x = \partial B_x/\partial y$, where $x$ and $y$ are respectively the radial and the vertical coordinate (see Fig. 2.1). It is therefore necessary a method based on alternating magnets

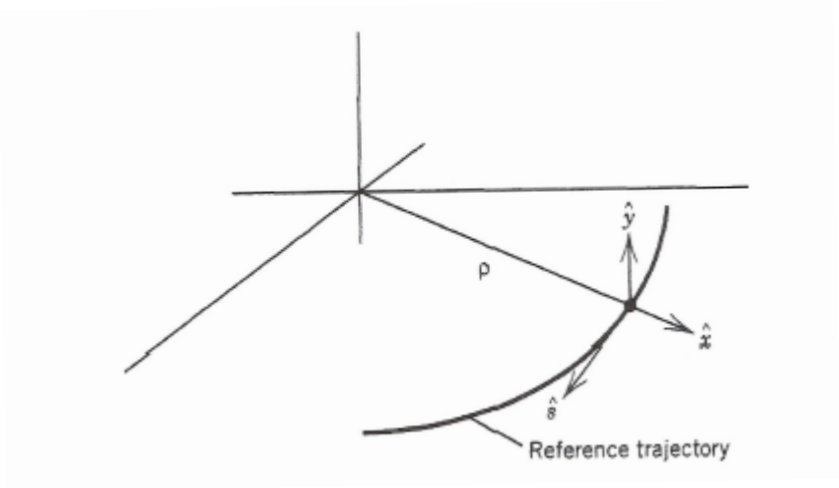


Figure 2.1: *Coordinate system for development of the transverse equations of motion [22].*

focusing in the vertical and horizontal directions. This method, that involves the use of quadrupole magnets, is called *strong focusing*.

A quadrupole magnet, assuming condition $\vec{\nabla} \times \vec{B} = 0$ to be valid, provides a magnetic field defined as:

$$\vec{B} = B'(y\hat{x} + x\hat{y}) \tag{2.1}$$

where the field gradient $B' = \partial B_y/\partial x = \partial B_x/\partial y$ is evaluated at the center of the quadrupole, and $\hat{x}$ and $\hat{y}$ are the unit vectors associated, respectively, to the radial and vertical directions. For a displacement $(x, y)$ from the reference trajectory, the Lorentz force acting on a particle with electric charge $e$ and velocity $v$ is:

$$\vec{F} = evB'\hat{s} \times (y\hat{x} + x\hat{y}) = evB'y\hat{y} - evB'x\hat{x} \tag{2.2}$$

with $\hat{s}$ being the unit vector associated to the longitudinal direction (see Fig. 2.1). It is evident, looking at Eq. (2.2), that the Lorentz force is focusing in the radial direction ($\hat{x}$) and

defocusing in the vertical direction ($\hat{y}$), meaning that a quadrupole affects simultaneously the two directions in an opposite way.

### 2.1.2 Betatron motion

In a storage ring particles are held in circular motion on a closed orbit, that is the trajectory closing on itself after one revolution and is defined by bending magnets. The transverse motion of a particle consists of this circular motion plus small amplitude oscillations, called *betatron oscillations*, around the closed orbit, that depend on the disposition of quadrupole magnets in the ring.

Let us assume the coordinate system to be the one represented in Fig. (2.1). Locally the *reference orbit*, thus the designed trajectory, has curvature $\rho$ and the path length along this curve is $s$, that will be the independent variable. At every point along the reference orbit it is possible to define the three unit vectors $\hat{s}$, $\hat{x}$, and $\hat{y}$. Therefore, the position of a particle can be expressed as a vector in the form:

$$\vec{R} = r\hat{x} + y\hat{y} \tag{2.3}$$

where $r \equiv \rho + x$. The particle having the right momentum $p_0 = eB\rho$ and phase to be synchronized with the RF cavity, known as reference or synchronous particle (see section 2.2), will be identified by $\vec{R} = \rho\hat{x}$. We are interested in the behaviour of the deviations $x$ and $y$ of a non-idea particle from the reference orbit. In general, the equations of motion we want to derive will not be linear. Anyway, if we take into account only fields that are linear functions of $x$ and $y$, being this the case of dipoles and quadrupoles, and keep only the lowest order terms in $x$ and $y$, we will get the Hill's equations of *betatron motion* [22]:

$$\frac{d^2x}{ds^2} + \left[\frac{1}{\rho^2} + \frac{1}{B\rho}\frac{\partial B_y(s)}{\partial x}\right]x = 0 \tag{2.4}$$

$$\frac{d^2y}{ds^2} - \frac{1}{B\rho}\frac{\partial B_y(s)}{\partial x}y = 0 \tag{2.5}$$

Let ($q$,$q'$) represent the couple of canonical phase space variables either for the radial or the vertical coordinate, where $q' = dq/ds$. Eq. (2.4) and (2.4) are both of the form

$$q'' + K(s)q = 0 \tag{2.6}$$

and differ from a simple harmonic oscillator only because the "spring constant" $K$ depends on position $s$. The general solution of the equation of motion can then be written as:

$$q(s) = A\sqrt{\beta_q(s)}\cos\left[\psi_q(s) + \psi_q(s_0)\right] \tag{2.7}$$

with $A$ and $\psi_q(s_0)$ constants of integration to be determined using initial conditions, and $\beta_q(s)$ the *betatron amplitude function*, characterizing an oscillation with varying amplitude $\sqrt{\beta_q(s)}$. Substituting Eq. (2.7) in the generic form of the equation of motion (2.6), one obtains for the phase advance of the particle oscillation:

$$\psi_q(s_0 \to s) \equiv \Delta\psi_q = \int_{s_0}^{s} \frac{ds}{\beta_q(s)} \tag{2.8}$$

and $\beta_q(s)$ can be interpreted as the local wavelength of the betatron oscillation divided by $2\pi$. Finally, for a circular machine, starting from the definition of the phase advance it is possible to derive the number of oscillations per particle revolution in the ring, that is:

$$\nu_q \equiv \frac{1}{2\pi}\oint \frac{ds}{\beta_q(s)} \tag{2.9}$$

which is called *betatron tune* of the accelerator.

### 2.1.3 Courant-Snyder parameters

Since, as we saw in the previous section, the betatron amplitude function $\beta(s)$ (from this point on, we do not explicit the subscript $q$ anymore) is a fundamental quantity for the description of the transverse motion, it is convenient to define two new variables:

$$\alpha(s) \equiv -\frac{1}{2}\frac{d\beta(s)}{ds} \tag{2.10}$$

$$\gamma(s) \equiv \frac{1+\alpha^2(s)}{\beta(s)} \tag{2.11}$$

that together, with $\beta(s)$ itself, are referred to as *Courant-Snyder parameters* or *Twiss parameters*. Using the new set of variables to rewrite the equations of motion, it is possible to define a constant of motion, whose derivation can be found in reference [22], that is called the *Courant-Snyder invariant*:

$$A^2 = \gamma q^2 + 2\alpha q q' + \beta q'^2 \tag{2.12}$$

This invariant form describes an ellipse at any point in the accelerator. Each time that a particle passes a particular position in the ring, its betatron oscillation coordinates will appear as

a point on the ellipse given by the amplitude function and its slope at that point, as shown in Fig. (2.2). For different locations through the lattice, the ellipses will have different shapes and orientations, but they will always have a constant area equal to $\pi A^2$. The phace space

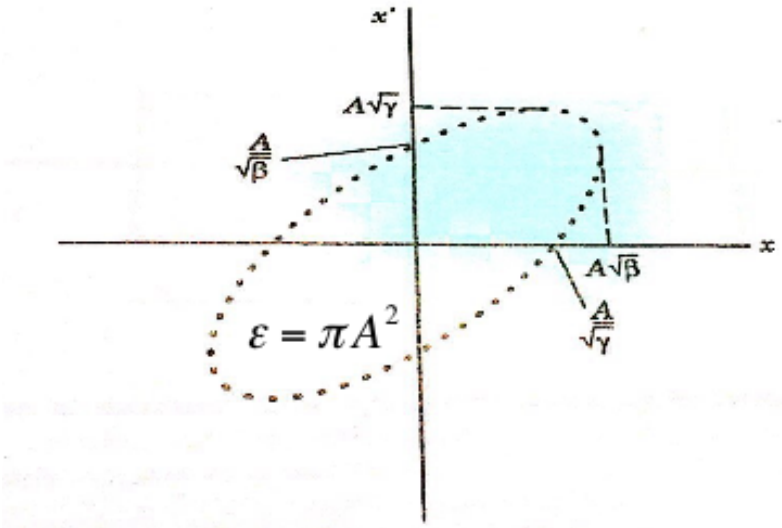


Figure 2.2: *The Courant-Snyder ellipse defined by the Twiss parameters $\alpha$, $\beta$, and $\gamma$ in the $x - x'$ phase space. The area of the ellipse is equal to $\varepsilon = \pi A^2$, and it is constant all along the orbit. The sketch shows the maximum amplitude of the betatron oscillation $A\sqrt{\beta}$ and the maximum angle $A\sqrt{\gamma}$ [22].*

area associated with the largest ellipse accepted by the accelerator is called the *admittance*, and it is equal to $(\pi a/\beta_{max}(s)$, being $a$ the half aperture available to the beam, and $\beta_{max}(s)$ the maximum value of the amplitude function. The phase space area occupied by the beam is called the *emittance*, and it is equal to the area of the Courant-Snyder ellipse $\varepsilon = \pi A^2$. In terms of the emittance, the maximum displacement $q$ and angle $q'$ in a particular position $s$ around the ring are:

$$q_{max} = \sqrt{\frac{\varepsilon \beta_{max}(s)}{\pi}} \tag{2.13}$$

$$q'_{max} = \sqrt{\frac{\varepsilon \gamma_{max}(s)}{\pi}} \tag{2.14}$$

It is often convenient to speak of the emittance for a particle distribution in terms of the rms transverse beam size. Assuming the particle distribution to be Gaussian in both transverse degrees of freedom, and the beam to be in an equilibrium situation where the distribution is

indistinguishable from turn to turn, the emittance can be calculated as:

$$\varepsilon = -\frac{2\pi\sigma_q^2}{\beta(s)}\ln(1-F) \tag{2.15}$$

where $\beta(s)$ is the amplitude function in the point $s$, $\sigma_q$ is the rms transverse beam size, and $F$ is the fraction of particles included in the phase space area $\varepsilon$. If the transverse beam width $\sigma_q$ is measured, for instance with an Ionization Profile Monitor (IPM), then the emittance can be calculated as:

$$\varepsilon = \frac{\sigma_q^2}{\beta(s)} \tag{2.16}$$

### 2.1.4 Momentum dispersion

In the previous section we examined the motion of particles having the same momentum as the reference particle but different transverse coordinates. Now we want to focus on the motion of particles differing in momentum from that of the reference particle ($p_0$) of a quantity $\Delta p = p - p_0$. Since the bending field of dipole magnets depends on the particle momentum ($B\rho = p/e$), we will find that these off-momentum particles perform betatron oscillations around a new class of closed orbits which are displaced from that of the reference particle. This displacement is described by a new lattice function, known as the *momentum dispersion function* $D(p,s)$, that has its origin in the fact that a particle of higher momentum is deflected through a lesser angle in a bending magnet. The displacement from the ideal trajectory of a particle with fractional momentum deviation $\Delta p/p_0$ is then given by:

$$x = D(p,s)\frac{\Delta p}{p_0} + x_\beta \tag{2.17}$$

where the first term represents the contribution of the closed orbit of the off-momentum particle and the second the betatron oscillation about that closed orbit.

In addition, higher momentum particles are bent less effectively in the focusing elements. That is, there is an effect completely analogous to chromatic aberration in conventional optics. The dependence of focusing on momentum will be responsible for the dependence of betatron oscillation tune on momentum. The lattice parameter quantifying this relationship is called the *chromaticity*, and it is indicated with the symbol $\xi(p)$. The change in tune $\delta\nu$ due to momentum is then defined as:

$$\delta\nu = \xi(p)\frac{\Delta p}{p_0} \tag{2.18}$$

where $\Delta p/p_0$ is the particle fractional momentum deviation. The source of chromaticity we are discussing is the dependence of focusing strength on momentum for the ideal accelerator fields, and it is called the *natural chromaticity*. There are additional sources, coming for instance from field imperfections, but we are not treating them here. The main reason to worry about chromaticity is that, if the beam has a large momentum spread, then a large chromaticity may place some portions of the beam on resonances that, amplifying the particles displacement from the reference trajectory, will cause the loss of the beam.

### 2.1.5 Sextupoles

In order to provide chromaticity adjustments, what is needed is a set of magnets presenting a field gradient that is a function of particle momentum. A distribution of sextupole magnets is normally used for this purpose. In the horizontal plane, the sextupole field is of the form

$$B = kx^2 \tag{2.19}$$

and so the field gradient on a displaced equilibrium orbit is

$$B' = 2kx = 2kD(p,s)\frac{\Delta p}{p_0} \tag{2.20}$$

Unfortunately, the sextupoles inevitably introduce nonlinear aberrations that cannot be described in this brief description of linear beam dynamics.

One of the goals of this work is to prove that sextupole magnets, that provide a position dependent focusing, can be used to compensate the decoherence effects of betatron oscillations and, consequently, lengthen the horizontal polarization lifetime by an opportune choice of sextupole strength, defined as:

$$K_2 = \frac{1}{B\rho}\frac{\partial^2 B}{\partial x^2} \tag{2.21}$$

where $B$ is the magnetic field within the magnet and $\rho$ is the curvature. This topic will be treated in details in Sec. 5.4.

### 2.1.6 Betatron oscillations effect

For the purpose of this thesis, we want to highlight the crucial contribution of betatron oscillations to the horizontal polarization lifetime (see Chap. 5). In general, a particle undergoing betatron oscillations travels a longer path than the reference particle. The fractional

orbit lengthening due to the betatron motion is the sum in quadrature of the radial ($x$) and vertical ($y$) contributions, giving as result

$$\frac{\Delta L}{L} = \frac{(\Delta x')^2 + (\Delta y')^2}{4} \tag{2.22}$$

where $L$ is the path length of the reference particle, while $\Delta x'$ and $\Delta y'$ are the maximum angle deviations from the ideal path in the radial and vertical directions, respectively. Since, as we will see in Sec. 2.2.1, the RF cavity effect is to keep all particles on average isochronous, betatron oscillations lead to a longer beam path and, therefore, a higher particle velocity, meaning a change in the spin precession rate. It will be shown in Chap. 5 how such a change during the beam motion affects the horizontal polarization lifetime.

## 2.2 The longitudinal motion

It has been already mentioned that charged particles in a synchrotron storage ring are held in a circular motion by bending dipole magnets and focusing quadrupole magnets. The beam can be kept circulating in "packages" (*bunched beam*) or it can occupy the whole ring circumference (*coasting beam*). Since the measurements and, therefore, the simulations presented in this thesis concern the bunched beam case, this is the one that will be discussed in this section.

The bunched beam is provided by means of a radio-frequency cavity that produces an oscillating longitudinal electric field that accelerates the particles. There is a particle, called *synchronous particle* (or *reference particle*), that at each moment of time has exactly the right momentum and the right transit time through the accelerating cavity so that it receives exactly the right increment of energy to move on a closed orbit passing through the center of all magnets in the ring. Nevertheless a particle beam is composed by a distribution of particles differing in momentum and, then, in transit time through the RF cavity. We thus have to deal with a stability issue: do particles initially nearby in momentum and transit time to those of the reference particle remain close in the phase space throughout the acceleration process? The answer is provided by the so called *phase stability* principle, that will be explained in the next section.

### 2.2.1 Phase stability

During each revolution in the ring, a particle with electric charge $e$ goes through the resonant cavity, being its energy gain per turn equal to:

$$\varepsilon = eV_0 \sin(\omega_{RF} t + \phi_s) \tag{2.23}$$

where $V_0$ is the amplitude of the accelerating voltage, $\omega_{RF}$ is the angular frequency of the RF cavity, and $\phi_s$ is the RF phase angle. A particle synchronized with the RF cavity has the same phase $\phi_s$ and is called synchronous (reference) particle. The system is designed so that the synchronous particle arrives at the cavity each turn with the same phase $\phi_s$ (modulo $2\pi$) and receives the same energy difference at each passage, always moving on the *reference trajectory*, that corresponds to a closed orbit passing through the center of all the magnets in the ring. If $\phi_s = 0$, the synchronous particle will neither gain nor lose energy when it goes through the cavity.

In general the particles in the beam will deviate from the designed motion described above. Let us consider a case of a particle with momentum $p$ that differs from the one of the synchronous particle $p_0$. If $L$ is the length of the ring circumference, and $v$ is the velocity of the particle considered, the time needed for one complete revolution will be $\tau = L/v$. The fractional change in $\tau$ associated with deviations in $L$ or $v$ is by logarithmic differentiation:

$$\frac{\Delta\tau}{\tau} = \frac{\Delta L}{L} - \frac{\Delta v}{v_0} \tag{2.24}$$

where $v_0$ is the velocity of the synchronous particle. Eq. (2.24) shows how a particle moving with speed greater than the one of the ideal particle will take less time to make one complete revolution. But if its path length is larger, this deviation will increase the time needed to reach the RF cavity. The fractional change in the velocity can be expressed in terms of the fractional momentum deviation [22] in the following way:

$$\frac{\Delta v}{v_0} = \frac{1}{\gamma^2}\left(\frac{\Delta p}{p_0}\right) \tag{2.25}$$

with $\gamma$ being the relativistic factor. In a storage ring, and generally in a circular accelerator, the magnetic rigidity is defined as $B\rho = p/e$. Since it is proportional to the momentum, one can expect the orbit circumference to be larger for a particle of momentum slightly above the momentum of the ideal particle. Indeed the variation of the orbit length with momentum is determined by the *momentum compaction factor* $\alpha_c$, whose value depends on the design

of the accelerator, and it is defined as:

$$\frac{\Delta L}{L} = \alpha_c \frac{\Delta p}{p_0} \tag{2.26}$$

After substituting Eq. (2.25) and (2.26) in Eq. (2.24), we obtain the relation between the fractional change in $\tau$ and the one in momentum, that is:

$$\frac{\Delta \tau}{\tau} = \left(\alpha_c - \frac{1}{\gamma^2}\right) \frac{\Delta p}{p_0} = \eta \frac{\Delta p}{p_0} \tag{2.27}$$

where the coefficient

$$\eta = \left(\alpha_c - \frac{1}{\gamma^2}\right) \tag{2.28}$$

is the *slip factor*. The energy

$$\gamma_t = \frac{1}{\sqrt{\alpha_c}} \tag{2.29}$$

for which the slip factor vanishes is called *transition energy*, and it is a characteristic of

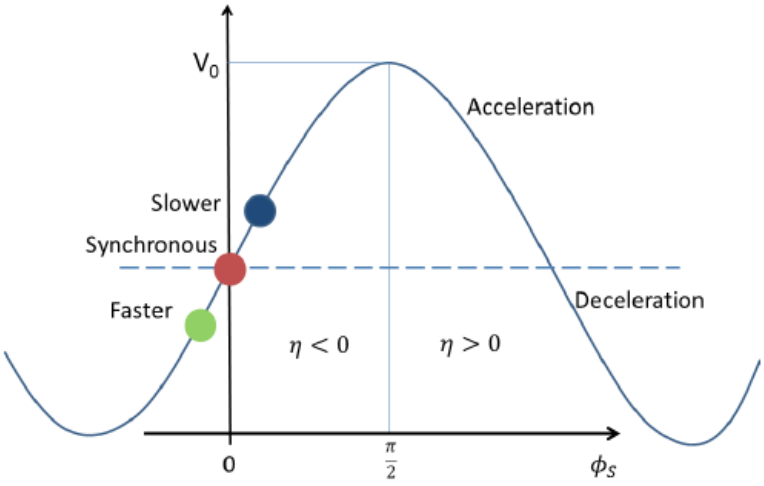


Figure 2.3: *Sketch of an RF wave where the phase angles of the synchronous particle (red) and the higher ($\Delta p/p_0 > 0$; green) and lower ($\Delta p/p_0 < 0$; blue) energy particles are shown [23]. In order to provide a stable synchrotron motion, the phase stability requires $\phi_s = 0$ for $\eta < 0$ and $\phi_s = \pi$ for $\eta > 0$.*

the particular accelerator design. Eq. (2.27) can be also written in terms of the revolution frequency, thus:

$$\frac{\Delta f}{f_0} = -\frac{\Delta \tau}{\tau} = -\eta \frac{\Delta p}{p_0} \tag{2.30}$$

where $f_0$ is the revolution frequency for the synchronous particle. The sketch in Fig. (2.3), together with Eq. (2.30), helps to understand the *phase stability* principle. If we consider a system below the transition energy ($\gamma < \gamma_t$), thus with $\eta < 0$, a particle with a momentum higher than $p_0$ ($\Delta p/p_0 > 0$) will have a revolution frequency higher than $f_0$, meaning that it will pass through the RF cavity earlier than the synchronous particle. Therefore the partical phase is negative, so that it acquires less energy than the ideal particle and is decelerated. In the same way, a particle with a momentum lower than $p_0$ ($\Delta p/p_0 < 0$) will arrive at the RF cavity later and will get more energy in comparison with the ideal particle, being then accelerated. The effect of this process is the reduction of both the phase change and the energy difference from turn to turn between particles in the beam, providing then the phase stability of the synchrotron motion.

### 2.2.2 Synchrotron motion

The equations of the *synchrotron motion* can be derived from the phase stability process described in the previous section. The demonstration of this derivation can be found in [22].

The synchrotron motion of a particle with arbitrary energy $E$ and phase angle $\phi$ with respect to the synchronous particle is described by two difference equations, that are:

$$\phi_{n+1} = \phi_n + \frac{\omega_{RF}\tau\eta c^2}{v^2 E_s}\Delta E_{n+1} \tag{2.31}$$

$$\Delta E_{n+1} = \Delta E_n + eV(\sin\phi_n - \sin\phi_s) \tag{2.32}$$

where $n$ stands for the $n$-th particle transit of the RF cavity and $\Delta E = E - E_s$ is the difference in energy between the particle in question and the reference particle.

The $\phi - \Delta E$ phase space is represented in Fig. (2.4), where the application of the synchrotron equations of motion is shown for 8 different values of initial energy difference $\Delta E$, each one corresponding to one orbit. In each case the starting value of the phase is the synchronous one. We see in the picture that there is a well defined boundary between confined and unconfined motion. This boundary is called the *separatrix*. The area in phase space within the separatrix is called a *bucket*, whose number corresponds to the *harmonic number*, while the collection of particles sharing a particular bucket is called a *bunch*. The figure depicts three different buckets.

It is possible to approximate the difference equations, Eq. 2.31 and Eq. 2.32, by one differential equation of the second order, considering phase and energy as continuous variables

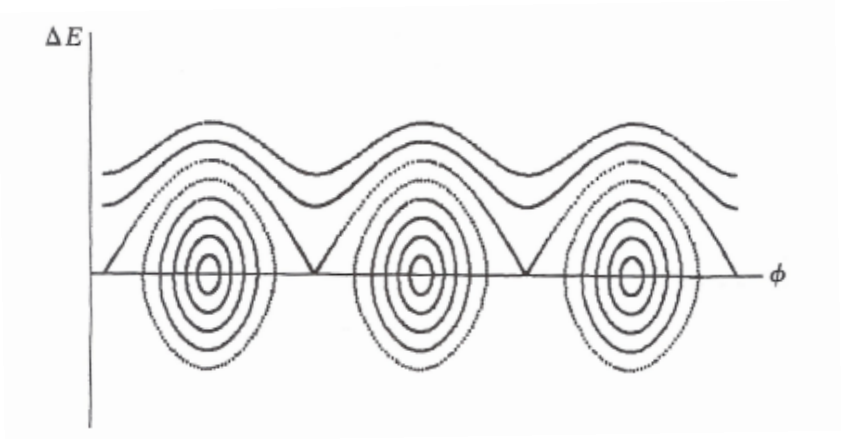


Figure 2.4: *Application, in the stationary case (the reference particle is not accelerated), of the difference equations of synchrotron motion for 8 different values of initial energy difference $\Delta E$, each one represented by one orbit. The starting value of the phase is the synchronous one for all the cases. The regions within the separatrices are called stationary buckets [22].*

and the turn number $n$ as an independent variable. After a first integration, assuming that $\Delta\phi = \phi - \phi_s$ is small, we obtain [22]:

$$\frac{d^2\Delta\phi}{dn^2} + (2\pi\nu_s)^2\Delta\phi = 0 \tag{2.33}$$

where $\nu_s$ is the number of synchrotron oscillations per turn, known as *synchrotron oscillation turn*, and is defined as:

$$\nu_s = \sqrt{-\frac{\eta\,\omega_{RF}\,\tau c^2 eV_0\cos\phi_s}{4\pi^2\nu^2 E_s}} \tag{2.34}$$

The stability condition, discussed in the previous section, is satisfied by requiring $\eta\cos\phi_s < 0$, that establishes the correct choice for the synchronous phase depending on $\eta$.

# Chapter 3

# Experimental setup

## 3.1 The COoler SYnchrotron storage ring

The COoler SYnchrotron (COSY) is a 184 *cm* long storage ring situated at the Institute for Nuclear Physics (IKP) of the Forschungszentrum-Jülich, and it represents an ideal environment for the EDM experiment's feasibility tests.

The storage process starts with negative ions sources producing unpolarized and polarized hydrogen and deuterium ions, which are then accelerated in the JULIC cyclotron up to, respectively, a momentum of 300 $MeV/c$ and 600 $MeV/c$. These pre-accelerated ions are stripped off their electrons, and the remaining protons or deuterons are injected into the COSY ring where they can be accelerated and stored in a momentum range from 300 $MeV/c$ (600 $MeV/c$ for deuterons) to 3.7 $GeV/c$. The phase space cooling of the stored beam is provided by an electron cooler (electron energy: 25-100 $KeV$) at or near injection momentum and completed by a stochastic cooling covering the momentum range above 1.5 $GeV/c$. The achieved beam intensity is $\sim 10^{10}$ particles stored in the accelerator.

At the injection energy, the Low Energy Polarimeter (LEP) provides a polarization measurement of the states generated by the polarized source. During the experiments that are the subject of this thesis, the RF solenoid placed in one arc of COSY was used to move the polarization from the vertical axis to the horizontal (ring) plane by inducing a spin resonance. The horizontal and vertical polarization components have been then measured using the EDDA scintillator detectors, as explained in the next section.

An overview of the COSY ring is shown in Fig. (3.1) indicating the main experiments,

and in particular the EDDA polarimeter.

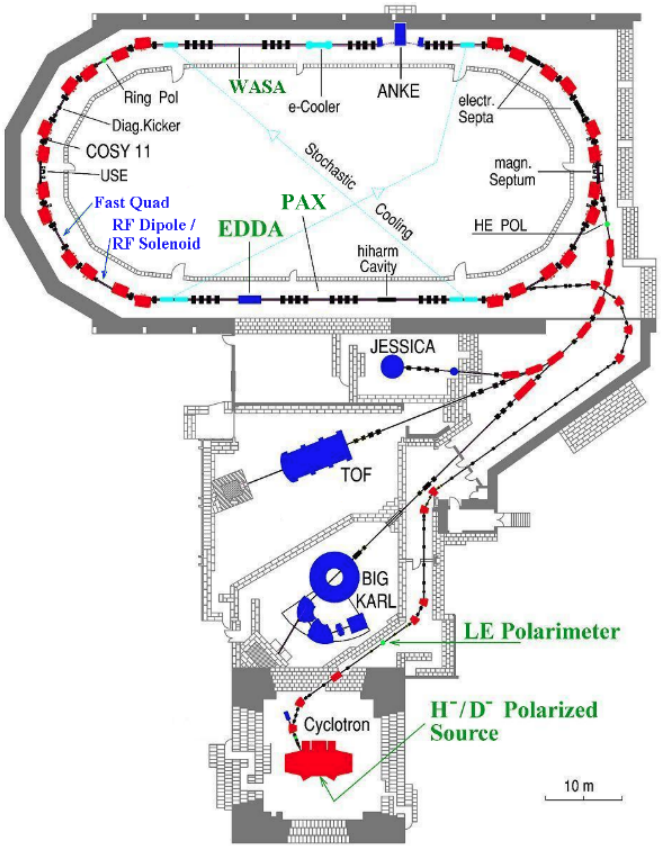


Figure 3.1: *The figure shows a sketch of the COSY ring, where the EDDA polarimeter and the RF solenoid are indicated. In the bottom we can see the sources providing polarized and unpolarized protons and deuterons, the cyclotron that accelerates the particles to the injection energy and the Low Energy Polarimeter (LEP), which measures the beam polarization.*

## 3.2 Beam polarization and its measurement

The polarization of a particles beam is defined as the ensemble average of the individual particles spins. In a spin-one system [24], like deuterons, there are three possible magnetic states along the quantization axis. In Cartesian notation, the fractional populations

of deuterons in terms of the magnetic quantum number along the spin axis are given by $f_1$, $f_0$ and $f_{-1}$, for which is valid the relation $f_1 + f_0 + f_{-1} = 1$. The unpolarized state is characterized by the condition $f_1 = f_0 = f_{-1} = 1/3$, while the vector $p_V$ and the tensor $p_T$ polarization states are defined by the following equations:

$$p_V = f_1 - f_{-1} \tag{3.1}$$

$$p_T = 1 - 3f_0 \tag{3.2}$$

The vector polarization $p_V$ can assume values in the range from $-1$ to 1, while the tensor polarization range goes from $-2$ to 1. With atomic beam sources, a pure vector polarization with no tensor polarization, thus $f_0 = 1/3$, can only reach the value $|p_V| = 2/3$; if a large tensor polarization is allowed, values may reach $|p_V| \sim 1$.

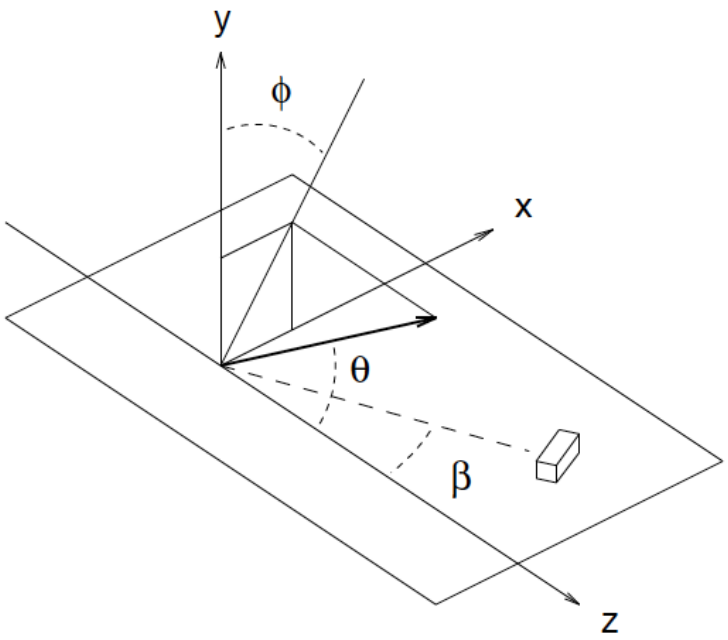


Figure 3.2: *The coordinate system for polarization direction (bold arrow) based on the observation of a reaction product in a detector (small box). The beam travels along the $\hat{z}$ axis. The detector position at an angle $\beta$ defines, along with the beam, the reaction plane and positive $\hat{x}$. The quantization axis for the polarization (bold arrow) lies in a direction given by the polar angles $\theta$ and $\phi$ (as measured from the $\hat{y}$ axis.*

The polarization of a deuteron beam can be determined by measuring deuteron-induced reactions on a target, provided that the relevant analyzing powers (or sensitivities to the po-

larization) are sufficiently large. The large vector analyzing power available with suitably chosen targets makes it preferable to focus on the vector polarization measurement rather than the tensor. Fig. (3.2) shows the definition of the spin direction with respect to a coordinate system determined by the detected reaction products. The beam defines the positive $\hat{z}$ axis. The location of the particle detector, along with the beam axis, defines the scattering plane and the dorection of the positive $\hat{x}$ axis. The scattering angle is $\beta$. In this coordinate system we can specify the orientation of the deuteron beam quantization axis by using the two angles of a spherical coordinate system, $\theta$ and $\phi$, where $\phi$ is measured from the $\hat{y}$ axis and increases toward the positive $\hat{x}$ axis. The interaction cross section between a polarized deuteron beam and an unpolarized carbon target is given by:

$$\begin{aligned}\sigma(\beta,\theta,\phi) &= \sigma_{unp}(\beta)[1+\sqrt{3}p_V iT_{11}(\beta)\sin\theta\cos\phi \\ &+ \frac{1}{\sqrt{8}}p_T T_{20}(\beta)(3\cos^2\theta-1) \\ &- \sqrt{3}p_T T_{21}(\beta)\sin\theta\cos\theta\sin\phi \\ &- \frac{\sqrt{3}}{2}p_T T_{22}(\beta)\sin^2\theta\cos 2\phi]\end{aligned} \tag{3.3}$$

where the $T_{kq}$ are the analyzing powers ($k=1$ for vector, $k=2$ for tensor). Both the unpolarized cross section and the analyzing powers are properties of the reaction.

The reaction is most sensitive to the vertical (along the $\hat{y}$ axis) component of the vector polarization when $\sin\theta\cos\phi$ is near 1 or $-1$. If both $p_V$ and $iT_{11}$ are positive, for example, then the rate at th detector (shown by the small box in Fig. 3.2) will increase relative to the unpolarized beam rate when $\sin\theta\cos\phi \sim 1$. Likewise, a detector on the opposite side of the beam (on the $-\hat{x}$ side) will see a reduce rate. The *asymmetry* in these two rates is a measure of the product $p_V iT_{11}$ and, for $iT_{11}$ known, of the **vertical component** of $p_V$. If the left and right rates are, respectively, $l$ and $R$, then the asymmetry is given by

$$\varepsilon_{LR} = \sqrt{3}p_{V,y}iT_{11}(\beta) = \frac{L-R}{L+R} \tag{3.4}$$

Over the length of a beam store, the size of $p_{V,y}$ will steadily increase due to the accumulated contributions from the interaction of the deuteron EDM with the radial electric field. This is the signal that will reveal the presence of the EDM (see Chap. 1).

If the polarization lies in the $x-z$ plane (COSY ring plane), there will be a large and oscillating $\hat{x}$ component of the deuteron polarization due to the precession of the magnetic moment in the dipole fields of the ring. In a storage ring with just horizontal bending, the

stable spin direction $\hat{n}$, called *spin invariant axis*, coincides with the vertical axis, orthogonal to the ring plane. Any horizontal polarization component would precess about $\hat{n}$ while the beam circulates in the ring. In a similar manner as described above, this will generate a difference in count rates for detectors mounted above and below the beam, giving an asymmetry defined as:

$$\varepsilon_{DU} = \sqrt{3} p_{V,x} i T_{11}(\beta) = \frac{D-U}{D+U} \tag{3.5}$$

that is a measure of the **horizontal component** of $p_V$. This asymmetry will oscillate with the $g-2$ frequency. The number of spin precessions about $\hat{n}$ per beam revolution in the ring is called the **spin tune**, and it is defined as:

$$\nu_s = G\gamma \tag{3.6}$$

thus, the spin precession rate depends on the particle anomalous magnetic moment $G$ and on the particle velocity through the relativistic factor $\gamma$.

### 3.2.1 The EDDA polarimeter

The concept for the polarimeter used for the feasibility tests at COSY involves stopping detectors that deliver their largest signals for elastic scattering events, since they are the most sensitive to spin interactions. In order to reduce the background of other processes, such as deuteron break-up interactions, an absorbing medium between the target and the detector is installed. This setup was already developed for a previous experiment [28], using a thick carbon target and the scintillators of the EDDA detector (see Fig. 3.3) [25]. Long scintillators, called *bars*, run parallel to the beam and their signal is read out by photomultiplier tubes mounted on the downstream end. These 32 scintillators are divided into groups of 8, corresponding to scattering to the left, right, down and up directions. Outside the bars there are *rings* that intercept particles scattering through a range of polar angles beginning at 9.1°. In order to extend the sensitive angle range up to 21.5°, four consecutive EDDA rings were included in the "polarimeter group" [29]. Over this angle range, the vector analyzing power for the deuteron-carbon elastic scattering is positive and crosses the first interference maximum (see Fig. 3.4) [27], making this range excellent for operation as a polarimeter. The requirement that elastically scattered deuterons stop within the forward angle ring detectors led to the choice of 970 $MeV/c$ as the optimum beam momentum.

The EDDA polarimeter scheme provides a continuous monitor of the polarization during

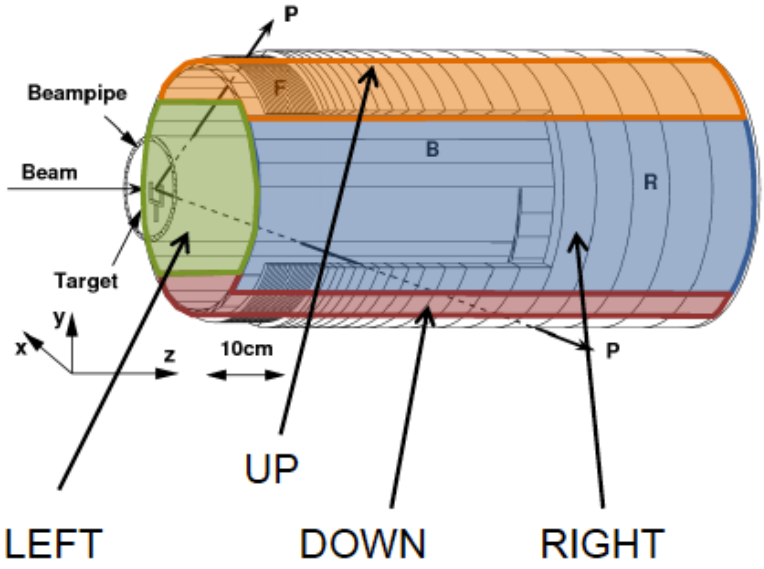


Figure 3.3: *The EDDA detector, with the thick carbon target placed in front of it. B: scintillator bars; R: scintillator rings; F: rings made of scintillating fibers. The different sectors are highlighted in different colors: green for the left sector, blue for the right, orange for the up, and red for the down. [25, 26].*

the beam storage time, in contrast to previous experiments techniques that offered observation at only one time during the measurement process. In order to achieve that, the deuteron beam is slowly and continuously extracted onto the thick carbon target, which is a carbon tube of length 15 *mm* that surrounds the beam. This slow extraction is obtained by locally steering the beam in the vertical upward direction into the top edge of the tube. Deuterons intercepting the target front face pass through the full target thickness, increasing their scattering probability into the EDDA scintillator system [29].

## 3.3 Data Acquisition

### 3.3.1 Vertical polarization measurement

The triggers from the four segments (left, right, up, down) of the EDDA detector were recorded in a single computer file for each run. A run consists of a number of stores whose events could be added as a function of time since the start was synchronized to polarization

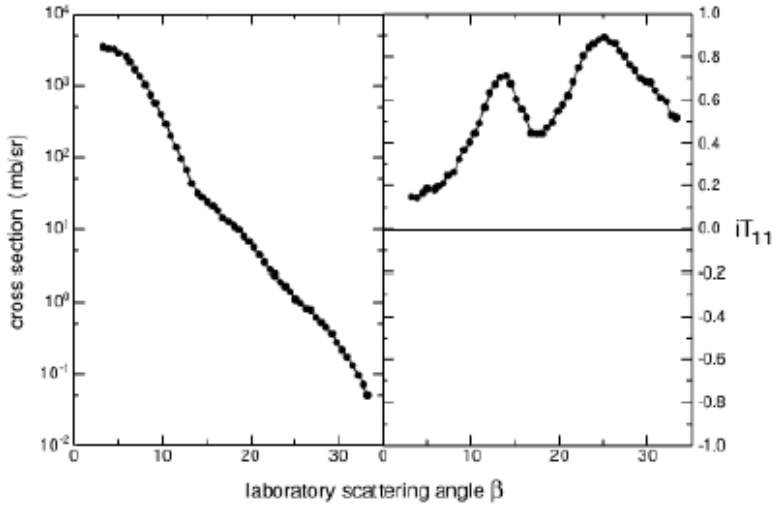


Figure 3.4: *Measurements of deuteron elastic scattering cross section and vector analyzing power $iT_{11}$ from carbon at* 270 *MeV [27].*

precession operations through the use of a reproducible start time marker.

If both positive $(+\hat{y})$ and negative $(-\hat{y})$ vector polarizations are available from the polarized source, the vertical component of the vector polarization can be determined from the *cross ratio* formula given by:

$$\varepsilon_{CR} = \frac{r-1}{r+1} \qquad \text{with} \qquad r^2 = \frac{L(+)R(-)}{L(-)R(+)}$$

where $L$ and $R$ are the count rates for the left and right segments of the EDDA detector, for the positive $(+)$ and negative $(-)$ polarization states. Analysis of the stores produced two cross ratio asymmetries, one for vector and one for vector-tensor polarized states. The two sets of cross ratio (see Eq. 3.3.1) data from each run were normalized to one based on the asymmetries recorded before making any polarization manipulation. The two measurements were then averaged. This procedure combined all the polarized beam data from a given run into one time-dependent set of vector polarization measurements [23, 29].

### 3.3.2 Horizontal polarization measurement

The most challenging new skill needed to measure the spin coherence time (see Sec. 1.4.1) was the development of a "time-stamp system" which made possible recording the horizontal polarization as a function of time while it precessed at 120 $kHz$.

The first direct measurement ever of the rapidly rotating horizontal polarization was accomplished at COSY facility using the Data Acquisition (DAQ) software written by V. Hejny. A vertically polarized beam was injected into the COSY ring, and then the polarization was rotated to the horizontal plane, reaching a state of null vertical polarization, using an RF-solenoid operating at the spin resonance frequency:

$$f_{res} = f_{cyc}(1 - G\gamma) \tag{3.7}$$

where $f_{cyc}$ is the COSY cyclotron frequency and $G\gamma$ is the spin tune. The RF solenoid spin resonance frequency was determined at the beginning of the experiment using a variable-frequency *Froissart-Stora scan* [30] across the resonance, whose effect is to flip the vertical polarization component, and refined with a series of fixed-frequency scans to locate the center of the resonance within an error of about 0.2 $Hz$ (see Sec. 6.1.1).

The Time-to-Digital Converter (TDC) ZEL GPX, created at the Forschungszentrum-Jülich, marked the polarimeter events with the elapsed time from a continuously running clock. The clock period of the TDC was 92.59 $ps$, a much smaller value than the COSY beam revolution time of 1.332 $\mu s$. This allowed good resolution on the longitudinal position

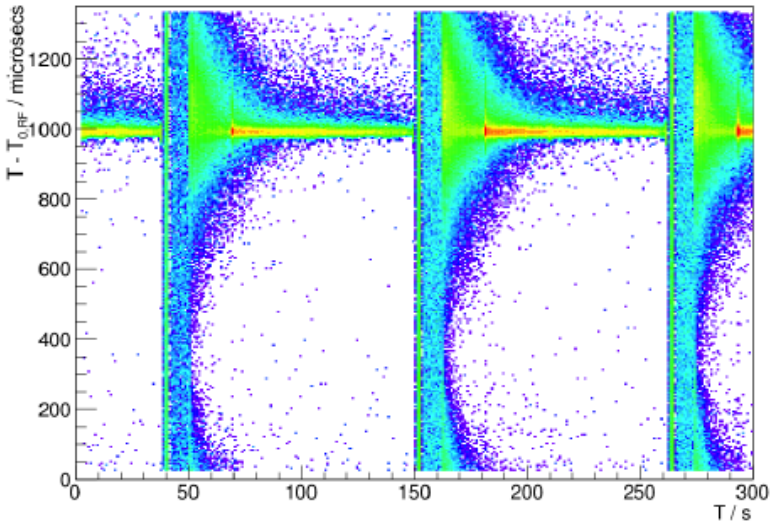


Figure 3.5: *Scatterplot of polarimeter events as a function of location around the ring (vertical axis) and clock time in seconds (horizontal axis). Parts of four different machine cycles are shown. The intensity scale starts with violet and goes on through blue, green, yellow and red [23].*

of a detected particle within the beam bunch. Once the RF cavity signal and the TDC

oscillator were cross-calibrated, so that the turn number since DAQ start could be calculated, it became possible to use the fractional part of the turn number to provide a map of the particle distribution within the beam bunch. This means that the fractional part of the turn number may be interpreted as the location of particles around the ring with respect to the center of the bunch. A scatterplot of polarimeter events as a function of the fractional part of the turn number (vertical axis) and clock time in secons (horizontal axis) is shown in Fig. (3.5). This plot shows that, at the beginning of the cycles, the beam is spread around the ring. The initial few seconds are for injection, ramping, bunching, and the start of cooling. The bunching moves events out of the area near 300 and toward the center of the bunch near 1000 along the vertical axis. Electron cooling makes the bunch more compact (narrow yellow-red band). Outliers are slowly gathered into the main beam. After about 30 $s$, the extraction of the bunch onto the polarimeter target starts and, after that, the height of the cooling peak declines until the beam is nearly gone [23]. One machine cycle represents about $8.8 \times 10^7$ turns.

In order to calculate the total spin precession angle, only the integral part of the turn number is needed. This calculation requires the knowledge of the spin tune frequency, which can be derived from Eq. (3.7) by making the difference between the RF solenoid resonance frequency and the cyclotron frequency, giving as result $G\gamma f_{cyc} \sim 120\ kHz$. Therefore, the total horizontal polarization precession angle was calculated for each event as:

$$\omega_{tot} = 2\pi G\gamma\, \mathrm{Int}(N_{turns}) \tag{3.8}$$

being $G\gamma$ the spin tune, and $\mathrm{Int}(N_{turns})$ the integral part of the turn number.

In order to finally measure the beam horizontal polarization, the circle around which the particle spins precessed was divided into 9 bins, and then the polarimeter events collected in the up and down sectors of the EDDA detector were sorted separately into each bin. The high frequency of the polarization precession represented an issue. In fact, one full precession corresponded to only 6 revolutions of the beam around the COSY ring (about 8.3 $\mu s$), while the rate of the elastic scattered deuterons was approximately one every 700 turns. In order to enhance the statistics, an accumulation time of 3 $s$ was chosen, and the down-up asymmetries were calcuated for each bin and reproduced with a sine wave with variable magnitude, phase and offset, defined as:

$$\frac{D-U}{D+U} = A\sin(\omega+\phi)+B \tag{3.9}$$

The magnitudes from successive 3-seconds accumulation times were put together to create a history of the horizontal polarization during the store.

In the last part of the measuring process, the spin tune was varied over a small range in each accumulation time in order to find the value that gave the largest polarization magnitude. A peak was always evident. The spin tune is typically known up to $10^{-8}$ in each accumulation time and varies by $10^{-7}$ during a beam store [23]. This variation seems to be associated with the spin tune change across the beam profile during its extraction onto the carbon target of the polarimeter.

# Chapter 4

# The COSY INFINITY code

In order to design and study particle optical systems, several simulation codes have been developed in the recent past. It is possible to divide these codes in two different categories:

- Ray tracing codes, which determine the trajectory of the single rays through electromagnetic fields by using numerical integration techniques. Although they generally have a core easy to set up, they often result to be quite slow for many apllications, without giving access to other informations than ray coordinates values.

- Map codes, which compute the transfer matrix of the Taylor expansion coefficients that describe the action of the optical system on the phase space. They are usually faster than the integration codes and, through the expansion coefficients, they provide more specific informations about the system than only the coordinates values. On the other hand, the majority of these codes has a limited expansion order and, therefore, a limited accuracy in determining the system parameters.

The goal would be to merge the advantages of these two categories in one code able to compute Taylor maps for arbitrarily complicated fields and to arbitrary order. The usage of differential algebraic (DA) tecniques [31] allows to do that efficiently, up to high order and with the speed of classical mapping codes.

This is the purpose of the **COSY INFINITY** code [32, 33], created by Prof. Martin Berz at the Michigan State University. Besides tracking particles during their motion, this code offers the possibility to track also the particle spins (see Sec. 4.3.4) by using DA to

calculate the spin transfer matrix of the system.

This chapter will define how the COSY INFINITY language, COSYScript, works by presenting the basic structure of a program. It will then explain in details how the beam physics is included in the code and how the spatial coordinates and the spin transfer maps are computed. The optical elements used to build the COoler SYnchrotron lattice will be defined. Finally, details about the position and spin tracking procedure are given.

## 4.1 The COSY INFINITY language

COSY INFINITY is a new generation code based on differential algebra for the study and design of optical systems like accelerators, spectrometers, beamlines, electron microscopes, etc. It has an object oriented language environment, called **COSYScript**, that allows, by defining different subsequent procedures, to call and use powerful DA operations up to high order of Taylor expansion and, at the same time, to reduce the computational time to the minimum. It is a recursive language with a PASCAL based syntax; for compatibility reasons, the compiler is written in Fortran 77 that, because of its portability, serves as a machine independent assembly language [34].

Most commands of COSYScript consist of a keyword, followed by names of variables and expressions, that are terminated by a semicolon; the individual entries are separated by blanks. The assignment statements represent an exception because they do not have a keyword, but they are identified by the assignmen identifier :=. When a procedure is called, the pocedure name is used instead of the keyword. Commands can extend over several lines, and several commands can be written in one line; furthermore line breaks are not significant. It is possible to add comments to the program script by writing them within curly brackets, so that the compiler ignores them. Finally, the language is not case sensitive [32].

## 4.2 Basic structure of a program

A COSY input program consists of a tree-structured arrangement of nested program segments. The user generally uses three types of these segments. The first and also indispensable one is the main program, which opens and closes the input files and contains all the other segments; its keywords are

**BEGIN** ; and **END** ;

The other two types of program segments are procedures and functions; they are identified respectively by the commands

**PROCEDURE** $<$ *name* $>$ $\{<$ *name* $>\}$ ; and **ENDPROCEDURE** ;

or

**FUNCTION** $<$ *name* $>$ $\{<$ *name* $>\}$ ; and **ENDFUNCTION** ;

The first $<$ *name* $>$ is the identification expression that allows to call a procedure or a function; the $<$ *name* $>$ in curly brackets is optional and defines the local names of variables passed into the routine. While the call to a procedure is a separate statement, the identification name of a function can be used as a mathematical object in arithmetic expressions.

Each one of the segments just described is constituted by three sections: the first one contains the declaration of the local variables, the second one contains the local procedures and functions, and the third one contains the executable commands. Concerning the last part, it is important to specify that both procedure and function segment must contain at least one executable line.

To declare a variable there is the command

**VARIABLE** $<$ *name* $>$ $<$ *expression* $>$ $\{<$ *expression* $>\}$ ;

where the $<$ *name* $>$ is the identifier of the variable that has to be declared. The first $<$ *expression* $>$ represents the size of the memory that has to be allocated when the variable is used. Since no type of variable has to be specified at declaration, the amount of memory has to be sufficient to hold the different types that the variable can assume in the program. For instance, a real or double precision number requires a memory allocation length equal to 1, while a complex double precision number requires a length of 2; a DA vector, which is the type we are mainly interested in, requires at least a length of $(n+v)!/(n!\cdot v!)$, expression that represents the number of partial derivatives in $v$ variables to order $n$.

It is also possible to use a declared variable as an array; in that case, the second $<$ *expression* $>$ has to indicate the number of components of the array. For example, the line

**VARIABLE** K 50 3 ;

declares the variable K as an one-dimensional array with 3 components, each of which has a memory allocation length of 50.

All variables declared inside a specific program segment are available also for the proce-

dures and functions defined inside it. This ensemble of local procedures and functions is the second section of the segment. When a routine is called, all the executable lines contained in it are processed, and this includes also the commands specified inside local routines.

The final section of the program segment is the one containing the executable statements. Among this class of commands we find the assignment statement that, as already introduced, is characterized by the identifier := and is not associated to any keywords. It has the form

$<$ *variable or array component* $>:=<$ *expression* $>$ ;

where the $<$ *expression* $>$ is an arithmetical combination of numbers, variables and array elements visible in the routine where the assignment is defined.

The call to a procedure or a function is an executable statement too. In order to use it, it is necessary to write the first $<$ *name* $>$ that appears in the definition of the selected procedure or function, followed by the name of the local variables needed to define it.

In order to control the program flow, there are statements consisting of command pairs indicating the beginning and ending of the control structure. Such statements are called by the keywords

**IF** $<$ *expression* $>$;

**WHILE** $<$ *expression* $>$;

and

**LOOP** $<$ *name* $><$ *beginning* $><$ *end* $>$;

where $<$ *expression* $>$ in the **IF** and **WHILE** commands indicates one or more operations that have to be done when certain conditions occur. The **LOOP** flow controller is used to iterate one or more operations: $<$ *name* $>$ is the variable that is incremented in the process, while $<$ *beginning* $>$ and $<$ *end* $>$ represent the initial and the final value of this variable. Control sequences can be arranged in a nested arrangement, with the constraint of including completely the beginning and ending of the lower level control structure inside the beginning and ending of the higher level control structure.

As last example of executable instructions, it is important to mention the input and output statements. These have respectively the form

**READ** $<$ *unit* $><$ *name* $>$ ;

and

**WRITE** $<$ *unit* $><$ *expression* $>$;

where the $<$ *unit* $>$ stands for a unit number that specifies where the input has to be read

and where the output has to be written; unit 5 indicates the keyboard and unit 6 denotes the screen, while other numbers can be associated with file names by using the procedures **OPENF** and **CLOSEF** in order to read from or write in a file. In the **READ** command, the $< name >$ following the $< unit >$ refers to the variable to be read, that can be either of type number or string; in the **WRITE** command, the $< expression >$ after the $< unit >$ is the output quantity that, also in this case, can be a number or a string.

Inside the program structure just described, the user has the possibility to call beam physics elements in order to create and study complex systems such as a particle accelerator. This physics environment deserves a more detailed treatment.

## 4.3 Beam physics in COSY

The physics part of COSY INFINITY is written in its own input language in a separate file named *cosy.fox*, where all the elements necessary to the study of a beam physics system are defined as procedures. Therefore, most commands in the user's input file are simply calls to those previously defined procedures. The user can also decide to create new commands simply by defining new procedures. In this optic, beamlines are formed by a sequence of calls to procedures representing individual elements [33].

Using the DA techniques and the powerful environment described above, COSY INFINITY proves to be a very flexible code that allows map computation and particle tracking in a compact way. This approach permits, in particular, to avoid many approximations in the resolution of the particles equation of motion in the accelerator by computing the transfer map of the system to high order.

The transfer map $M$ is the flow of the Ordinary Differential Equation (ODE)

$$\vec{z_f} = M(\vec{z_i}, \vec{\delta}) \tag{4.1}$$

where $\vec{z_i}$ and $\vec{z_f}$ are the vectors of, respectively, the initial and the final conditions, while $\vec{\delta}$ is the vector of the system parameters, among which there is time. So, for any initial state $\vec{z_i}$ of the system, the time dependent map tells us the final state of the system after a certain interval of time. Note that, for a repetitive system like, for instance, a beam line, only a one turn map has to be computed, making the particle tracking much faster than with ray tracing codes, that trace each individual particle through the system.

As well as for the orbital motion, it is possible to calculate the spin transfer map $\hat{A}$ for

the investigated system, that represents the ensemble of solutions of the ODE

$$\vec{S_f} = \hat{A}(\vec{z_i}, \vec{\delta}) \cdot \vec{S_i} \tag{4.2}$$

where $\vec{S_i}$ and $\vec{S_f}$ are the spin vectors of, respectively, the initial and the final state. A fundamental charachteristic of this form of the spin equation of motion, deriving from the Thomas-BMT equation [19, 20], is that the orthogonal matrix $\hat{A}(z)$ does not depend on the spin components, but only on the orbital quantities. This means that, once the orbital transfer map is computed, it is straightforward to obtain the spin one by calculating the solution of Eq. (4.1) and consider it as the new initial condition.

Every time COSY INFINITY computes a map, it stores it in a global variable called MAP that is updated by each particle optical element that is called. It is always possible to print both the orbital and the spin transfer map using respectively the commands **PM** and **PSM**, that print the desired map to a chosen unit.

### 4.3.1 Optical elements

Among the several optical elements supported by COSY INFINITY, it is opportune to discuss about the main of them used to build a lattice (see App. A) as close as possible to the COooler SYnchrotron (COSY), being this the system we are interested in simulating.

The simplest particle optical element is the field-free and material-free drift length, that can be applied to the transfer map with the command

**DL** $< length >$ ;

where the parameter $< length >$ is given in meters and specifies how long the drift space is wanted.

Since the aim is to recreate a circular trajectory, bending elements are needed. It is possible to call a parallel faced bending magnet with the call

**DP** $< \rho > < \theta > < aperture >$ ;

that applies on the map a vertical magnetic field $B \propto (1/\rho)$, being $\rho$ the bending radius; the angle $\theta$ denotes the bending angle and the $< aperture >$ corresponds to the half gap width of the magnet.

Other necessary elements are quadrupole and sextupole magnets. In order to call a quadrupole magnet, that acts on the beam as a focusing device, there is the command

**MQ** $< length > < B > < aperture >$ ;

where $< length >$ is the length of the magnet in meters, $B$ is the magnetic flux density at the pole tip, and $< aperture >$ denotes the half gap width of the magnet. This element acts on the map with a magnetic field defined as:

$$\begin{cases} B_x = ky \\ B_y = kx \end{cases} \tag{4.3}$$

where $k$ is the related multipole strength parameter [35]. For a sextupole, that provides a position dependent focusing, the call is similar

**MH** $< length > < B > < aperture >$ ;

This type of magnets is used for non linearity and chromaticity corrections, since the generated magnetic field depends on the second order of the spatial coordinates:

$$\begin{cases} B_x = mxy \\ B_y = \frac{1}{2}m(x^2 - y^2) \end{cases} \tag{4.4}$$

where $m$ is again the related multipole strength parameter [35].

The last important element to be introduced is the Radio-Frequency (RF) cavity. There is a simple model for the cavity in COSY INFINITY, based on a potential depending on position and time according to the relation:

$$V(x,y) = P(x,y) \cdot \sin\left[2\pi(\nu \cdot t + \phi/360)\right] \tag{4.5}$$

where $\nu$ is the frequency in Hertz and $\phi$ is the phase in degrees at which the reference particle enters the cavity. The command tha allows to call the RF device is

**RF** $< V > < I > < \nu > < \phi > < aperture >$ ;

being $V$ a two dimensional array containing the coefficients of a polynomial of order $I$ describing the dependence on the position of the potential $V(x,y)$, defined as:

$$P(x,y) = \sum_{j,k=0}^{I} V(j+1,k+1) \cdot x^j \cdot y^k \tag{4.6}$$

For the purpose of this thesis, $I$ has been chosen to be equal to zero.

### 4.3.2 Implementation

The COSY INFINITY input file that contains all the user commands is a *.fox* file and it is compiled by *foxy.f*, that is the compiler and executor of COSYScript written in Fortran 77. The first line of this input file must be

**INCLUDE 'COSY'** ;

which allows the use of all the compiled code contained in the program *cosy.fox*. The user input itself is contained in the main COSY procedure, that has to be named RUN. According to the COSYScript syntax precedently described, all commands must then be included between the statements

**PROCEDURE RUN** ; and **ENDPROCEDURE** ;

As for all the procedures, also the procedure RUN must be called to be executed, then the ENDPROCEDURE statement has to be followed by the call

**RUN** ;

followed by the final line that completes the input file

**END** ;

Before any DA operation can be executed, thus before any maps can be computed, it is necessary to set up the DA tools via the call

**OV** $<$ *order* $>$ $<$ *phase space dimension* $>$ $<$ *number of parameters* $>$ ;

The order specifies the maximum order of computation required by the user and it can be changed during the run time, but it can never exceed the one set in OV. The phase space dimensionality can assume the value 1, 2 or 3: if it is 1, only the horizonthal motion is computed; if it is 2, also the vertical motion is taken into account; if it is 3, the code computes also the time of flight and the chromatic effects. The number of parameters is the number of additional quantities that the transfer map of the system will depend on, besides the phase space variables.

### 4.3.3 Beam parameters

All the calculations are performed in COSY INFINITY in the following set of coordinates:

$$
\begin{aligned}
r_1 &= x & r_2 &= x' = \frac{p_x}{p_0} \\
r_3 &= y & r_4 &= y' = \frac{p_y}{p_0} \\
r_5 &= l = \frac{-(t-t_0)v_0\gamma}{1+\gamma} & r_6 &= \delta_K = \frac{K-K_0}{K_0} \\
r_7 &= \delta_m = \frac{m-m_0}{m_0} & r_8 &= \delta_Z = \frac{Z-Z_0}{Z_0}
\end{aligned}
\tag{4.7}
$$

The first six variables form three canonically conjugate pairs in which the map is symplectic; $x$ and $y$ are, respectively, the radial and the vertical position in meters with respect to the reference trajectory, thus the trajectory corresponding to an ideal orbital motion; $p_0$, $K_0$, $v_0$, $t_0$ and $\gamma$ are, respectively, the momentum, kinetic energy, velocity, time of flight and total energy in unit of $m_0c^2$ of the reference particle, that is the particle travelling on the reference trajectory; $m_0$ and $Z_0$ are, respectively, the mass and the charge of the reference particle.

We understand therefore that all the optical coordinates are calculated relatively to a reference particle, that has to be defined within the input file with the command

**RP** $<$ *kinetic energy in MeV* $>$ $<$ *mass in amu* $>$ $<$ *charge in units of e* $>$ ;

It is also possible to set the reference particle by assigning a value in $MeV/c$ to the momentum:

**RPM** $<$ *momentum in MeV/c* $>$ $<$ *mass in amu* $>$ $<$ *charge in units of e* $>$ ;

Finally, in order to activate the spin computation, it is necessary to call the procedure

**RPS** $< LS > < G >$ ;

where $< LS >$ is the spin mode, with 1 indicating spin computation ON and 0 no spin computation, while $G = (g-2)/2$ is the anomalous magnetic moment of the selected particle.

### 4.3.4 Tracking

One of the main features of COSY INFINITY is its ability to trace rays through the system. To every selected ray is applied the map of the system as result of the compositions of the maps of the single elements called by the user. It is possible to print the coordinates of these rays, and also to plot their trajectories. In order to set a ray that has to be traced through the system, it is given the command

**SR** $< x > < x' > < y > < y' > < l > < \delta_K > < \delta_m > < \delta_Z > < color >$ ;

where the specified quantities are the particle optical coordinates defined in Eq. (4.7); the unit $< color >$ indicates a number that can be specified to choose the line color for the plot.

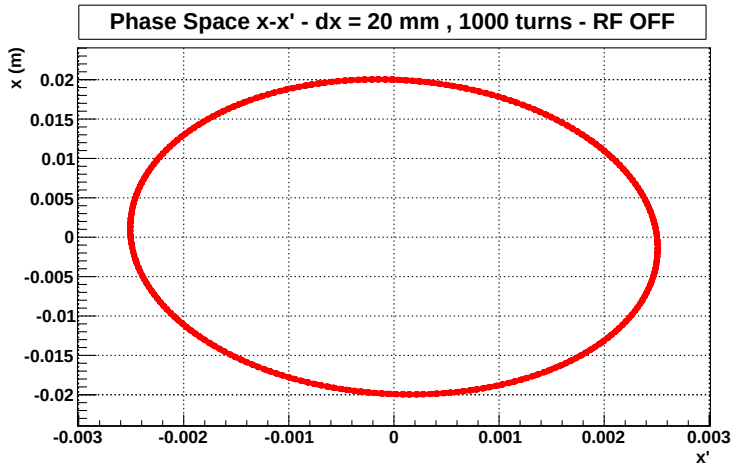


Figure 4.1: *Phase space $x - x'$ for a deuteron with momentum* 970 *MeV*$/c$ *and initial radial position* $x = 20$ *mm. The tracking is here performed for 1000 turns.*

If the spin computation is ON, it is necessary to set the spin coordinates of the particle. This can be achieved using the command

**SSR** $< S_x > < S_y > < S_z >$ ;

where $S_x$, $S_y$ and $S_z$ are, respectively, the radial, vertical and longitudinal components of the normalized spin vector $\vec{S}$. This call has to be made immediately after the coordinates setting via **SR**.

An aspect of the feature of the code just described that is very important for the aim of this work is the repetitive tracking of particles through the defined lattice. Using the call

**TR** $< N > < NP > < ID1 > < ID2 > < D1 > < D2 > < TY > < NF > < IU >$ ;

COSY INFINITY tracks each of the particles selected with **SR** through the map of the system for the required number of iterations $N$. After each $NP$ iterations, the position of the phase space projection $ID1 - ID2$ is drawn to the selected unit $IU$. The phase space identification numbers $ID1$ and $ID2$ can assume values going from 1 to 6, corresponding to the group of optical variables $r_1 \rightarrow r_6$ defined in Eq. (4.7); it is also possible to select the $x$, $y$ and $z$ components of the spin by assigning to the identifiers, respectively, the numbers -1, -2, -3. The maximum value that these components can get, is set with $D1$ and $D2$. The parameter $TY$ specifies the symplectification mode. Notice that it is also possible to store

the output of the tracking procedure in a file, that can be analyzed with different softwares. An example of repetitive tracking is shown in Fig. (4.1).

# Chapter 5

# Spin Coherence Time simulations

To investigate the actual feasibility of an electric dipole moment experiment in a storage ring, dedicated studies are being performed at the COoler SYnchrotron (COSY) facility. Such experiments investigate the polarization lifetime of a horizontally polarized deuteron beam in the COSY storage ring.

The realization of a Storage Ring EDM experiment requires a long time during which the longitudinal polarization remains stable. This requirement comes from the fact that the EDM signal is detected as a build-up of a vertical polarization component in a horizontally polarized system (see Sec. 1.4). Therefore, for such a high precision experiment, it is necessary a perfect knowledge of the spatial motion of the beam and the evolution of the spin motion inside the ring.

The aim of the work at the base of this thesis is to benchmark the COSY INFINITY code for the spin tracking, probing its reliability for a future use in the design of the new generation EDM storage ring. To achieve that, the results obtained from the simulations have been compared with the experimental results of the precursor experiments performed at the COoler SYnchrotron.

In this chapter both the simulations and the comparison with the experiments will be shown. In the first part, after defining the spin tune and the spin coherence time in COSY INFINITY, the calculation of the latter starting from the spin tune spread dependence on radial and vertical position, and on the momentum offset is presented. Both the cases with and without the RF cavity will be treated. The second part will be about the correction of these decoherence effects through the use of sextupole magnets installed in the ring.

## 5.1 Spin tune

The *spin-tune* of the particles composing a beam is defined as the number of spin rotations around the vertical axis during one revolution in the ring. It depends on the particles velocity through the relation:

$$\nu = |G|\gamma \tag{5.1}$$

where $G$ is the particles anomalous magnetic moment, and $\gamma$ is the relativistic factor. This dependence is responsible for introducing a *spin-tune spread* ($\Delta\nu$) among the particles composing the beam. Each particle will have then a spin tune differing from the one of the reference particle ($\nu_{RP}$) by the quantity:

$$\Delta\nu = \nu - \nu_{RP} \tag{5.2}$$

Therefore, since in a real beam all the particles do not have the same velocity, they will precess with different frequencies and, after a certain amount of time depending on the spin tune spread, called spin coherence time, they will be all out of phase in the horizontal plane (see Fig. 1.5) ending in the vanishing of the initial horizontal polarization of the beam.

### 5.1.1 Spin tune calculation in COSY INFINITY

The first step towards the investigation of the dependence of the spin coherence time on the machine parameters through simulations with COSY INFINITY, is the development of an effective procedure for computing the spin tune. As explained in Chap. 4, COSY INFINITY allows to track the spin of the particles of the beam and print out the spin vector coordinates for each particle after every time they complete a revolution in the ring. With this information it is possible to calculate the spin-invariant axis by making use of the normalized cross product of each couple of spin vectors for two consecutive turns:

$$\hat{n}_i = \frac{\vec{S}_i \times \vec{S}_{i+1}}{|\vec{S}_i||\vec{S}_{i+1}|} \tag{5.3}$$

where $i$ is the number of turns counter, that can assume values $0 \leq i \leq N$, being $N$ the total number of turns. The spin invariant axis is the axis around which the spin vector is precessing. As the spin tune is defined as the number of spin rotations around this particular axis in one beam revolution, we can calculate the spin phase advance around $\hat{n}_i$ in one turn

as:

$$\theta_i = \arcsin\left(\frac{|\vec{S}_i \times \vec{S}_{i+1}|}{|\vec{S}_i||\vec{S}_{i+1}|}\right) \tag{5.4}$$

and then obtain the spin tune by:

$$\nu_i = \frac{\theta_i}{2\pi} \tag{5.5}$$

It emerges from Eq. 5.5 that get several spin tune values, specifically as many as the number of turns $N$. The choice of an high number of turns has been made in order to increase the accuracy of the calculation by averaging the spin tune over $N$. The procedure can be

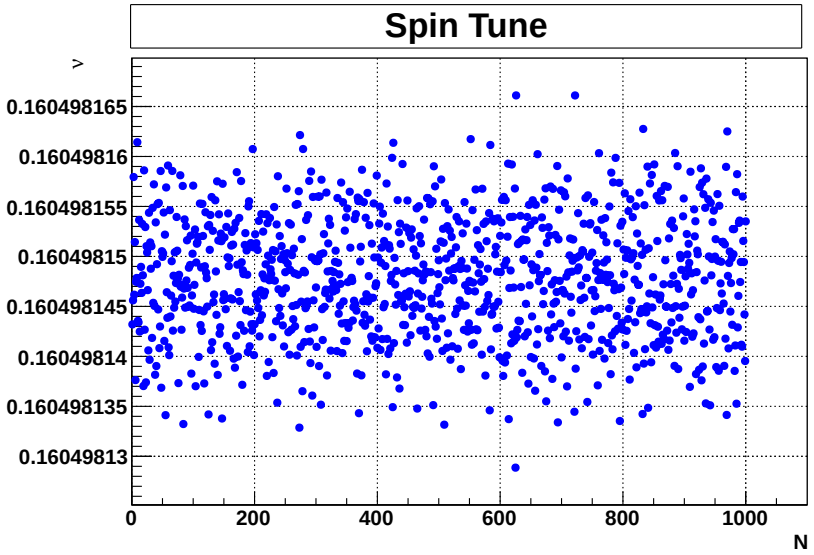


Figure 5.1: *Spin tune's dependence on the number of revolutions in the ring for a reference deuteron with momentum $p = 970\ MeV/c$. The tracking has been performed for $N = 2 \times 10^5$, and the average over this number of turns gives as result $\langle \nu \rangle_{RP} = 0.1604981$. Only the values for the first 1000 turns are shown, to avoid confusion.*

clarified by looking at Fig. 5.1, that shows the spin tune's dependence on the number of turns for the reference particle. The presented case is that of a deuteron with momentum $p = 970\ MeV/c$ and initial spin vector $\vec{S} = (S_x, S_y, S_z) = (0, 0, 1)$. $S_x$, $S_y$, and $S_z$ are, respectively, the radial, vertical and longitudinal spin components. Spin tracking has been performed for $N = 2 \times 10^5$ turns, and the spin tune values obtained are within the interval

$0.16049812 < \nu < 0.16049817$

with an average over $N$ calculated to be:

$$\langle \nu \rangle_{RP} = 0.1604981 \tag{5.6}$$

The differences between the spin tune values occur to the 8th digit, due to the limitation in the number of digits used in the code. These differences are therefore due to numerical approximations in the analysis.

As a cross-check, the same result can be obtained by making use of the spin tune definition $\nu = |G|\gamma$ (see Eq. 5.1), where in this case $G = -0.1425617$ is the deuteron anomaly [36], and $\gamma$ is the relativistic factor. This evidence represents a first confirmation that the code is correctly computing the spin motion.

An additional check that can be done is looking at the horizontal spin precession around the spin invariant axis. Fig. (5.2a) shows the radial $S_x$ and the longitudinal $S_z$ components

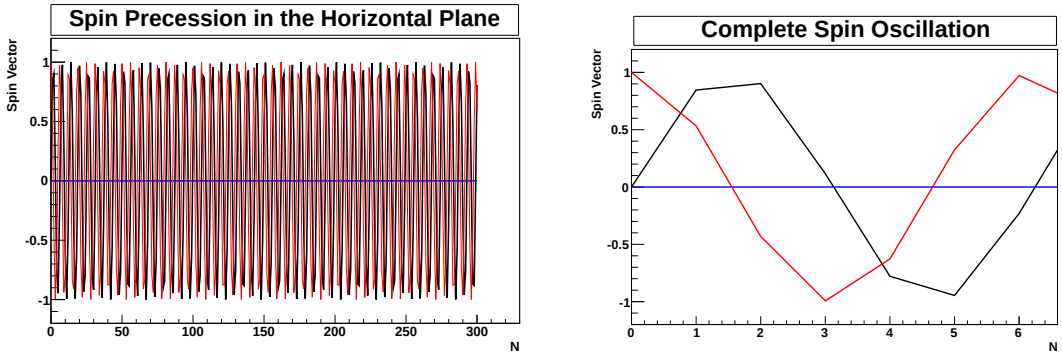


(a) (b)

Figure 5.2: *Fig. (a) shows the spin precession in the horizontal plane during 300 revolutions around the ring. The black line refers to the $S_x$ component, starting from 0, the red line refers to the $S_z$ component, starting from 1, and finally the blue line refers to the $S_y$ component that starts and stays constant at 0. This is in agreement with the initial condition $\vec{S} = (0,0,1)$. Fig. (b) shows the period of the spin precession, thus one complete oscillations of $S_x$ and $S_z$.*

oscillating between $-1$ and $+1$ with a phase difference of $\pi/2$, while the vertical component $S_y$ remains constant at its starting value 0, consistently to the motion of a spin vector $\vec{S} = (0,0,1)$ in a vertical magnetic field. $S_x$ and $S_z$ make a complete oscillation in $N_\nu \sim 6.23$ revolutions of the particle in the ring, as it is shown in Fig. (5.2b), meaning that the spin tune can be derived also from this plot as:

$$\nu = 1/N_\nu \simeq 0.1605 \tag{5.7}$$

This result is close to the one obtained with the average method, suggesting again that COSY INFINITY calculates the reference deuteron's spin tune correctly.

## 5.2 Spin tune spread evaluation

So far we have talked about the spin tune of the reference particle, that represents the spin precession frequency that, for an ideal beam, would be the same for all the particles. Our aim is to study a real system where the particles have parameters, like momentum and position, that differ from the reference ones and change during the storing time.

In a real beam, there are three different contributions to the spin tune spread coming from beam dynamics:

- a first order contribution due to the momentum spread $\Delta p/p$ of the particles in the beam;
- a second order contribution due to betatron oscillations that cause both a radial and a vertical position offset with respect to the reference trajectory, ending in a lengthening of the beam path, a change in the particles speed, and a resulting spin tune spread;
- a second order contribution due to $(\Delta p/p)^2$.

The method described in the previous section has been applied to calculate the spin tunes of the offset particles.

Three different offsets have been studied in this work: the radial and vertical position with respect to the reference orbit, respectively $\Delta x$ and $\Delta y$, and the momentum spread $\Delta p/p$. Their contributions to the spin tune spread have been considered indipendently. The computation order of COSY INFINITY has been set to 2.

### 5.2.1 Transverse phase space

The first case considered is the one with RF cavity switched off. For studying the radial offset effect on the spin tune, an ensemble of 15 deuterons was declared in COSY INFINITY with initial spin vector $\vec{S} = (0,0,1)$ and an assigned value of $\Delta x$ included in the interval $-35\ mm \leq \Delta x \leq 35\ mm$ with a difference of 5 *mm* between one particle and the following. This spread was chosen to resemble the size of an uncooled beam. The spin tracking was performed for $N = 2 \times 10^5$ turns, and the spin tune was calculated as average over $N$. The result of the simulation is shown in Fig. (5.3), representing the spin tune dependence on $\Delta x$.

The obtained spin-tune values are fitted by the second order polynomial

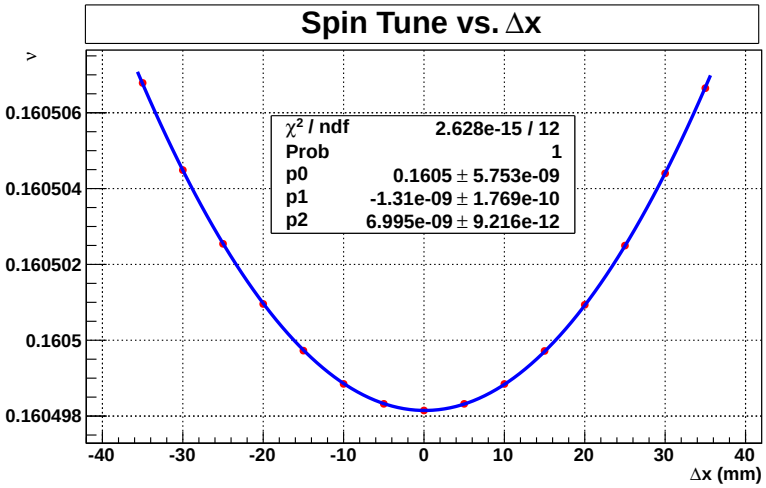


Figure 5.3: *Dependence of the spin-tune on the radial offset $\Delta x$ with respect to the reference orbit. Each one of the red dots represents the spin tune, averaged over the number of turns $N = 2 \times 10^5$, of one particle with an assigned offset. The blue curve corresponds to the $2^{nd}$ order polynomilal fit, indicating a quatratic dependence of the spin tun on $\Delta x$.*

$$\nu = p_0 + p_1 \Delta x + p_2 (\Delta x)^2 \tag{5.8}$$

where $p_0$, $p_1$ and $p_2$ are the fit parameters shown in the fit box in Fig. (5.3). The $p_0$ coefficient, that indicates the position of the vertex of the parabola, is the spin tune of the reference particle, as defined in Eq. (5.6); $p_2 > 0$ indicates that the parabola has an upward concavity, meaning that the average spin tune increases with respect to the reference value as the module of the radial offset increases. Finally, $p_1 \neq 0$ shows that the axis of the parabola does not coincide with the ordinate axis, probably because there is not a perfect symmetry between the spin tune values corresponding to positive and negative offsets. The obtained spin-tune spread varies in the region:

$$10^{-7} < \Delta\nu_x < 10^{-5} \tag{5.9}$$

where

$$\Delta\nu_x = \langle\nu\rangle_{\Delta x} - \langle\nu\rangle_{RP} \tag{5.10}$$

The same procedure was adopted to study the vertical offset effect on the spin tune. Also in this case, to each of the 15 deuterons, with initial spin vector $\vec{S} = (0,0,1)$, was assigned a value of $\Delta y$ included in the interval $-35\ mm \leq \Delta y \leq 35\ mm$ with a difference of 5 *mm*

between the particles. The spin tune dependence on $\Delta y$ is shown in Fig. (5.4). The ensemble

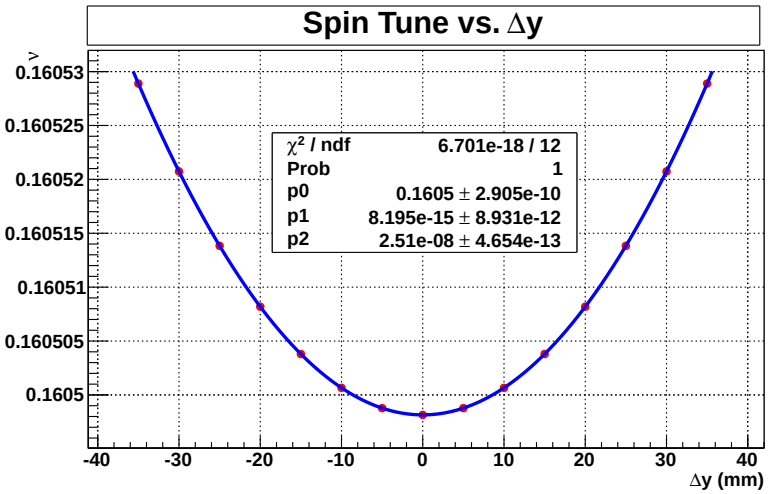


Figure 5.4: *Spin tune's dependence on the vertical offset $\Delta y$ with respect to the reference orbit. Each one of the red dots represents the spin tune, averaged over the number of turns $N = 2 \times 10^5$, of one particle with an assigned offset. The blue curve corresponds to the 2nd order polynomilal that fits the spin tune values ensemble, indicating a quatratic dependence of the spin tun on $\Delta y$.*

of spin tune values obtained is fitted by the second order polynomial:

$$\nu = p_0 + p_1 \Delta y + p_2 (\Delta y)^2 \tag{5.11}$$

where $p_0$, $p_1$ and $p_2$ are the fit parameters shown in the fit box in Fig. (5.4). The obtained interval of spin-tune spread is comparable to the radial one:

$$10^{-7} < \Delta \nu_y < 10^{-5} \tag{5.12}$$

where

$$\Delta \nu_y = \langle \nu \rangle_{\Delta y} - \langle \nu \rangle_{RP} \tag{5.13}$$

### 5.2.2 Longitudinal phase space

The last contribution to be considered is the one due to the momentum offset $\Delta p/p$ of particles of the beam with respect to the reference one. An ensemble of 13 deuterons was declared, each one with initial spin vector $\vec{S} = (0,0,1)$ and an initial value of momentum

offset included in the interval $10^{-4} \leq |\Delta p/p| \leq 3.2 \times 10^{-3}$. This choice of $\Delta p/p$ replicates the average momentum spread that is present among particles of an uncooled beam. The spin tracking was performed for $N = 2 \times 10^5$ turns, and the spin tune was calculated as average over $N$. The result of this investigation is shown in Fig. (5.5), presenting the spin tune dependence on $\Delta p/p$. In this case, the relation between the spin tune and the offset is linear,

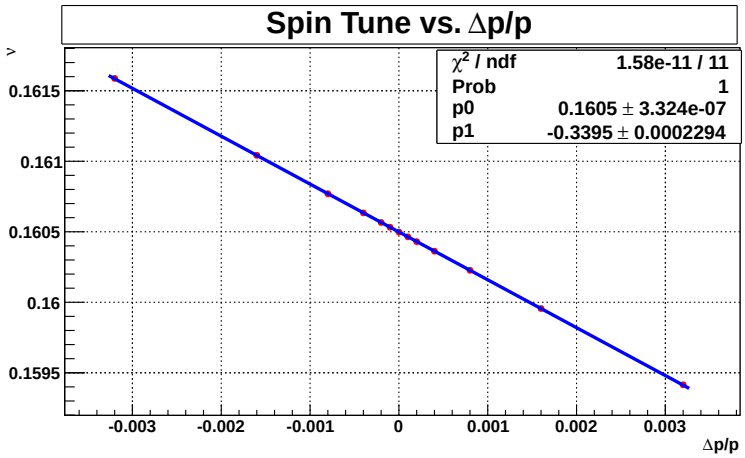


Figure 5.5: *Spin tune's dependence on the momentum offset $\Delta p/p$ with respect to the reference particle. Each one of the red dots represents the spin tune, averaged over the number of turns $N = 2 \times 10^5$, of one particle with an assigned offset. The blue curve corresponds to the 1st order polynomilal that fits the spin tune values ensemble, indicating a linear dependence of the spin tune on $\Delta p/p$.*

as expected considering the linear dependence existing between the momentum and the relativistic factor $\gamma$. The spin-tune, according to its definition (see Eq. 5.1), is proportional to $\gamma$ too, explaining the relation derived by the simulations. The polynomial that fits the values obtained is:

$$\nu = p_0 + p_1 \frac{\Delta p}{p} \tag{5.14}$$

where $p_0$ and $p_1$ are the fit parameters reported in the fit box in Fig. (5.5). The $p_0$ coefficient indicates the ordinate of the point where the straight line crosses the vertical axis, and represents the value of the spin tune of the reference particle, defined in Eq. (5.6); $p_1$ is the angular coefficient of the line and it is negative, indicating that the spin tune decreases while the momentum offset increases ($\Delta p = p - p_0$). This point is controversial and deserves some discussion. From the definition of spin tune $\nu = G\gamma$, it is clear that to a higher $\gamma$ should correspond a bigger $\nu$, thus an increase in the momentum should lead to a bigger spin-tune. The

authors of the code have been informed of this discrepancy: the latest possible explanation concerns the computation of fringe fields of dipoles and quadrupoles in COSY INFINITY, which seem to have a conflict when a momentum offset is inserted. Further investigations are required in order to understand if this is the real problem and find a solution to it. Nevertheless this situation does not affect our capability to probe the code because, as we will see later in this chapter, the quantity that matters to the calculation of the spin coherence time is the absolute value of the spin tune spread.

Finally, it is important to point out that $\Delta p/p$ induces a much bigger spin tune spread than $\Delta x$ and $\Delta y$, being its order of magnitude:

$$10^{-5} \leq \Delta\nu_p \leq 10^{-3} \tag{5.15}$$

where

$$\Delta\nu_p = \langle\nu\rangle_{\Delta p} - \langle\nu\rangle_{RP} \tag{5.16}$$

### 5.2.3 Introduction of the RF cavity

The following step in the simulation of a lattice as close as possible to the real COSY ring, is the introduction in the simulations of the effect of the RF cavity. The COSY INFINITY procedure calling a RF cavity has been described in Sec. (4.3.1); in Eq. (4.6), describing the position dependence of the cavity's potential, the choice $I = 0$ has been made so that the potential is a simple sinusoid, whose amplitude has been set to $V = 0.7\ kV$. The RF cavity effect on the beam can be seen in Fig. (5.6) that shows the $\Delta p/p$-$l$ phase space, where $l$ is the distance travelled by a particle with respect to the reference one (see Eq. 4.7), for a particle with initial momentum offset $\Delta p/p = 4 \times 10^{-4}$ in the cases with and without RF. When the RF cavity is off, the phase space plot is the one shown in Fig. (5.6a). In this case, the particle considered has a larger momentum with respect to the reference one, meaning that it is faster and this condition will not change turn after turn. Therefore the particle will always be ahead of the reference one, and the distance between them will increase turn by turn. The situation changes if the RF cavity is switched on, as shown in Fig. (5.6b). In this case $\Delta p/p$ does not stay constant at the initial value because the cavity changes turn by turn the momentum of the offset particle in order to compensate its being in advance. This action leads to oscillations of the particle around the reference position, called synchrotron oscillations, as it is shown by the characteristic ellipse-shaped curve. In this example, only one particle was considered, but the same thing happens in a real beam composed by particles

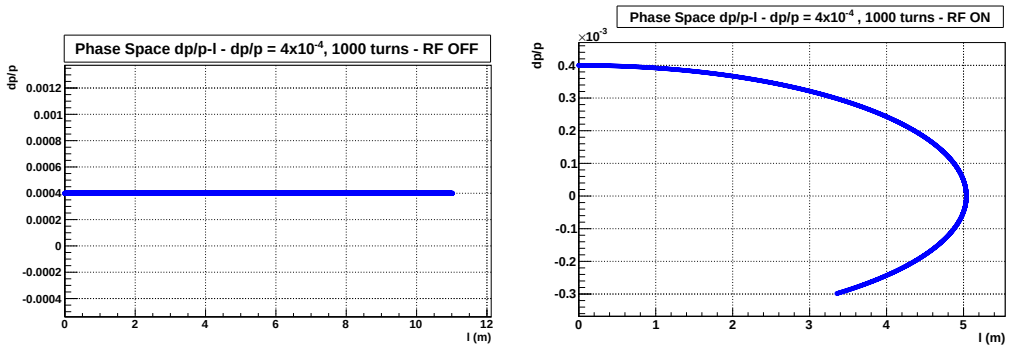


(a) (b)

Figure 5.6: *$\Delta p/p$-$l$ phase space for a case where the RF cavity is off: $\Delta p/p$ remains constant at the initial value $4 \times 10^{-4}$ during the motion, while $l$ keeps on increasing, meaning that the particle will be further and further from the reference one. Fig (b) shows the same situation, but with the RF cavity on: both $\Delta p/p$ and $l$ starts oscillating around $0$, showing that the RF is trying to compensate the effect of the initial momentum offset by inducing synchrotron oscillations. Here only a tracking for 1000 turns is shown; when the ellipse is closed, one synchrotron oscillation is complete.*

with different momenta: the RF cavity cancels the first order contribution of the momentum spread. In fact, each particle has an average momentum offset equal to zero in a complete synchrotron oscillation, thus its contribution to the path lengthening (see Eq. 2.26), and then to the spin-tune, vanishes. This underlines the importance of the RF cavity in the achievement of high spin coherence times, since it cancels the only first order contribution to the spin-tune spread, leaving only the second order ones to be dealt with.

Once defined that COSY INFINITY reproduces the action of the RF cavity on the beam correctly, the spin tune spread calculations for position and momentum offsets were repeated, in order to study the effect of the RF on the beam and spin dynamics. The adopted procedure is the same already described for the case with no cavity, except for an important detail: synchrotron oscillations occur even if the starting value of the momentum offset is zero. In facts, a particle having a position offset with respect to the reference trajectory, would be ahead or delayed with respect to the reference particle, and the RF cavity will induce a momentum offset, varying like in Fig. (5.6b), in order to compensate this difference. The induced $\Delta p/p$ are generally small, of the order $10^{-5}$; anyway, since a change in momentum is involved, they affect the spin tune vs. number of turns distribution (see

Fig. 5.1), introducing an oscillation frequency in such distribution. This means that it is not possible anymore to average the calculated spin tune over an arbitrary number of turns, but instead the chosen number of turns has to be the closest possible to a multiple of the number of revolutions needed for the phase space ellipse in Fig. (5.6b) to close, thus to an integer number of synchrotron oscillations. Notice that it is not assured that a complete synchrotron oscillation occurs in an integer number of revolutions in the ring, but it is not possible to average on a fractional number of turns. This will imply a systematic in the calculation of the spin tune spread and, later, of the spin coherence time, that has to be taken into account.

**Transverse phase space**

The result of the simulation confirms also in this case the quadratic dependence of the spin tune on $\Delta x$ (see Fig. 5.7a). Each spin tune is the result of an average over $N = 199363$ turns, corresponding to 73 complete synchrotron oscillations ($\simeq 2731$ revolutions per period). The differences with respect to the case without RF cavity are mainly two: first, the concavity of the parabola is now downward, implying that the spin tune is decreasing while the offset becomes larger. This is probably due to effect of the RF cavity on the spin-tune vs. number of turns distribution. In facts, due to the RF, the distribution starts oscillating with the synchrotron oscillations frequency, and the average spin-tune dramatically changes depending on the number of turns chosen to calculate it. This dependence can lead to either an increase or a decrease of the spin-tune with respect to the reference one, affecting the direction of the concavity of the parabola. It is important to highlight that we are interested in the absolute value of the spin tune change, not in its sign, because that is the quantity involved in the calculation of the spin coherence time. Second, the $p_2$ coefficient is about half of the one calculated without cavity, meaning that the spin tune change is slower than in the previous case. This leads also to a smaller magnitude of the spin tune spread, defined in Eq. (5.10), that in this case is evaluated to be:

$$10^{-8} < \Delta\nu_x < 10^{-6} \tag{5.17}$$

The quadratic dependence of the spin-tune on $\Delta x$ in the presence of the RF cavity is confirmed also for the case of a vertical offset, as shown in Fig. (5.8). In this case the parabola is not reversed, and the quadratic coefficient $p_2$ is about two orders of magnitude smaller than the one calculated without cavity, showing that the spin tune change is much

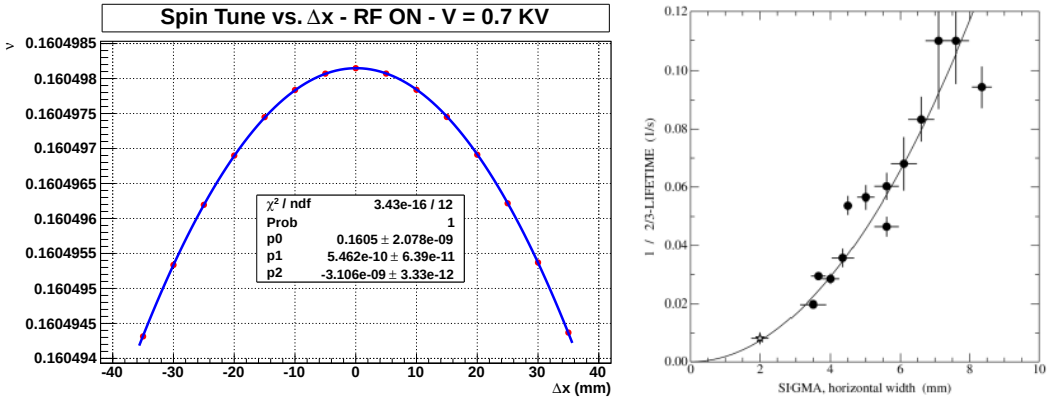


(a) (b)

Figure 5.7: *The left plot shows the spin tune's dependence on the radial offset $\Delta x$ with respect to the reference orbit when the RF cavity is switched on. Each red dot represents the spin tune, averaged over the number of turns $N = 199363$, of one particle with an assigned offset. The blue curve corresponds to the 2nd order polynomial that fits the spin tune values ensemble, indicating a quadratic dependence of the spin tune on $\Delta x$. The right plot [26] shows the dependence of the reciprocal of the beam polarization lifetime, thus the module of the tune spread (see next section), on the beam horizontal width for the data taken in May 2012 at COSY. The quadratic dependence has been confirmed experimentally.*

slower than in the previous case. As already reported for the radial offset effect, this decrease of $p_2$ leads to a smaller spin tune spread:

$$10^{-8} < \Delta\nu_x < 10^{-6} \tag{5.18}$$

that is comparable to the spread induced by $\Delta x$. This drastic reduction of the spin-tune spread is due to the effect of the RF cavity on the particles momenta. As explained above, the RF induces a varying momentum offset on the particles that, having a position offset, either radial or vertical, are ahead or delayed with respect to the reference one. This momentum offset, like for the phase stability principle (see Sec.2.2.1), in part compensates the path lengthening due to the position difference.

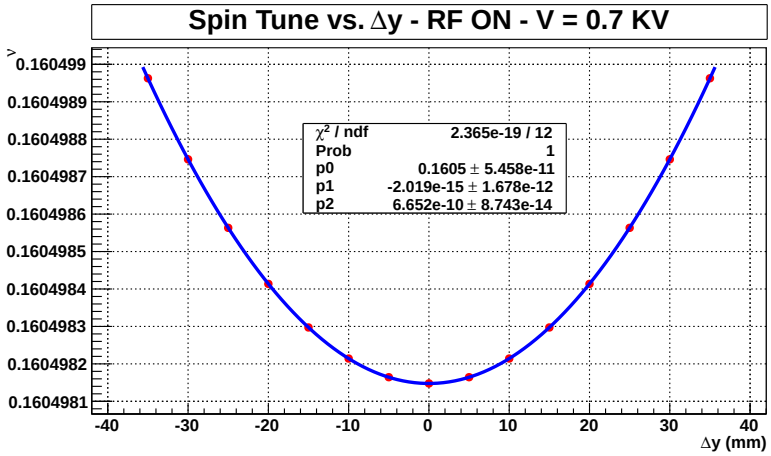


Figure 5.8: *Spin tune's dependence on the vertical offset* $\Delta y$ *with respect to the reference orbit when the RF cavity is switched on. Each one of the red dots represents the spin tune, averaged over the number of turns* $N = 199363$*, of one particle with an assigned offset. The blue curve corresponds to the 2nd order polynomial that fits the spin tune values ensemble, indicating a quatratic dependence of the spin tune on Deltay.*

### Comparison with experimental results

As it will be shown in the next chapter, the quadratic dependence of the spin-tune from the horizontal beam width has been experimentally confirmed by the data taken during the spin coherence time tests at the COSY ring, as it is possible to see looking at Fig. (5.7b) [26] where the data points related to the accelerator run occured in May 2012 are shown. This comparison is only qualitative, but represents a rather strong hint about the right approch of COSY INFINITY to the spin dynamics in a storage ring. One of the following steps will be the attempt to find a quantitative equivalence between simulation and experiment.

There were no data taken at the COSY ring with a vertically wide beam; in fact, due to the limited vertical acceptance of the accelerator, the attempts to increase the vertical profile of the beam resulted in its complete loss. This makes not possible the comparison between experiment and simulation.

### Longitudinal phase space

The effect of the RF cavity on the spin tune is even more evident for the case involving momentum offset as initial condition. As already specified, the cavity should cancel the first order contribution of $\Delta p/p$ to the spin tune spread, leaving a residual quadratic dependence. This is in part confirmed by Fig. (5.9), that shows the dependence of the spin tune on $\Delta p/p$ when the cavity is switched on. The curve that fits the spin tune values ensemble is not a

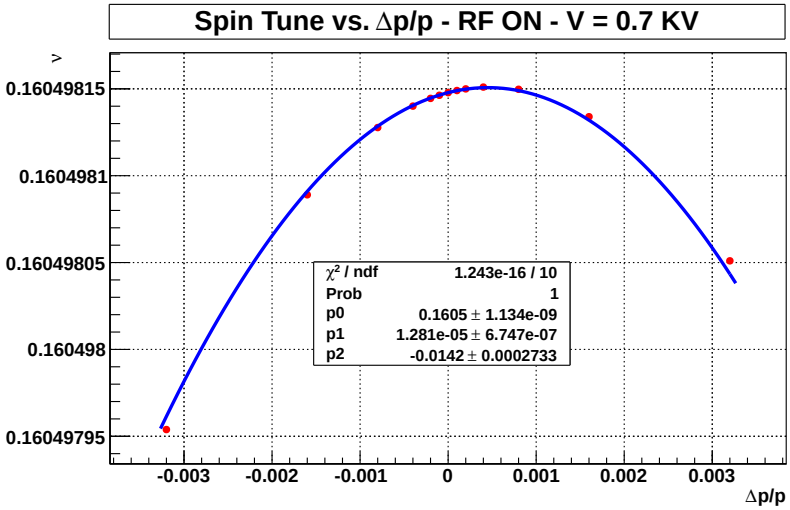


Figure 5.9: *Spin tune's dependence on the momentum offset $\Delta p/p$ with respect to the reference particle when the RF cavity is switched on. Each one of the red dots represents the spin tune, averaged over the number of turns $N = 199363$, of one particle with an assigned offset. The blue curve corresponds to the $2^{nd}$ order polynomial that fits the spin tune values ensemble; the parabola does not have its vertex in corrispondence of $\Delta p/p = 0$, suggesting some residual linear contribution.*

straight line anymore (see Fig. 5.5), but a second order polyomial of the type:

$$\nu = p_0 + p_1 \frac{\Delta p}{p} + p_2 \left( \frac{\Delta p}{p} \right)^2 \tag{5.19}$$

The spin tune spread is much smaller than the one calculated without RF cavity (see Eq. 5.15), and its order of magnitute is

$$10^{-8} < \Delta \nu_p < 10^{-6} \tag{5.20}$$

One would expect the parabola to have its vertex in corrispondence of $\Delta p/p = 0$, that would lead to a quadratic dependence just like in the case of the position offsets shown above.

This is not the case, suggesting that there is still a residual linear dependence affecting the relation. A possible explanation could be connected to the number of turns $N$ chosen for the average; in fact the synchrotron oscillation frequency depends on the starting value of $\Delta p/p$ assigned to the particles composing the ensemble considerated, meaning that $N$ could be slightly different for each of the particles selected. It could be possible to improve the situation by increasing the order of computation of the Taylor coefficients in COSY INFINITY, in order to better calculate the synchrotron oscillation period for each of the particles and, then, the correct $N$. This has been made for the $3^{rd}$ order of computation, and the results are shown in Fig.(5.10). The offset values $|\Delta p/p| > 4 \times 10^{-4}$ have not been

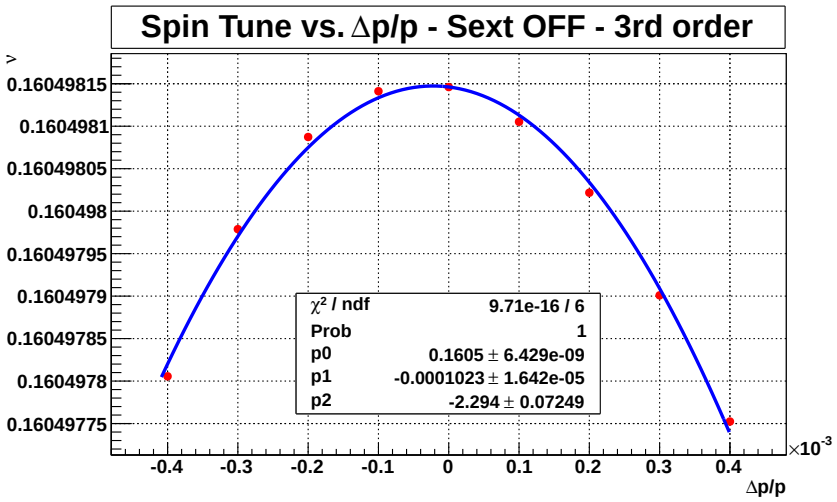


Figure 5.10: *Spin tune's dependence on the momentum offset $\Delta p/p$ with respect to the reference particle when the RF cavity is switched on. The computation order was set to 3. The vertex of the parabola is now in $\Delta p/p = 0$.*

considered, because this more accurated calculation showed that such values could be too big for the RF cavity to succeed in compensating them and lead to a miscalculation of the spin tune-momentum offset relation. This could be indeed another factor explaining the plot in Fig. (5.9). The new calculation shows a parabola with its vertex back in $\Delta p/p = 0$, but still not symmetric around it.

Now that we have the way to calculate the spin tune spread for an ensemble of particles, it is necessary to understand how to extract from this information a good extimate for the spin coherence time. This is the topic of the next section.

## 5.3 Spin Coherence Time estimation

As shown in Sec. 2.1.6, the change in path length depends on the square of the maximum angular deviation from the reference trajectory. It is therefore reasonable to expect the reciprocal of the spin coherence time to go as the square of the width of the beam profile:

$$\frac{1}{\tau_{SC}} = A\langle(\Delta x)^2\rangle + B\langle(\Delta y)^2\rangle \tag{5.21}$$

where $\Delta x$ and $\Delta y$ are connected to the angular deviations $\Delta x'$ and $\Delta y'$ through the emittance. Since in the previous section we saw how the spin-tune has a quadratic dependence on $\Delta x$ and $\Delta y$, it is possible to define a relation between the spin-tune spread and the horizontal polarization lifetime:

$$|\Delta\nu| \propto \frac{1}{\tau_{SC}} \tag{5.22}$$

Given that the polarization is a property of an ensemble of particles, we assume that these particles are distributed with a Gaussian shape, as shown by the heavy solid curve below the spin tune points in Fig. (5.11). The Gaussian width is shown by the long-dashed line; the curve on the right shows the distribution of the spin tune shifts that is produced by the calculation of the shift itself for each Gaussian width selected. We assume, therefore, that each of the offset values chosen for the spin tune spread evaluation represents the Gaussian width of the beam in the simulation, in order to be able to compare its polarization lifetime to the one coming from the experiment. The measurements (see next chapter) show that the Gaussian width is, in most cases, a reasonable measure of the beam width [37].

In the measurements that we will present in Sec. 6.2, the spin coherence time $\tau_{SC}$ of a particles beam was defined as the time for which the spin tune spread produces a polarization equal to $p = 0.606$ of the initial value of one. This definition derives from the analysis of the time dependence of the measured up-down asymmetry, whose shape is neither Gaussian nor exponential. A numerical template was therefore needed in order to associate a value of the spin coherence time to this shape. It was determined that, at small time, the template function behaves like a Gaussian, whose width corresponds to a drop in the polarization from 1 to $p = 0.606$.

In order to estimate the spin coherence time for a Gaussian-distributed beam, we start with the width of the Gaussian distribution of displacements, that in our case is a value included in the chosen $\Delta x$ or $\Delta y$ intervals. If we project this width onto the spin tune spread quadratic curve obtained (see Fig. 5.11), it corresponds to some value of the spin tune shift.

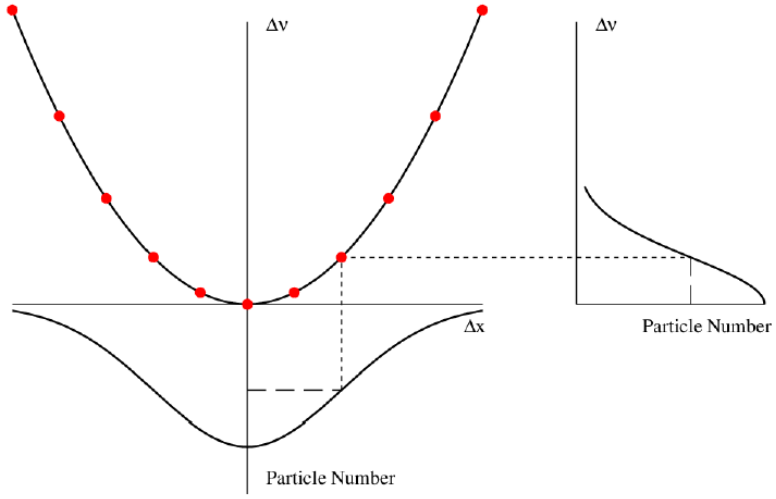


Figure 5.11: *Association of a spin tune spread value to a selected beam Gaussian width, in order to exctract an estimation for the spin coherence time [37].*

That shift represents the spin tune change for one turn. After many turns ($N$), the phase difference between the particles spin vectors precessing in the horizontal plane will be $N$ times the difference after one turn. A simulation, whose details are reported in Sec. 6.2, carried out by Ed Stephenson with a simple no-lattice model [38], shows that, when the polarization drops to 0.606, the angle indicating the phase spread of the spin vectors in the horizontal plane has increased to a value of 1.254 *rad*. A reasonable estimate of the spin coherence time would then be to use the number of turns needed for the phase difference of the spin vectors to reach 1.254 *rad*. Thus the spin coherence time becomes:

$$\tau_{SC} = \frac{1.254}{2\pi|\Delta\nu|f_{cyc}} \tag{5.23}$$

where $f_{cyc} = 750602.5\ Hz$ is the COSY cyclotron frequency, and $\Delta\nu$ is the spin tune spread calculated for different beam conditions in the previous section.

### 5.3.1 Horizontal betatron oscillations

Fig. (5.12) shows the spin coherence time dependence on the horizontal beam profile $\Delta x$ when the RF cavity is switched on. Each spin tune value has been averaged over $N = 199363$ turns, being $N$ close to the number of revolutions in the ring needed by the particles to complete 73 synchrotron oscillations. The function that fits the spin coherence time values

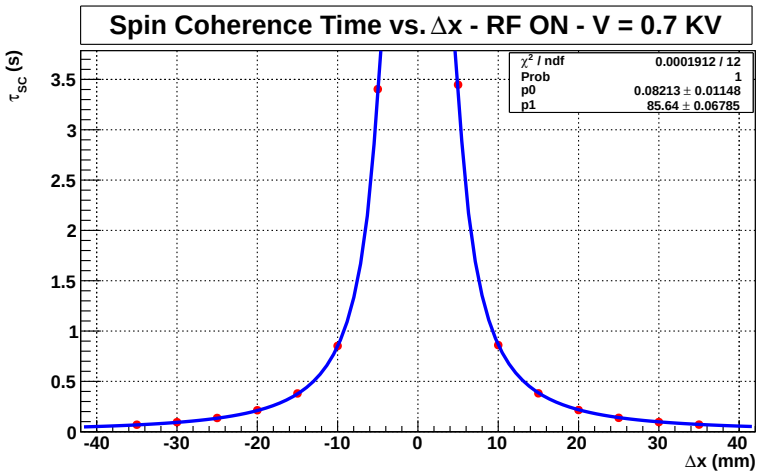


Figure 5.12: *Spin coherence time's dependence on the horizontal beam profile $\Delta x$ with respect to the reference orbit when the RF cavity is switched on. Each one of the red dots represents the spin coherence time corresponding to a spin tune shift calculated as in Eq. (5.10). The spin tune values for each particle with an assigned offset are averaged over the number of turns $N = 199363$. The blue curve corresponds to a fitting function that indicates a $1/(\Delta x)^2$ dependence of the spin coherence time.*

is the one defined in Eq. (5.23).

### Comparison with experimental results

In order to calculate an estimation of the spin coherence time for a certain value of $\Delta x$, data from the May 2012 run across a wide range of horizontal widths are available. As an example we pick a value of $\Delta x_{exp} = 5\ mm$, that is in the middle of the data set. For such width the measured spin coherence time is $\tau_{SC} = 11.4\ s$ [38]. To compare this number to the estimation coming from the simulations, it is necessary to consider that the $\Delta x$ used in COSY INFINITY is evaluated in a different position in the ring with respect to the one measured by the Beam Profile Monitor (BPM), thus in the middle of the target telescope in one of the straight sections, corresponding to the starting point of the tracking. Therefore we need to scale $\Delta x$ by making use of the relationship between emittance and the position, that is $\varepsilon\beta_x = (\Delta x)^2$. As the emittance does not vary over the ring, we have:

$$\Delta x_{code} = \sqrt{\frac{\beta_{code}}{\beta_{exp}}}\Delta x_{exp} \tag{5.24}$$

Using the beta functions values $\beta_{code} = 6.582\ m$ and $\beta_{exp} = 22.12\ m$, the COSY INFINITY width corresponding to 5 *mm* is $\Delta x_{code} = 2.727\ mm$. This yields, after substituting the right values in Eq. (5.23), an estimate for the spin coherence time of $\tau_{SC} = 11.5\ s$. The agreement between the measured and estimated spin coherence time for this example is excellent, but at the present stage of investigation might be accidental. It is important anyway that the order of magnitude is correct. In fact, there are still elements that are missing in the COSY INFINITY lattice, for example the electron cooler. Specified this, the important result to be pointed out is the possibility of calculating the spin coherence time of a particles beam by using the COSY INFINITY spin tracking tools and, furthermore, the order of magnitude of this characteristic time is comparable to the one measured in the experiments at the COSY ring.

### 5.3.2 Vertical betatron oscillations

The same described procedure for the $\Delta x$ case has been used in order to determine the spin coherence time dependence on the vertical beam profile $\Delta y$, shown in Fig. (5.13a), where we can see that it is of the same kind of the one described for the radial case, thus $\tau_{SC} \propto 1/(\Delta y)^2$. It is important to highlight that a vertical offset affects the polarization lifetime less than a horizontal one. In fact, comparing the quadratic fit parameters of Fig. (5.12) and Fig. (5.13a), that are respectively $p_2^x = 85.64$ and $p_2^y = 400.5$. Since $p_2^y > p_2^x$, we see that a vertical offset would cause a decrease in the spin coherence time that is smaller than the one caused by the same offset in the radial direction. This yields, for $\Delta x$ and $\Delta y$ equal to 5 *mm*, a spin coherence time respectively of 3.4 *s* and 16 *s*.

As already mentioned relatively to the spin tune spread calculation, because of acceptance problems in the COSY storage ring it was not possible to probe the polarization lifetime of a vertically wide beam. Therefore, no comparison can be made.

### 5.3.3 Synchrotron oscillations

In Fig. (5.13b) the spin coherence time dependence on the momentum offset is shown. For the reasons already explained in the previous section, this calculation has been performed up to the 3rd order of approximation and for a more limited ensemble of $\Delta p/p$ values than in the case with the RF cavity switched off. A second order polynomial fit to the data evi-

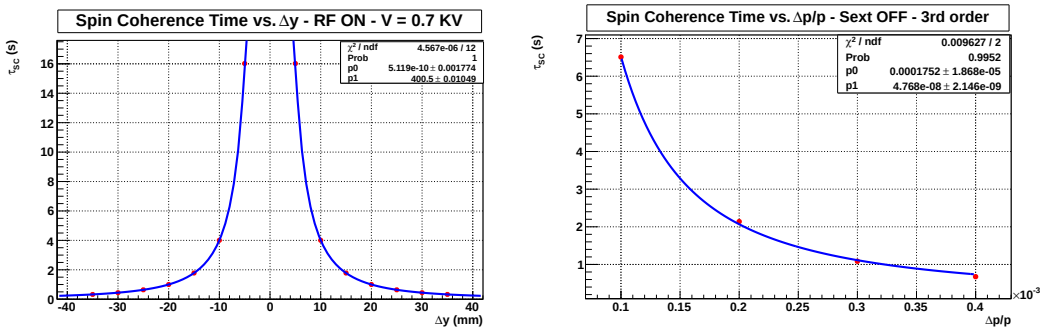


(a) (b)

Figure 5.13: *The left plot shows the spin coherence time dependence on the vertical offset $\Delta y$ with respect to the reference orbit when the RF cavity is switched on. Each one of the red dots represents the spin coherence time corresponding to a spin tune shift calculated as in Eq. (5.13). The blue curve corresponds to the fitting function that indicates a $1/(\Delta y)^2$ dependence of the spin coherence time. Fig. (b) shows the spin coherence offset on the momentum offset $\Delta p/p$. The spin tracking in this case has been performed up to the 3rd order.*

dences the persistence of a linear dependence from $\Delta p/p$. The data collected about the study of the effects of a momentum spread on the beam polarization lifetime are presently being analyzed; we need then to wait for these results in order to compare them to the simulations and check the exsistence of this linear dependence.

## 5.4 Use of sextupoles to enhance the SCT

The evidence that both position and momentum offsets affect dramatically the spin coherence time of the beam, and knowing that for a future EDM experiment we need at least $\tau_{SC} \sim 10^3$ *s*, we need to find a way to compensate these depolarizing effects. In this section it is described how this has been done for vertical and radial offsets by using sextupole magnets.

Sextupole magnetic fields, which vary as the square of the radius from the center (see Eq. 4.4), provides a position dependent focusing that can adjust the particle orbit and compensate for the emittance terms that originate a spread in the spin-tune. Referring to Eq. (5.21),

we can add the sextupole corrections as in the following way:

$$\frac{1}{\tau_{SC}} = A\langle(\Delta x)^2\rangle + B\langle(\Delta y)^2\rangle + (a_1 K_{2_{MXS}} + a_2 K_{2_{MXL}})\langle(\Delta x)^2\rangle + (b_1 K_{2_{MXS}} + b_2 K_{2_{MXL}})\langle(\Delta y)^2\rangle \tag{5.25}$$

where $K_{2_{MXS}}$ and $K_{2_{MXL}}$ are the sextupole strengths (see Eq. 2.21) for, respectively, the MXS and MXL sextupole families of the COSY ring. These magnets are installed respectively where the $\beta_x$ and $\beta_y$ are separately large, as shown in Fig. (5.14).

Within the COSY INFINITY code, the sextupole magnets are defined as described in

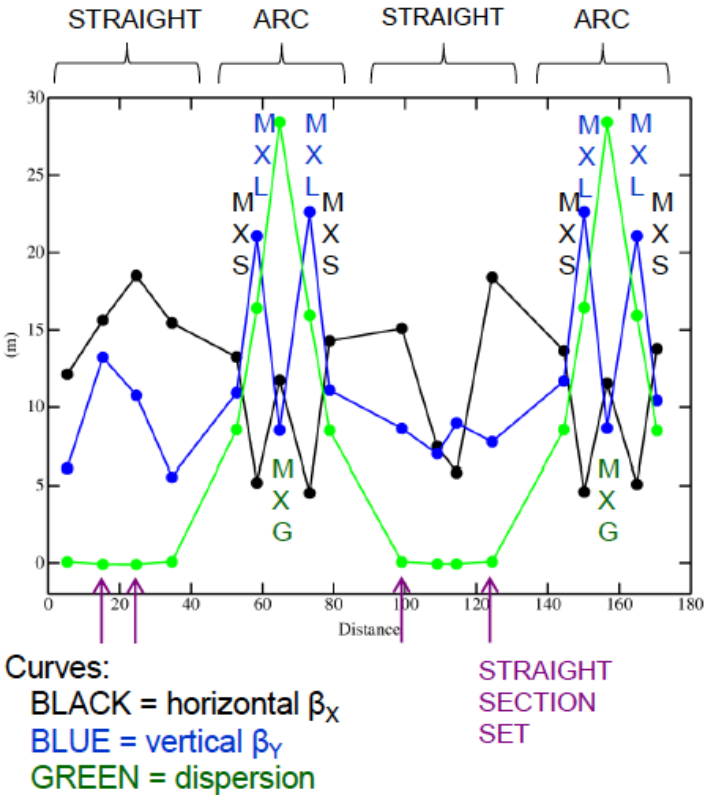


Figure 5.14: *Plot of the horizontal (black) and vertical (blue) beta functions, and of the dispersion function (green) around the ring. The position of the MXS and MXL sextupoles is shown: they are placed in the arc sections, respectively where the $\beta_x$ and $\beta_y$ are separately large [39].*

Sec. (4.3.1), and located in the same position as in the real lattice. In order to find the sextupole corrections that cancel the emittance effects on the spin coherence time, it is necessary

to set $1/\tau_{SC}$ to zero, then solve the system:

$$\begin{pmatrix} K_{2_{MXS}} \\ K_{2_{MXL}} \end{pmatrix} = - \begin{bmatrix} a_1 & b_1 \\ a_2 & b_2 \end{bmatrix}^{-1} \begin{pmatrix} A \\ B \end{pmatrix} \tag{5.26}$$

where $A$ and $B$ represent the known quadratic dependences of the spin tune spread on the radial and the vertical offset respectively. The coefficients $a_i$ and $b_i$, with $i = 1,\ 2$ represent the sextupole corrections and have to be determined in the simulations. Values of the spin coherence time have been calculated for different values of $K_{2_{MXS}}$ and $K_{2_{MXL}}$, separately varied, and for a certain value of the beam width $\Delta x$ or $\Delta y$. By setting the vertical offset to zero and operating exclusively with the MXS magnets, Eq. (5.25) becomes:

$$\frac{1}{\tau_{SC}} = (A + a_1 K_{2_{MXS}}) \langle (\Delta x)^2 \rangle \tag{5.27}$$

As an example, let us examine the case of a particle with a radial offset $\Delta x = 1\ mm$ and try to compensate the effect of this offset by varying the MXS family magnets strength. Fig. (5.15) represents the dependence of the spin coherence time on $K_{2_{MXS}}$. What we see

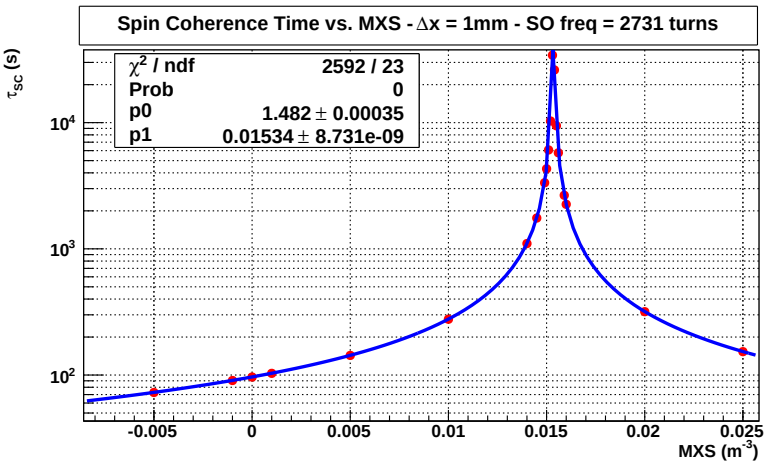


Figure 5.15: *Scan of the MXS sextupoles strength, showing how the polarization lifetime varies while the current circulating in the magnets is changing. The lifetime increases fast up to its maximum, that is reached at the strength of* $0.015344\ m^{-3}$*, and then decreases likewise. The blue curve fits the set of simulated spin coherence times.*

is a considerable increase of the polarization lifetime while the strength is varying, until a maximum value that is reached at $K_{2_{MXS}}^{max} = 0.015344\ m^{-3}$ where the spin coherence time reaches a value $\tau_{SC} \sim 2.12 \times 10^6\ s$. As a reference, the value of spin SCT for $K_{2_{MXS}} = 0\ m^{-3}$ is

around 86 $s$. The simulation supports the idea that the sextupoles could be effectively used to compensate for the spin-tune spread caused by the finite size of the beam and consequently increases the SCT. In particular for the presented study, the SCT has been increased by a factor $\simeq 2.5 \times 10^4$. The functional form, reproduced by the blue fitting curve in the plot, is defined as:

$$\tau_{SC} = \frac{p_0}{|K_{2_{MXS}} - p_1|} \tag{5.28}$$

where $p_1$ is the sextupole strength that maximizes the spin coherence time ($K^{max}_{2_{MXS}}$), and can be extracted from the fit. The other parameter $p_0$ is related to the curve's width. If the spin tune spread was exactly canceled, the spin coherence time would become infinity.

The simulations evidence how sensitive is the SCT from the changes in $K_2$; the strength values are then reported with six digits, considering that a shift of $10^{-6}$ $m^{-3}$ from the maximum means a change of one order of magnitude in $\tau_{SC}$, or, in some cases, even more.

**Comparison with experimental results**

Let us now compare the result obtained from the simulation to what has been observed during the beam time in May 2012. In Fig. (5.16) the comparison for the reciprocal of the spin coherence time is shown. The left side plot (5.16a) shows the same MXS scan shown in Fig. (5.15), this time with $1/\tau_{SC}$ on the ordinates axis, performed for $\Delta x = 1$ $mm$ (blue line) and $\Delta x = 3$ $mm$ (red line). The reciprocal of the spin coherence time becomes very close to zero in correspondance of $K^{max}_{2_{MXS}}$. It is important to highlight that the zero crossing point is the same for both the values of simulated beam width, suggesting that $K^{max}_{2_{MXS}}$ does not depend on the beam size. In order to determine whether this behavior is linear, the $1/\tau_{SC}$ values before or after such a zero crossing are reversed in sign. In Fig. (5.16a) this has been done for all the points above 0.015344 $m^{-3}$. The same linear behavior has been observed during the May 2012 run, as it is possible to see in Fig. (5.16b) where results for three different values of $\Delta x$ are shown. Also from the data emerges a common zero cross point for different values of $\Delta x$.

Despite of the correspondance in the linear dependence, there is a big difference in the scale of the MXS strength axis. In fact, the $K_{2_{MXS}}$ value that was experimentally found to maximize the spin coherence time is 5.4 $m^{-3}$, that is a factor $\sim 350$ bigger than the one determined from the simulations. This is a large difference, suggesting that something was missing in the COSY INFINITY lattice. The evidence triggered additional investigations.

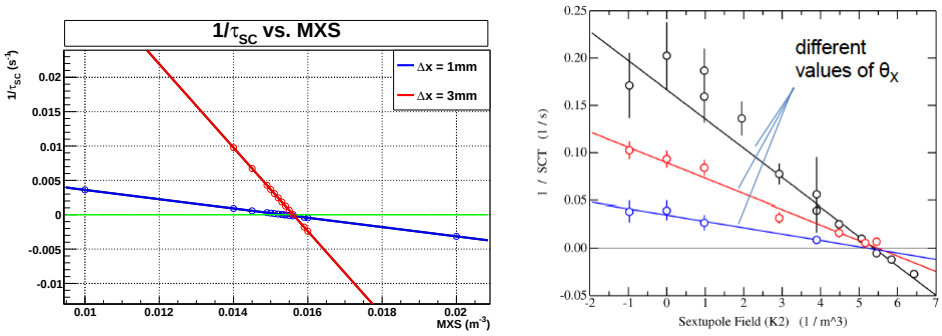


(a) (b)

Figure 5.16: *The left plot shows the reciprocal of the spin coherence time as function of the MXS sextupoles strength for* $\Delta x = 1$ *mm (blue line) and* $\Delta x = 3$ *mm (red line). In order to determine whether this behavior is linear, all the values above the zero crossing at* $0.015344\ m^{-3}$ *were reversed in sign. The two lines crosses zero in the same point, suggesting that* $K_{2_{MXS}}^{max}$ *does not depend on the beam size. In the right plot we can look at the same dependence, this time obtained from the data taken in May 2012 at COSY. The three lines correspond to three different beam profile widths. The behavior is again linear, but the common zero crossing is at* $5.4\ m^{-3}$*. The values above this point were reversed in sign to test the linearity.*

### 5.4.1 Implementation of the sextupole component of the dipoles

The real dipole magnets have a sextupole field component that was not taken into account for the performed simulations.The first attempt to reduce the $K_2$ scale factor between experiment and simulation involved the implementation of the dipole magnets sextupole component in COSY INFINITY. These multipole components are in fact responsible for the residual sextupole field present in the ring when all the sextupole magnets are switched off, and therefore they can affect the polarization lifetime exactly as the sextupole magnets do.

The result of the dipoles sextupole components measurement, carried out about twenty years ago at COSY, is reported in Fig. (5.17). The plot shows the sextupole components of the 24 dipoles of the COSY ring as function of the currents circulating in the coils. The large spread at the lowest current is due to errors in the magnetic fields measurements and the geometrical differences between the magnets. The dashed line represents a linear fitting

function, defined as:

$$y = \left(-1.18 \times 10^{-5} \, \frac{m^{-3}}{A}\right) x + 1.13 \times 10^{-3} \, m^{-3} \tag{5.29}$$

The current circulating in the dipoles during the May 2012 run is $1040\,A$, so we can calculate the sextupole strength, that is $K_2^{dip} = -0.011149\,m^{-3}$.

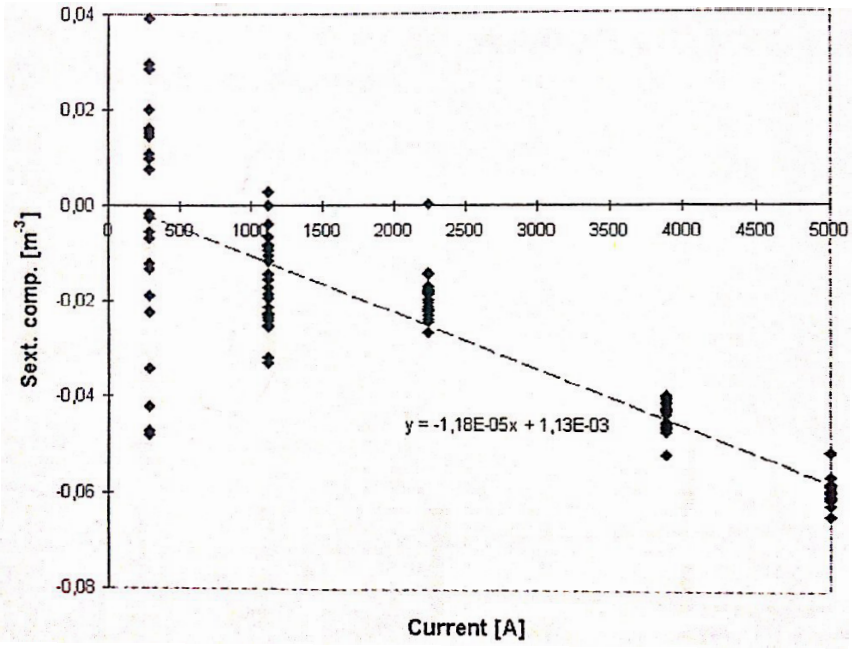


Figure 5.17: *Sextupole component of the 24 dipoles of the COSY ring as function of current.*

In order to take this multipole component into account in the simulations, the choice was to modify the dipole magnets field by using the thin lense approximation, that allows us to attach to both sides of each dipole a sextupole magnet and then consider the resultant field as the superposition of the dipole and the sextupole components. Each added sextupole has a length of $l_{sext} = 5\ cm$, and a strength equal to $K_2^{dip}/2$, scaled by the ratio between the length of the dipole and the length of the sextupole itself $l_{dip}/l_{sext}$. This scale factor is needed because the tranfer matrix element associated to the sextupoles is proportional to $K_2^{dip} l_{sext}$. We are actually defining a field component of a dipole, meaning that this component has to be considered over the total length of the dipole instead of only over $5cm$. Therefore the ratio $l_{dip}/l_{sext}$ transforms the matrix element into $K_2 l_{sext} l_{dip}/l_{sext} = K_2 l_{dip}$, and the contribution of the sextupole component is properly evaluated.

**Horizontal case** After the implementation of the sextupole component of the dipoles, a

new MXS scan was performed for the case $\Delta x = 1\ mm$; the results are shown in Fig. (5.18). The dependence of the spin coherence time on the MXS sextupoles strength is still described by Eq. (5.28); what has substantially changed is the sextupole strength scale. In fact now the lifetime reaches its maximum at 0.755958 $m^{-3}$, improving by a factor $\simeq 50$ the agreement with the measured value. This large increase in the sextupoles strength scale indicates

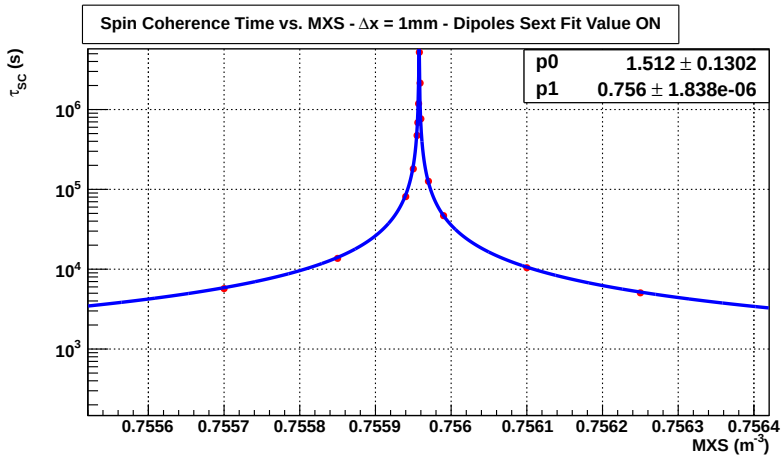


Figure 5.18: *Spin coherence time dependence on the MXS sextupoles strength when the dipoles sextupole component is taken into account. The lifetime maximum is reached at the strength of* 0.755958 $m^{-3}$*, and its value is* $\sim 4 \times 10^6$ *s. The blue curve fits the set of simulated spin coherence times.*

that it has been reasonable to consider sources of sextupole field other than the sextupole magnets themselves. Anyway, the new value is still a factor $\sim 7$ off the 5.4 $m^{-}3$ found experimentally, fact that tells us that there might still be sextupole components in the ring that are not accounted for. For instance, it is already known that the electron cooler, constituted by solenoid and toroid magnets, contributes to the residual sextupole component of the COSY ring. Since there is no element in the COSY INFINITY code that describes an electron cooler, it is not possible to include this further contribution in the simulations. At the moment it is not clear if this contribution would compensate the remaining factor $\sim 7$; for this reason it is necessary to understand which other effects could possibly change the sextupole field of the ring.

**Vertical case** As shown in Sec. (5.2), also a vertical position offset with respect to the reference orbit is responsible for the generation of a spin tune spread that reduces the beam

polarization lifetime. For this reason, a compensation of the $\Delta y$ offset effect is needed. The sextupoles of the MXL family are located where the function $\beta_y$ is large, and they are then the right choice for the vertical dimension. As the final aim is the cancellation of both the radial and the vertical offset effects, this requires the consideration of the cross terms, thus radial compensation changing MXL and vertical compensation changing MXS. A study has been performed to determine whether the MXS and MXL compensating effects add linearly, following the relation:

$$K_{2_{MXL}} = C_1 + C_2 K_{2_{MXS}} \tag{5.30}$$

Both the cases $\Delta x = 1$ *mm* and $\Delta y = 1$ *mm* were separately considered. In Tab. (5.1) the

| $\Delta x = 1$ *mm* | | $\Delta y = 1$ *mm* | |
|---|---|---|---|
| $K_{2_{MXS}}(m^{-3})$ | $K_{2_{MXL}}(m^{-3})$ | $K_{2_{MXS}}(m^{-3})$ | $K_{2_{MXL}}(m^{-3})$ |
| 0 | 1.3176 | -0.5 | 0.5221 |
| 0.2 | 0.9688 | 0 | 0.3288 |
| 0.4 | 0.6202 | 0.4 | 0.1742 |
| 0.7559 | 0 | 0.8505 | 0 |

Table 5.1: *MXS and MXL strength pairs that separately cancel the spin tune spread generated by a radial and a vertical position offset.*

pairs of MXS and MXL strengths that separately cancel the effect of a 1 *mm* radial and vertical offset are reported. In Fig. (5.19) the relative plot is shown. The points in the graphic represent the pairs $(K_{2_{MXS}}, K_{2_{MXL}})$ that maximize the spin coherence time in the two cases studied. The green line fits the values relative to the radial offset, while the blue line fits the ones relative to the vertical offset. Both curves are well described by the relation of Eq. (5.30), confirming that the two compensation effects of the MXS and MXL families add linearly, and also that it would be possible to simultaneously cancel the spin tune spread caused by the radial and vertical beam widths. The two lines cross each other indeed, and the pair of sextupole strengths that should provide the cancellation is:

$$\begin{cases} K_{2_{MXS}} = 0.7303\ m^{-3} \\ K_{2_{MXL}} = 0.0446\ m^{-3} \end{cases} \tag{5.31}$$

Unluckily is not possible to compare this result with an experimental one because, as already pointed out, due to acceptance problems it is not possible at COSY to study the vertical offset effect on the polarization lifetime. The simulations result is anyway very

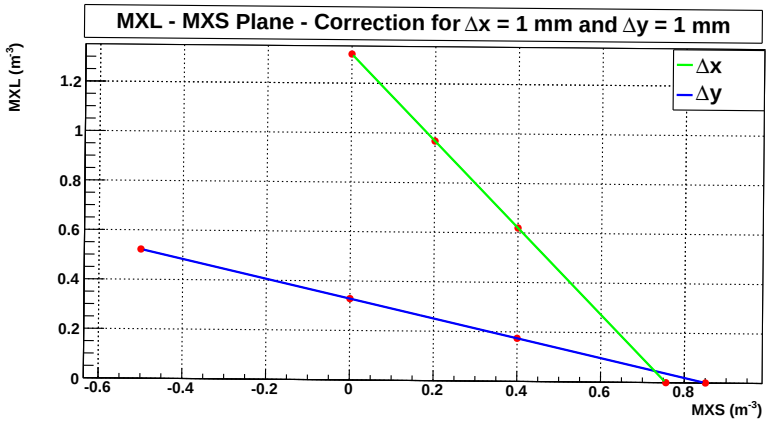


Figure 5.19: *The plot shows two sets of MXS and MXL strengths that cancel the spin tune spread caused separately by a radial (green line) and a vertical (blue line)* 1 *mm offset. The two lines cross each other, suggesting that it is possible to cancel both effects at the same time.*

promising, and confirms that the COSY INFINITY code is potentially a very powerful tool for spin dynamics studies in a storage ring.

# Chapter 6

# Measurements at the COSY ring

The purpose of this thesis is to benchmark beam and spin dynamics calculations in the COSY INFINITY code. The EDM feasibility experiments that have been taking place at the COSY ring, presented a unique opportunity to test the code on field.

The feasibility of the deuteron EDM experiment depends on the minimization of the spin tune spread, that is responsible for the vanishing of the beam horizontal polarization with time. In order to understand the mechanisms which cause it, a series of polarization studies were performed at COSY. These studies can be performed using either a *coasting* beam or a *bunched* beam.

In the case of a coasting beam, this is injected in the storage ring and it occupies the entire circumference. The main contribution to the spin tune spread comes from $\Delta p/p$ which, in the case of an uncooled beam, kills the spin coherence time in $\sim 10^{-3}$ $s$ ($\sim (f_{cyc}\Delta p/p)^{-1}$).

In the case of a bunched beam, an RF cavity confines the particles inside a bucket, as explained in Chap. 2. Particles with a different velocity from the reference particle will undergo synchrotron oscillations inside the bunch such that the first order contribution of $\Delta p/p$ averages to zero. Only a second order effect due to betatron oscillations is left.

This chapter presents how a vertically polarized beam was prepared in order to perform a measurement of the horizontal polarization lifetime. It will be shown how the polarization was precessed from the vertical to the horizontal plane by exciting an RF solenoid spin resonance, and then how the spin coherence time was extracted from the measures of the horizontal polarization asymmetry. Finally, beam emittance effects on SCT will be discussed, including the possibility to correct them by making use of sextupole magnets.

## 6.1 Beam preparation

In order to obtain a horizontally polarized beam with variable profile widths, suitable for use in the exploration of bem emittance effects on the spin tune spread, the following procedure was adopted:

1. Injection in the COSY ring of a vertically polarized beam.
2. Set up beam ramp up to 0.97 $GeV/c$ and bunch on the first harmonic.
3. Set up cooling/heating cycles, with the electron cooling running for 30 $s$, followed by 10 $s$ in weach selective heating is available to enlarge vertical or horizontal width.
4. Slow extraction into a thick carbon target.
5. Set up a Froissart-Stora scan that stops with zero vertical polarization, resulting in a horizontally polarized beam whose polarization rapidly precesses in the ring plane.

| Machine parameter | Value |
|---|---|
| Horizontal tune, $Q_x$ | 3.60 |
| Vertical tune, $Q_y$ | 3.62 |
| Compaction factor, $\alpha_c$ | $0.177 \pm 0.003$ |
| Slip factor, $\eta$ | $-0.612 \pm 0.003$ |
| Cycotron frequency, $f_{cyc}$ | 750602.5(5) Hz |

| Beam parameter | Uncooled | Cooled |
|---|---|---|
| $\Delta p/p$ | $(8.02 \pm 0.23) \times 10^{-4}$ | $(4.91 \pm 0.13) \times 10^{-5}$ |
| Horizontal width, $\Delta x$ | 6.01 $mm$ | 1.43 $mm$ |
| Vertical width, $\Delta y$ | 6.51 $mm$ | 1.77 $mm$ |
| Horizontal emittance, $\varepsilon_x$ | 1.6 $\mu m$ | 0.09 $\mu m$ |
| Vertical emittance, $\varepsilon_y$ | 5.8 $\mu m$ | 0.42 $\mu m$ |

Table 6.1: *Machine and beam parameters [29].*

The tests at COSY made use of a bunched vertically polarized deuteron beam with a momentum $p = 0.97$ $GeV/c$. Only three polarization states were used: positive and negative vector polarization states with no tensor polarization, and an unpolarized state. The beam

was bunched on the first harmonic ($h = 1$) with a maximum oscillator voltage of 400 $V$. For the uncooled beam, this captures most of the beam into about half of the ring circumference, as shown by Fig. (6.1a), that represents the oscilloscope traces of the RF (top) and beam pickup (bottom) for the uncooled beam [29]. When electron cooling is applied at the beginning of beam storage, the momentum spread and the size of the beam are greatly reduced (see Fig. 6.1b). A number of machine parameters were measured for the various running

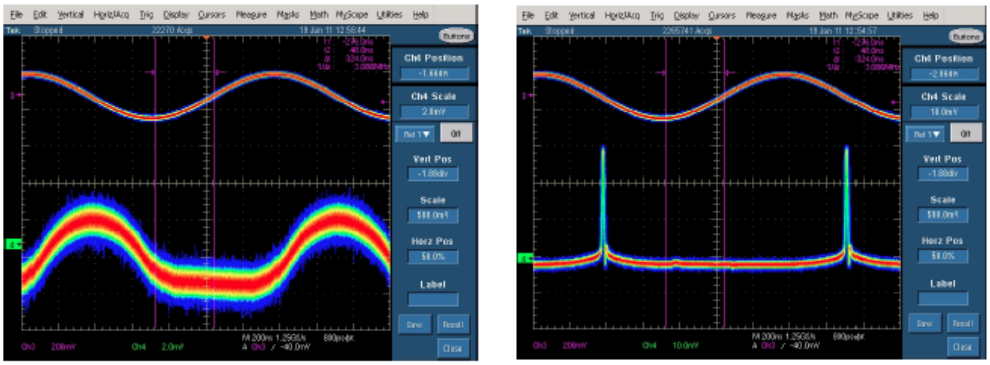

(a) (b)

Figure 6.1: *Oscilloscope traces of the RF (top) and beam pickup (bottom) for both the uncooled (see Fig. (a)) and the cooled (see Fig. (b)) beam. The time trace represents roughly* 1.5 *RF periods. In the uncooled case, the pickup sees no beam for about half of the machine cycle, while in the cooled case the beam is gathered into a narrow bunch and there is a long residual uncooled tale on the peak sides [29].*

conditions, and they are reported in in Tab. (6.1), where the slip factor $\eta$ is calculated from the measure of $\alpha_c$ using Eq. (2.28).

### 6.1.1 RF solenoid spin resonance

The vertical polarization was perturbed by a longitudinal radio-frequency (RF) magnetic field, provided by an RF solenoid, inducing an RF depolarizing resonance that can flip the spin direction of stored polarized particles. The resonance frequency is defined as:

$$f_{res} = f_{cyc}(k \pm G\gamma) \tag{6.1}$$

where $f_{cyc}$ is the cyclotron frequency and $k$ is an integer.

The studies began by exciting the $1 - G\gamma$ resonance, whose frequency was estimated by

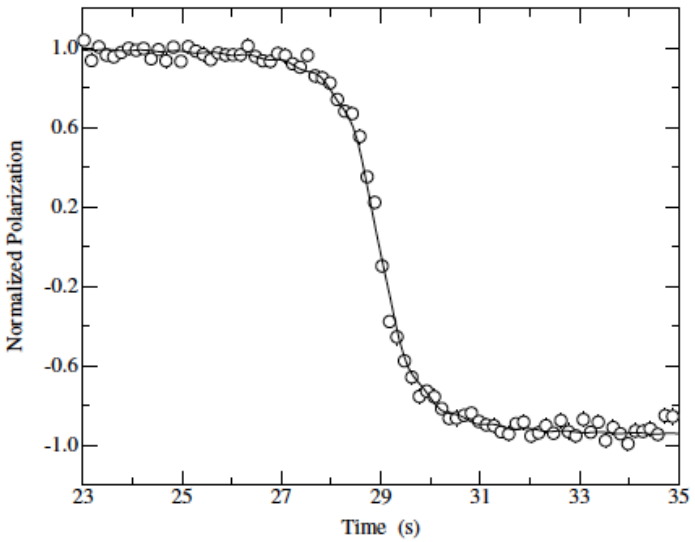


Figure 6.2: *Froissart-Stora scan for the uncooled beam. The zero crossing was used to make a first estimate of the spin resonance frequency. The curve is calculated assuming a resonance frequency of* 871434 $Hz$ *and a ramp rate of* 10 $Hz/s$ *starting from* 871200 $Hz$ *at* 5.8 $s$ *[29].*

making a Froissart-Stora frequency sweep [30] across the expected location of the resonance using the uncooled beam. The frequency at which the polarization changed sign was taken as the initial resonance location. Fig. (6.2) shows the data from this scan, which was started at 871200 $Hz$ (at a time of 5.8 $s$ and ramped at a speed of 10 $Hz$ for a total of 40 $s$. The zero crossing is clearly evident near 29 $s$, corresponding to 871434 $Hz$. The polarization does not completely reverse, an issue that is consequence of synchrotron oscillations effects on the spin resonance [29].

The cooled beam measurements on resonance are shown in Fig. (6.3). The data represent a slow oscillation of the vertical component of the polarization with a period of about $2/3$ $s$. It persists for the 55 $s$ that the RF solenoid was kept running after the initial ramp-up, which lasted 200 $ms$. This allows a very precise determination of the mgnetic field strength of the RF solenoid. The oscillation pattern requires an effective strength of $\varepsilon = (4.05 \pm 0.01) \times 10^6$ $rev/turn$.

Refinements to the position of the resonance were made using the RF solenoid operating

at a fixed frequency in the immediate neighborhood of the resonance. Being off resonance by even a fraction of 1 $Hz$ creates clear changes in the polarization oscillation pattern. The most

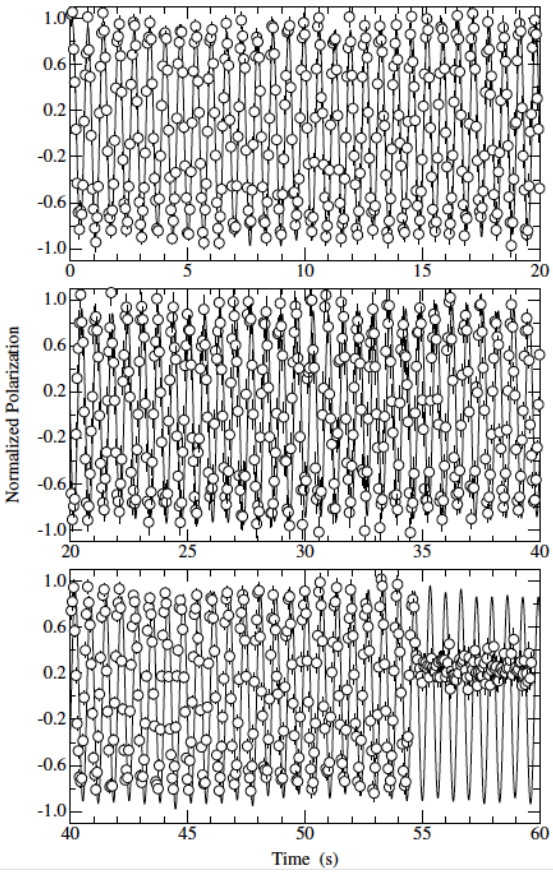


Figure 6.3: *Cooled beam measurements on resonance ($f_{res} = 871434\ Hz$), with a solenoid field strength of $\varepsilon = (4.05 \pm 0.01) \times 10^6\ rev/turn$. The vertical polarization oscillates for 55 s. The curve is a model calculation [29].*

accurate results were obtained in the cooled beam case, in which the beam has a very narrow profile and the synchrotron oscillation contribution is small. The resonance frequency value obtained with such a procedure is $871434.13 \pm 0.04\ Hz$.

The RF solenoid was run at this frequency in order to precess the vertical polarization of the beam towards the horizontal plane, at which point the solenoid strength is ramped to zero. Fig. (6.4) shows the left-right asymmetry in function of the measure time. While the RF solenoid is on, the vertical polarization oscillates. The solenoid was switched off when the vertical polarization reached zero, staying zero for the rest of the cycle, meaning that the

only left component of the beam polarization is now the horizontal one.

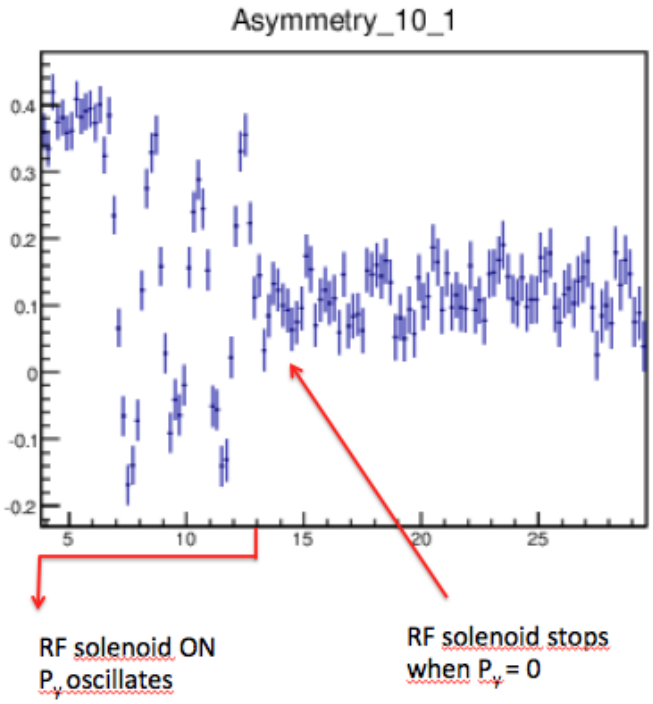


Figure 6.4: *Vertical polarization behaviour during the measure time. While the RF solenoid is on, the vertical polarization oscillates. The solenoid is then switched off when* $P_y = 0$*. The vertical polarization stays zero for the rest of the cycle, suggesting that the only left component is the horizontal one. [40]*

### 6.1.2 Machine cycles

Once we had a horizontally polarized beam in a "non-magic" machine (see Sec. 1.4), we had to deal with the precession motion of the particle spins in the ring plane, due to the particle anomalous magnetic momentum. This required the development of a method for measuring the rapidly rotating ($\sim 120\ kHz$) horizontal polarization as a function of time. The procedure applied, involving the use of a new data acquisition software, is described in Sec. 3.3.2.

In order to have good statistics on the time evolution of the horizontal polarization, many beam storage cycles are required. Each of these machine cycles begins with a vertically polarized beam. At a given moment, an RF solenoid is ramped on at the $1 - G\gamma$ harmonic of

the spin tune (see previous section). If the solenoid frequency is on resonance, then it will precess the vertical polarization toward the horizontal plane, at which point the solenoid strength is ramped to zero. This preparation, adjusted in advance to minimize the final vertical polarization, was initiated with a start signal that was also passed to the data acquisition as an event with a clock time. For each machine cycle, this was taken as the data acquisition start time. The RF solenoid process was assumed to be reproducible on each cycle.

The intention is to prepare a horizontally wide beam of variable width suitable for use

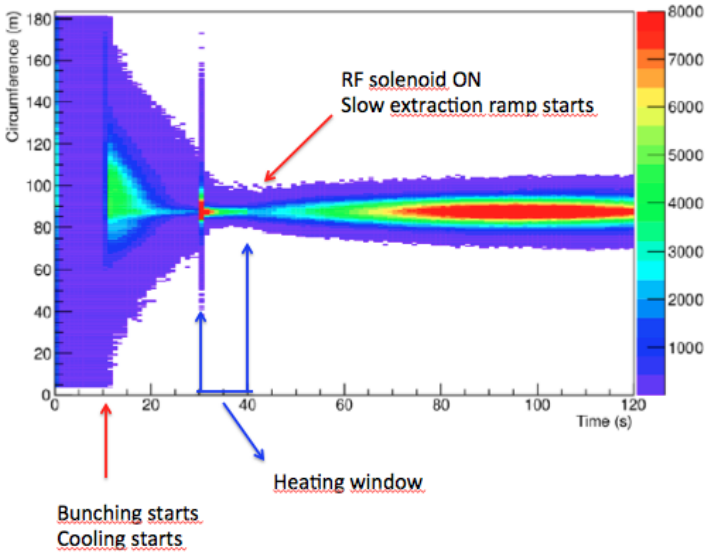


Figure 6.5: *The distribution of polarimeter events for one machine cycle shown as a function of the circumference of the ring and as a function of the time during the store [40].*

in the exploration of sextupole field effects on the spin tune spread. Fig. (6.5) shows the distribution of polarimeter events for one machine cycle as a function of the circumference of the ring and as a function of the time during the store.

In the early part of the machine cycle, after the initial few seconds used for injection, ramping and bunching, electron cooling ran for 30 *s* to minimize the momentum spread and transverse size of the beam. The next 10 *s* provided a time window in which selective heating with *white noise* applied to electric field plates could be used to enlarge the horizontal size of the beam depending on the power being applied. After heating, the signal for the data acquisition start was issued and the RF solenoid began the process of precessing the polarization into the ring plane.

In order to monitor the polarization during the beam storage time, the deuteron beam is

slowly and continuosly extracted onto the thick carbon target, consisting of a carbon tube 15 *mm* thick with a rectangular interior opening for the beam, that is placed in front of the EDDA scintillators. The extraction of the beam was made through a vertical steering bump that brought the beam close to the thick polarimeter target (see Sec. 3.2).

In the COSY arcs there are two sextupole families (groups of four magnets), MXS and MXL, which are located respectively where $\beta_x$ and $\beta_y$ functions are large. The original goal was indeed to study separately the emittance effects in both radial ($x$) and vertical ($y$) directions. Nevertheless, it was not possible during the run, due to an acceptance issue, to find a machine condition where the vertical emittance could be varied while keeping the beam bunched. Therefore, only the effects of the MXS family on a beam with large horizontal emittance were studied.

## 6.2 Spin Coherence Time extraction

In order to explore the effect of sextupole magnetic fields on the longevity of polarization in a storage ring such as COSY, it was necessary to have a way to define the spin coherence time and to provide a procedure through which it may be extracted from horizontal polarization measurements.

Horizontal polarization asymmetries, measured for small to large horizontal beam profiles, are shown in Fig. (6.6). As the profile becomes larger, the horizontal polarization lifetime shrinks because of the larger spin tune spread. The time dependent shapes visible in the three plots are neither Gaussian nor exponential, so a numerical template was needed in order to match the data and characterize the shape with a value of the spin coherence time.

The template assumes that spin decoherence is driven only by the lengthening of the particle path (see Sec. 2.1.4) associated with the finite $\varepsilon_x$ and $\varepsilon_y$ emittances of a bunched beam. At any point in the ring with known beta functions, the emittance may be characterized by the angles $\theta_x$ and $\theta_y$ that represent the maximum deviation from the direction of the reference orbit at the location of the rms deviation of the distribution. The change in spin tune depends on the combination $\theta_x^2 + \theta_y^2$ for each particle track. The values for $\theta_x$ and $\theta_y$ where chosen from two separate Gaussian distibutions, each characterized by a width, $\sigma_x$ and $\sigma_y$ respectively. Changing these widths one with respect to the other, changes the time-dependent shape of the template curve, which therefore may be described by a new parameter $\alpha = \sigma_y/\sigma_x$ [23]. As already mentioned, during the experiment it was possible to

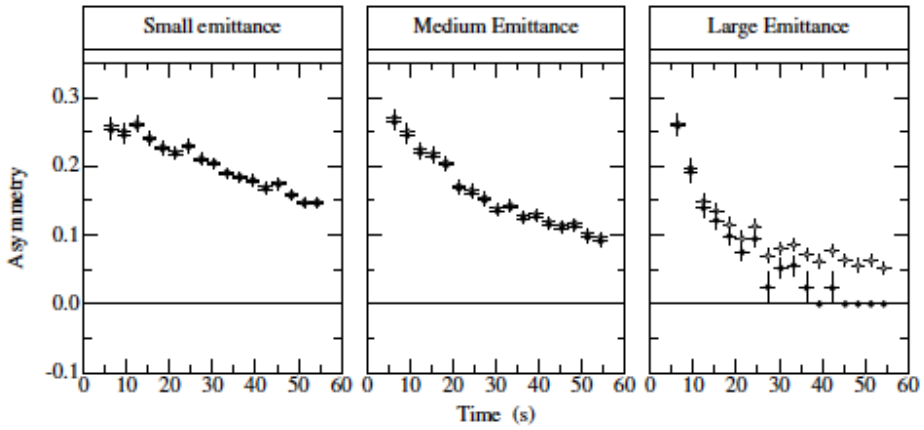


Figure 6.6: *The three plots show horizontal polarization asymmetries measured for small, medium and large horizontal beam profiles. As the profile becomes larger, the spin coherence time shrinks. [23].*

make $\sigma_x$, originally reduced through electron cooling, wider by applying white noise to a set of horizontal field electric plates. All tests were then made with horizontal ribbon beams whose shape represented cases with $\alpha < 1$.

A simple model of the process from our experiment begins with the assumption that, after the RF solenoid has precessed the polarization into the horizontal plane, all of the particle spins stay aligned with each other at the maximal polarization. Then, over time, they spread around a unit circle in the horizontal plane. The template shapes were built by taking $10^6$ spins and distributing them around this unit circle for a particular value of $\alpha$. Fig. (6.7) shows an example of such a distribution for 300 spin vectors and a single non-zero emittance ($\alpha = 0$). At $t = 0$ *s* all of the spins were at $(x, y) = (0, 1)$, thus the beam polarization was $p = 1$. As time increases, the points revolve around the unit circle in one direction (increasing spin tune) since the quadratic sum of the angles is always positive. The distribution was allowed to spread linearly with time. At each time point, the $x$ and $y$ components of the polarization were calculated and the total polarization determined by adding these components in quadrature. The resulting polarization time dependence for the $\alpha = 0$ case was matched by a template curve departing from one quadratically at small time, just like a Gaussian function. The spin coherence time was then chosen as the width corresponding to a polarization value of $p = 0.606$, the same value that corresponds to the amplitude of a Gaussian function whose argument is the function's width $\sigma$.

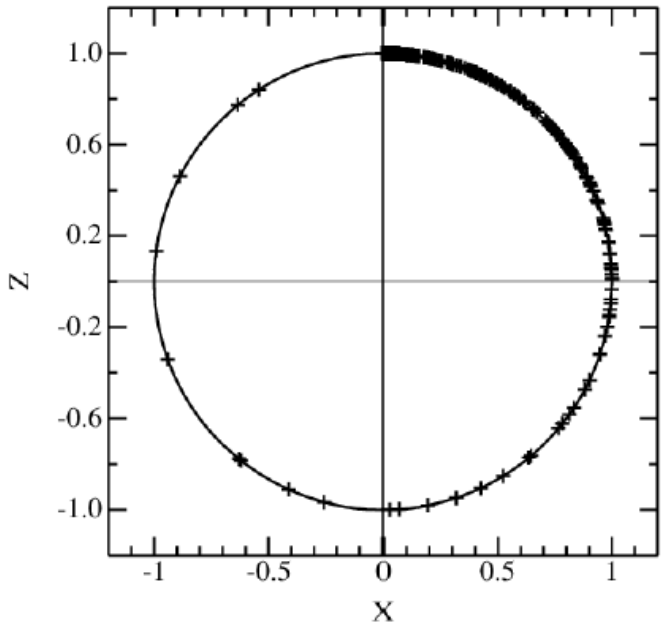


Figure 6.7: *Unit circle in the ring plane where the spins are distributed following the square of a Gaussian distribution. It represents the spin vectors positions in the plane.*

## 6.3 Emittance effects

The contributions to the spin tune spread from beam dynamics have been illustrated in Sec. 5.2. We saw how the change in path length goes as the square of the maximum angle of deviation from the reference trajectory. Therefore, the reciprocal of the spin coherence time should depend on the square of the width of the beam profile (see Eq. 5.21), as it is confirmed by Fig. (6.8). The plot shows a set of measurements where the effect on the spin coherence time of increasing horizontal emittance is evident. The vertical axis is the inverse of the horizontal polarization lifetime (or spin coherence time), that was extrapolated with the method described in the previous section. The horizontal axis is the average beam profile Gaussian width in *mm* at the location of the profile monitor. These data were taken with electron cooling off, following a period with cooling on in order to reduce the phase space size, and with another short period of heating to expand the beam profile horizontally. The blue circles are the data recorded without sextupole field corrections ($MXS = 0\%$, see Sec. 5.4 and next section), the red circles with $MXS = 5\%$, and the magenta circles with $MXS = -5\%$. The black line through the data is only a guide to the eye to suggest that a

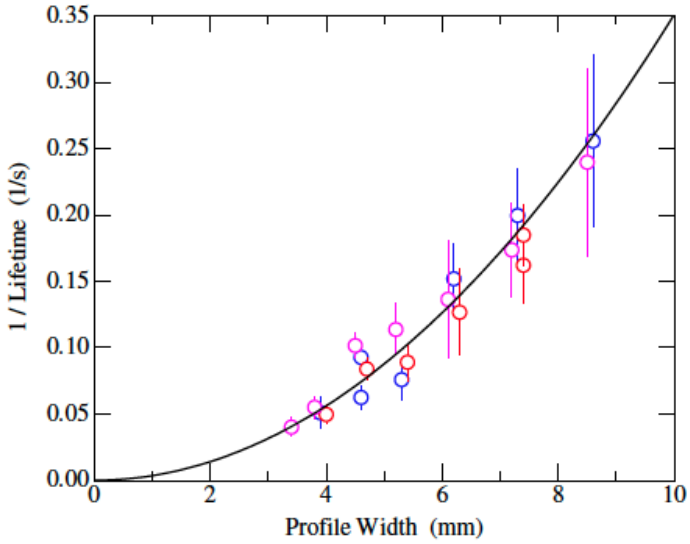


Figure 6.8: *The plot shows part of the data taken for several horizontal profile widths. These data were taken with electron cooling off, following a period with cooling on in order to reduce the phase space size, and with another short period of heating to expand the beam profile horizontally. The blue circles are the data recorded without sextupole field corrections ($MXS = 0\%$, see Sec. 5.4 and next section), the red circles with $MXS = 5\%$, and the magenta circles with $MXS = -5\%$. The black line through the data is only a guide to the eye to suggest that a quadratic dependence is reasonable. [23].*

quadratic dependence is reasonable.

Fig. (6.9) shows two examples of horizontal polarization measurements for a narrow (a) and a wide (b) beam, in the case of $MXS = 0\%$. It is clear that there is a large emittance effect on the spin coherence time, which is $50.0 \pm 2.5$ *s* in the first case and $5.5 \pm 0.6$ *s* in the second case.

## 6.4 Sextupole corrections

In Sec. 5.4 it has been explained how sextupole corrections were added starting from Eq. 5.21

During the beam time in May 2012, it was observed that changes in the MXS sextupole current were capable of lengthening the polarization lifetime. The results are shown

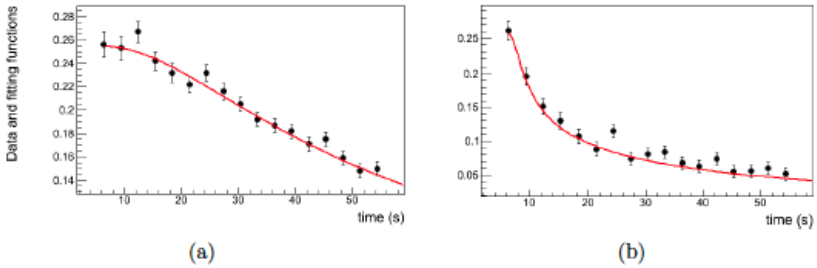


(a) (b)

Figure 6.9: *Comparison of the horizontal polarization as a function of time for a narrow beam (a) and for a wide beam (b) for MXS* $= 0\%$*. It is evident how emittance affects the spin coherence time. [23].*

in Fig. (6.10) that reports the plot of the reciprocal of the spin coherence time as a function of the strength (see Eq. 2.21) of the MXS sextupole magnets. We can observe how changing the value of the sextupole field has a dramatic effect on the horizontal polarization lifetime, that gets close to infinity as $1/SCT$ goes to zero. The linearity of the effect comes from the matching of the quadratic sextupole field as a correction to the quadratic path lengthening, which is a function of the size of the horizontal emittance.

Another test was made to measure the spin coherence time of a beam that was cooled during all the storage time, since it represents the case where the particle momentum distribution and the emittances are the smallest. In this case the beam was extracted onto the EDDA thick carbon target for only a short time at the beginning and end of the horizontal polarization window, as it is shown in Fig. (6.11). Under these conditions, the longest polarization lifetime measured was $316 \pm 40$ $s$, that is the time required for the polarization to fall to $1/e$ of its initial value. Without the polarization values in the gap, this lifetime cannot be converted into a spin coherence time using the previous definition.

Although this result is promising, since it approaches the goal value ($\tau_{SC} > 1000$ $s$) for dedicated EDM measurements, the adopted cooling tecnique, making use of the electron cooler, cannot be directly applied to the final experiment because the magnetic fields used in the electron cooling system would destroy the EDM signal. As a possible alternative, the use of stochastic cooling has been proposed, but its effects on the spin dynamics of a stored beam have to be investigated.

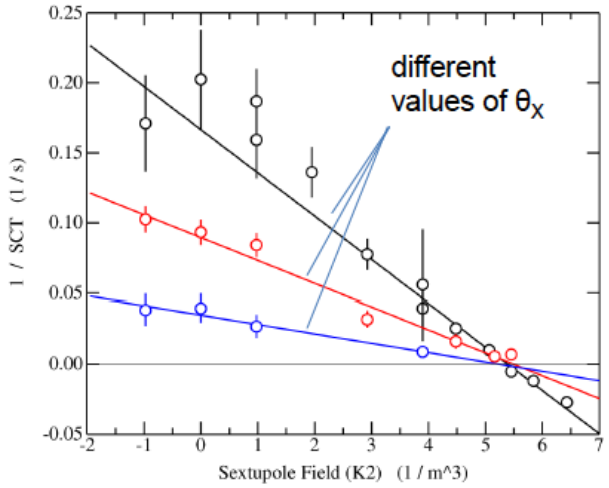


Figure 6.10: *Dependence of the reciprocal of the spin coherence time on the MXS sextupole strength. The three lines correspond to three different beam profile widths, starting from a narrow (bottom, blue) to a wide (top, black) profile. In order to determine wether this behavior is linear, all the points above the zero crossing at* $5.4\ m^{-3}$ *were reversed in sign. [23].*

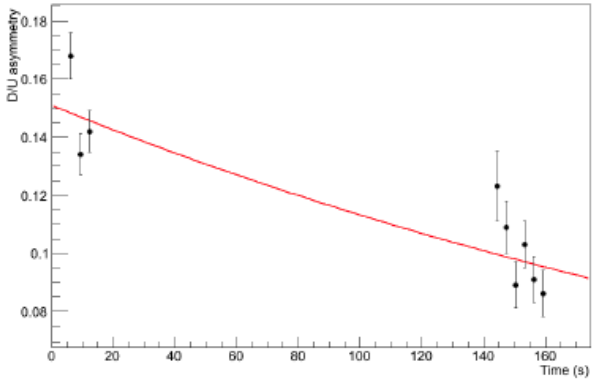


Figure 6.11: *Measurements of the spin coherence time for an electron cooled beam. Due to the lack of polarization values in the gap, the polarization lifetime is defined as the time required for the polarization to fall to* $1/e$ *of its initial value, and corresponds to* $316 \pm 40\ s$.

# Conclusions

This thesis is intended as a support to the feasibility studies for the search for an Electric Dipole Moment (EDM) of charged particles in a storage ring. The discover of a non-zero EDM at the sensitivity of present or planned experiments would clearly point to new sources of *CP* violation beyond the Standard Model. The basic idea proposed to measure the EDM of charged particles, is to inject in a storage ring a longitudinally polarized beam and keep it circulating while interacting with a radial electric field. The EDM signal would then be detected as a polarization precession starting from the horizontal plane and rotating towards the vertical direction. For such an experiment to succeed, a long horizontal polarization lifetime is required, since it defines the observation time available to measure the EDM signal. In the case of a deuteron EDM experiment, in order to reach a sensitivity of about $10^{-29}\ e \cdot cm$, a spin coherence time of at least 1000 $s$ is required, together with the capability of measuring microradians of vertical polarization rotation.

Such a high precision experiment requires a powerful tracking tool that allows to track both the position and the spin of the particles circulating in the storage ring. The code I used to perform the simulations presented in this thesis is COSY INFINITY, created by Prof. Martin Berz at the Michigan State University.

The purpose of this work is to benchmark the COSY INFINITY code against the feasibility studies for the deuteron EDM experiment that have been performed at the COoler SYnchrotron (COSY) storage ring, located at the Forschungszentrum-Jülich (Germany).

The simulations carried out with COSY INFINITY concern the investigation of the dependence of the spin coherence time from beam dynamics mechanisms occurring to a deuteron beam stored in the COSY ring.

The first part of the work regarded the evaluation of the betatron oscillations and the beam momentum spread contribution to the spin coherence time of a coasting beam. The change in the spin tune due to either a position or a momentum offset of a particle with

respect to the reference trajectory was calculated by selectively setting a certain value of $\Delta x$, $\Delta y$ and $\Delta p/p$. The spin-tune spread was determined and the associated spin coherence time was calculated. These simulations highlighted a quadratic dependence of the spin-tune on the horizontal and vertical beam profile widths, while a linear dependence from $\Delta p/p$ was found.

In order to compare the simulation results to the data emerging from the measurements, the case of a bunched beam was studied. An RF cavity was implemented in the code, and the spin coherence time was calculated for these new conditions. The quadratic dependence of the spin-tune on the profile widths was confirmed, but a significant reduction of the spin-tune spread was observed. This has to be related to the action of the RF cavity, which partially compensates for the particle path lengthening, due to the position difference with respect to the reference trajectory, by bunching the beam. In this case, the spin-tune depence on the momentum offset is not linear anymore, but quadratic, since the cavity cancels the first order contribution of $\Delta p/p$ to the spin-tune spread, leaving a residual quadratic effect.

The following step consisted of verifying the possibility of lengthening the polarization lifetime by correcting emittance effects using sextupole magnets, whose field varies as the square of the distance from the reference trajectory providing a position dependent focusing, and can compensate the decoherence effects due to betatron oscillations. Sextupoles were then implemented in the code and placed in the same position as in the real lattice. In order to take into account the residual sextupole field present in the COSY ring when all the sextupole magnets are switched off, the sextupole components of the dipole magnets were also implemented.

The vertical and horizontal beam emittance cases were treated separately. The sextupoles of the MXS family of the COSY ring, placed were $\beta_x$ is large, were used for the vertical case, while the sextupoles of the MXL family, placed were $\beta_y$ is large, were used for the horizontal one. For a particular value of sextupole strength, the reciprocal of the spin coherence time, which is proportional to the spin-tune spread, became zero, confirming the cancellation of the beam emittance effects on the horizontal polarization lifetime. This is a fundamental result because it confirms the hypothesis of lengthening the spin coherence time by making use of sextupole magnets. The zero crossing point was found to be independent of the chosen value of beam width, qualitatively reproducing the behavior of the experimental data. The MXS sextupole strength corresponding to the maximum spin coherence time is a factor $\sim 7$ off the measured value, suggesting the presence in the ring of further sextupole components that were not accounted for. Due to acceptance issues, it was

not possible to obtain a vertically wide beam in COSY, making it impossible to compare the simulation results to the experimental ones.

The COSY INFINITY calculations demonstrated that the MXS and MXL compensating contributions add linearly and, furthermore, that it is possible to simultaneously cancel the effects of vertical and horizontal emittance on the horizontal polarization lifetime.

The comparison of the simulations to the measurements represented a unique possibility of testing the COSY INFINITY code with actual data. The presented results demonstrate that COSY INFINITY correctly computes the beam and spin dynamics of a charged particles beam in a storage ring. The dependence of the spin coherence time on betatron and synchrotron oscillations is qualitatively reproduced, as well as its dependence on the strength of the sextupole magnets implemented in the simulated lattice. Further investigations are needed in order to be able to reproduce the experimental results also quantitatively. A first step towards this achievement could be the implementation in the code of the electron cooler, whose components could contribute to the sextupole field present in the COSY ring. Future plans also forsee the study of the second order contribution of the beam momentum spread to the spin coherence time, which is not compensated by the RF cavity effect.

# Appendices

# Appendix A

# The COSY INFINITY lattice

In this appendix we report the COSY storage ring lattice, written in the COSYScript language, that have been used to obtain the results presented in Chap. 5.

## A.1 Code

```
INCLUDE 'COSY' ;

PROCEDURE RUN ;

   {Variables declaration}

  VARIABLE sext 1 ;
  VARIABLE ORDER 1 ; VARIABLE TY 1 ; VARIABLE TITLE 80 ; VARIABLE NR 1 ;
  VARIABLE ER 1 ; VARIABLE ES 1 ; VARIABLE I 1 ; VARIABLE ANG 1 ;
  VARIABLE TRACE 1 3 ; VARIABLE LTUNE 1 3 ; VARIABLE PHASESPACE 1 ;

  VARIABLE q1 1 ; VARIABLE q2 1 ; VARIABLE q3 1 ;
  VARIABLE APER_QUAD 1 ; VARIABLE APER_SEXT 1 ; VARIABLE APER_BEND 1 ;
  VARIABLE IDEMO 1 ; VARIABLE IWAIT 1 ; VARIABLE ONESEC 1 ;
  VARIABLE IGR 1 ; VARIABLE IPIC1 1 ; VARIABLE IPIC2 1 ;
```

```
{ GUI variables }
VARIABLE DONE 1; VARIABLE BUTTON 100;
VARIABLE SYMP 1; VARIABLE SYMPTYPE 1;
VARIABLE DISTX 1; VARIABLE NRAYLOCAL 1; VARIABLE NTURN 1;
VARIABLE NREP 1 ; VARIABLE Nfree 1 ; VARIABLE Nsweep 1 ;
VARIABLE DISTY 1; VARIABLE DISTE 1;
VARIABLE TXA 1; VARIABLE UNIT 1; VARIABLE PSFILE 1;
VARIABLE NSPIN 1; VARIABLE TSX 1; VARIABLE PROT 1; VARIABLE DOOPTIK 1;
VARIABLE TSXN 1; VARIABLE TSYN 1; VARIABLE TSZN 1;
VARIABLE TYB 1; VARIABLE TTD 1 ;
VARIABLE TSXY 1; VARIABLE TSXZ 1; VARIABLE TSYZ 1;
VARIABLE TXN 1; VARIABLE TYN 1; VARIABLE TEN 1;
VARIABLE ONLYX 1; VARIABLE ONLYY 1; VARIABLE ONLYE 1;
VARIABLE FGQU1 1; VARIABLE FGQU2 1; VARIABLE FGQU3 1; VARIABLE FGQU4 1;
VARIABLE FGQU5 1; VARIABLE FGQU5 1; VARIABLE FGQU6 1;
VARIABLE FGQT1 1; VARIABLE FGQT2 1; VARIABLE FGQT3 1; VARIABLE FGQT4 1;
VARIABLE FGQT5 1; VARIABLE FGQT6 1; VARIABLE FGQT7 1; VARIABLE FGQT8 1;
VARIABLE MXG 1; VARIABLE MXS 1; VARIABLE MXL 1;
VARIABLE MXL01 1; VARIABLE MXL02 1; VARIABLE MXL03 1; VARIABLE MXL04 1;
VARIABLE MXL10 1; VARIABLE MXL11 1; VARIABLE MXL12 1; VARIABLE MXL13 1;

VARIABLE DmassAmu 1; { deuteron mass in atomic units }
VARIABLE MD 1; { mass of the deuteron }
VARIABLE T0 1; { central kinetic energy }
VARIABLE P0 1; { central momentum }
VARIABLE Alpha 10 ; {Momentum Compaction Factor}
VARIABLE Epconv 1 ; {Conversion factor between dK/K and Dp/p}
VARIABLE a 1; { deuteron anomalous magnetic moment }
VARIABLE V1 1 2 2; {parameters for RF cavity potential shape}
VARIABLE Voltage 1 ;
VARIABLE fRF 1; {RF frequency in Hz}
VARIABLE phiRF 1; {RF phase in degrees}
VARIABLE HARM 1; {Harmonic number}
VARIABLE mu 1000 3; { variable for tunes }
```

```
VARIABLE mu2 1000 3; { variable for tunes }
variable spinvect 1000 3 ;
variable spinvect2 1000 3 ;
variable spintune 1000 ;
variable spintune2 1000 ;

VARIABLE CALIBT 1;
VARIABLE CALIBU 1;

VARIABLE BRHO 1 ; { magnetic rigidty }
VARIABLE RHO  1 ; { bending radius of the dipole }
VARIABLE AD   1 ; { aperture of the dipole }
VARIABLE LDP  1 ; {length of the dipole LDP = RHO*[(15*2pi)/360]}

VARIABLE LBS  1 ; {length of a sext attached to a dipole}
VARIABLE BES01 1; VARIABLE BES02 1; VARIABLE BES03 1; VARIABLE BES04 1;
VARIABLE BES05 1; VARIABLE BES06 1; VARIABLE BES07 1; VARIABLE BES08 1;
VARIABLE BES09 1; VARIABLE BES10 1; VARIABLE BES11 1; VARIABLE BES12 1;
VARIABLE BES13 1; VARIABLE BES14 1; VARIABLE BES15 1; VARIABLE BES16 1;
VARIABLE BES17 1; VARIABLE BES18 1; VARIABLE BES19 1; VARIABLE BES20 1;
VARIABLE BES21 1; VARIABLE BES22 1; VARIABLE BES23 1; VARIABLE BES24 1;

VARIABLE LQU  1 ; { length of a bend section quad }
VARIABLE AQU  1 ; { aperture of a bend section quad }
VARIABLE GQU1 1 ; { quad gradient }
VARIABLE GQU2 1 ; { quad gradient }
VARIABLE GQU3 1 ; { quad gradient }
VARIABLE GQU4 1 ; { quad gradient }
VARIABLE GQU5 1 ; { quad gradient }
VARIABLE GQU6 1 ; { quad gradient }

VARIABLE LQT  1 ; { length of a straight section quad }
VARIABLE AQT  1 ; { aperture of a straight section quad }
VARIABLE GQT1 1 ; { quad gradient }
```

```
 VARIABLE GQT2 1 ; { quad gradient }
 VARIABLE GQT3 1 ; { quad gradient }
 VARIABLE GQT4 1 ; { quad gradient }
 VARIABLE GQT5 1 ; { quad gradient }
 VARIABLE GQT6 1 ; { quad gradient }
 VARIABLE GQT7 1 ; { quad gradient }
 VARIABLE GQT8 1 ; { quad gradient }

 VARIABLE ALIGNX 1 ; VARIABLE ALIGNY 1 ; VARIABLE ALIGNROT 1 ;
 VARIABLE BRFADJUST 1 ;
 VARIABLE RFRANGE 1 ;
 VARIABLE BRFSOL 1 ; VARIABLE FRFSOL 1 ;
 VARIABLE J 1 ; VARIABLE K 1 ; VARIABLE L 1 ;
 VARIABLE SAVEFILE 1 ;
 VARIABLE pxave 1 ; VARIABLE pyave 1 ; VARIABLE pzave 1 ;
 VARIABLE pxref 1 ; VARIABLE pyref 1 ; VARIABLE pzref 1 ;
 VARIABLE pscalar 1 ;

 [.....]

 {*****************************************************************}

PROCEDURE BCELL1 Q1 Q2 ALIGNX ALIGNY ALIGNROT;
   { one unit cell of the bend; three cells make a 180 deg. turn }
   { length of each cell = 17.33m                                }
   DL 1.439      ;
   RA ALIGNROT ;
   MQ LQU Q1*AQU AQU ;
   DL 0.389      ;
   MH LBS (BES01/2)*(LDP/LBS)*brho*AD^2 AD;
   DP RHO 15 AD  ;
   MH LBS (BES01/2)*(LDP/LBS)*brho*AD^2 AD;
   RA -1*ALIGNROT ;
   DL 0.389    ;
```

```
  MQ LQU Q2*AQU AQU ;
  DL 0.389      ;
  MH LBS (BES02/2)*(LDP/LBS)*brho*AD^2 AD;
  DP RHO 15 AD  ;
  MH LBS (BES02/2)*(LDP/LBS)*brho*AD^2 AD;    {
  DL 1.389       ;
  {  ------------------ symmetry point ---------------- }
  DL 1.389      ;
  MH LBS (BES03/2)*(LDP/LBS)*brho*AD^2 AD;
  DP RHO 15 AD  ;
  MH LBS (BES03/2)*(LDP/LBS)*brho*AD^2 AD;
  DL 0.389      ;
  MQ LQU Q2*AQU AQU ;
  DL 0.062      ;
  MH 0.14 MXS*brho*AQU^2 AQU ;
  DL 0.187      ;
  MH LBS (BES04/2)*(LDP/LBS)*brho*AD^2 AD;
  DP RHO 15 AD  ;
  MH LBS (BES04/2)*(LDP/LBS)*brho*AD^2 AD;
  DL 0.389      ;
  MQ LQU Q1*AQU AQU ;
  DL 1.439      ;
ENDPROCEDURE ;

{*****************************************************************}

PROCEDURE BCELL2 Q1 Q2 ALIGNX ALIGNY ALIGNROT;
  { one unit cell of the bend; three cells make a 180 deg. turn }
  { length of each cell = 17.33m                                }
  DL 1.127      ;
  MH 0.243 MXL*brho*AQU^2 AQU ;
  DL 0.069      ;
  RA ALIGNROT ;
  MQ LQU Q1*AQU AQU ;
```

```
  DL 0.389      ;
  MH LBS (BES05/2)*(LDP/LBS)*brho*AD^2 AD;
  DP RHO 15 AD  ;
  MH LBS (BES05/2)*(LDP/LBS)*brho*AD^2 AD;
  RA -1*ALIGNROT ;
  DL 0.389      ;
  MQ LQU Q2*AQU AQU ;
  DL 0.389      ;
  MH LBS (BES06/2)*(LDP/LBS)*brho*AD^2 AD;
  DP RHO 15 AD  ;
  MH LBS (BES06/2)*(LDP/LBS)*brho*AD^2 AD;
  DL 0.233      ;
  MH 0.328 MXG*brho*AQU^2 AQU ;
  DL 0.828      ;
  {  ------------------ symmetry point ---------------- }
  DL 1.389      ;
  MH LBS (BES07/2)*(LDP/LBS)*brho*AD^2 AD;
  DP RHO 15 AD  ;
  MH LBS (BES07/2)*(LDP/LBS)*brho*AD^2 AD;
  DL 0.389      ;
  MQ LQU Q2*AQU AQU ;
  DL 0.389      ;
  MH LBS (BES08/2)*(LDP/LBS)*brho*AD^2 AD;
  DP RHO 15 AD  ;
  MH LBS (BES08/2)*(LDP/LBS)*brho*AD^2 AD;
  DL 0.389      ;
  MQ LQU Q1*AQU AQU ;
  DL 0.069      ;
  MH 0.243 MXL*brho*AQU^2 AQU ;
  DL 1.127      ;
ENDPROCEDURE ;

{*****************************************************************}
```

```
PROCEDURE BCELL3 Q1 Q2 ALIGNX ALIGNY ALIGNROT;
  { one unit cell of the bend; three cells make a 180 deg. turn }
  { length of each cell = 17.33m                                }
  DL 1.439      ;
  RA ALIGNROT ;
  MQ LQU Q1*AQU AQU ;
  DL 0.389      ;
  MH LBS (BES09/2)*(LDP/LBS)*brho*AD^2 AD;
  DP RHO 15 AD  ;
  MH LBS (BES09/2)*(LDP/LBS)*brho*AD^2 AD;
  RA -1*ALIGNROT ;
  DL 0.187      ;
  MH 0.14 MXS*brho*AQU^2 AQU ;
  DL 0.062      ;
  MQ LQU Q2*AQU AQU ;
  DL 0.389      ;
  MH LBS (BES10/2)*(LDP/LBS)*brho*AD^2 AD;
  DP RHO 15 AD  ;
  MH LBS (BES10/2)*(LDP/LBS)*brho*AD^2 AD;
  DL 1.389       ;
  {  ------------------ symmetry point ---------------- }
  DL 1.389      ;
  MH LBS (BES11/2)*(LDP/LBS)*brho*AD^2 AD;
  DP RHO 15 AD  ;
  MH LBS (BES11/2)*(LDP/LBS)*brho*AD^2 AD;
  DL 0.389      ;
  MQ LQU Q2*AQU AQU ;
  DL 0.389      ;
  MH LBS (BES12/2)*(LDP/LBS)*brho*AD^2 AD;
  DP RHO 15 AD  ;
  MH LBS (BES12/2)*(LDP/LBS)*brho*AD^2 AD;
  DL 0.389      ;
  MQ LQU Q1*AQU AQU ;
  DL 1.439      ;
```

```
  ENDPROCEDURE ;

{*****************************************************************}

   PROCEDURE BCELL4 Q1 Q2 ALIGNX ALIGNY ALIGNROT;
    {Same element disposition of BCELL1, different dipole's sext components}
    { one unit cell of the bend; three cells make a 180 deg. turn }
    { length of each cell = 17.33m                                }
    DL 1.439      ;
    RA ALIGNROT ;
    MQ LQU Q1*AQU AQU ;
    DL 0.389      ;
    MH LBS (BES13/2)*(LDP/LBS)*brho*AD^2 AD;
    DP RHO 15 AD  ;
    MH LBS (BES13/2)*(LDP/LBS)*brho*AD^2 AD;
    RA -1*ALIGNROT ;
    DL 0.389       ;
    MQ LQU Q2*AQU AQU ;
    DL 0.389      ;
    MH LBS (BES14/2)*(LDP/LBS)*brho*AD^2 AD;
    DP RHO 15 AD  ;
    MH LBS (BES14/2)*(LDP/LBS)*brho*AD^2 AD;
    DL 1.389       ;
    {  ------------------ symmetry point ---------------- }
    DL 1.389      ;
    MH LBS (BES15/2)*(LDP/LBS)*brho*AD^2 AD;
    DP RHO 15 AD  ;
    MH LBS (BES15/2)*(LDP/LBS)*brho*AD^2 AD;
    DL 0.389      ;
    MQ LQU Q2*AQU AQU ;
    DL 0.062      ;
    MH 0.14 MXS*brho*AQU^2 AQU ;
    DL 0.187      ;
    MH LBS (BES16/2)*(LDP/LBS)*brho*AD^2 AD;
```

```
  DP RHO 15 AD  ;
  MH LBS (BES16/2)*(LDP/LBS)*brho*AD^2 AD;
  DL 0.389      ;
  MQ LQU Q1*AQU AQU ;
  DL 1.439      ;
ENDPROCEDURE ;

{*****************************************************************}

PROCEDURE BCELL5 Q1 Q2 ALIGNX ALIGNY ALIGNROT;
  {Same elements disposition of BCELL2, different dipole's sext components}
  { one unit cell of the bend; three cells make a 180 deg. turn }
  { length of each cell = 17.33m                                }
  DL 1.127      ;
  MH 0.243 MXL*brho*AQU^2 AQU ;
  DL 0.069      ;
  RA ALIGNROT ;
  MQ LQU Q1*AQU AQU ;
  DL 0.389      ;
  MH LBS (BES17/2)*(LDP/LBS)*brho*AD^2 AD;
  DP RHO 15 AD  ;
  MH LBS (BES17/2)*(LDP/LBS)*brho*AD^2 AD;
  RA -1*ALIGNROT ;
  DL 0.389      ;
  MQ LQU Q2*AQU AQU ;
  DL 0.389      ;
  MH LBS (BES18/2)*(LDP/LBS)*brho*AD^2 AD;
  DP RHO 15 AD  ;
  MH LBS (BES18/2)*(LDP/LBS)*brho*AD^2 AD;
  DL 0.233      ;
  MH 0.328 MXG*brho*AQU^2 AQU ;
  DL 0.828      ;
  {  ------------------ symmetry point ---------------- }
  DL 1.389      ;
```

```
  MH LBS (BES19/2)*(LDP/LBS)*brho*AD^2 AD;
  DP RHO 15 AD  ;
  MH LBS (BES19/2)*(LDP/LBS)*brho*AD^2 AD;
  DL 0.389      ;
  MQ LQU Q2*AQU AQU ;
  DL 0.389      ;
  MH LBS (BES20/2)*(LDP/LBS)*brho*AD^2 AD;
  DP RHO 15 AD  ;
  MH LBS (BES20/2)*(LDP/LBS)*brho*AD^2 AD;
  DL 0.389      ;
  MQ LQU Q1*AQU AQU ;
  DL 0.069      ;
  MH 0.243 MXL*brho*AQU^2 AQU ;
  DL 1.127      ;
ENDPROCEDURE ;

{*****************************************************************}

PROCEDURE BCELL6 Q1 Q2 ALIGNX ALIGNY ALIGNROT;
  {Same elements disposition of BCELL3, different dipole's sext components}
  { one unit cell of the bend; three cells make a 180 deg. turn }
  { length of each cell = 17.33m                                 }
  DL 1.439      ;
  RA ALIGNROT ;
  MQ LQU Q1*AQU AQU ;
  DL 0.389      ;
  MH LBS (BES21/2)*(LDP/LBS)*brho*AD^2 AD;
  DP RHO 15 AD  ;
  MH LBS (BES21/2)*(LDP/LBS)*brho*AD^2 AD;
  RA -1*ALIGNROT ;
  DL 0.187      ;
  MH 0.14 MXS*brho*AQU^2 AQU ;
  DL 0.062      ;
  MQ LQU Q2*AQU AQU ;
```

```
    DL 0.389      ;
    MH LBS (BES22/2)*(LDP/LBS)*brho*AD^2 AD;
    DP RHO 15 AD  ;
    MH LBS (BES22/2)*(LDP/LBS)*brho*AD^2 AD;
    DL 1.389       ;
    {  ------------------ symmetry point ---------------- }
    DL 1.389      ;
    MH LBS (BES23/2)*(LDP/LBS)*brho*AD^2 AD;
    DP RHO 15 AD  ;
    MH LBS (BES23/2)*(LDP/LBS)*brho*AD^2 AD;
    DL 0.389      ;
    MQ LQU Q2*AQU AQU ;
    DL 0.389      ;
    MH LBS (BES24/2)*(LDP/LBS)*brho*AD^2 AD;
    DP RHO 15 AD  ;
    MH LBS (BES24/2)*(LDP/LBS)*brho*AD^2 AD;
    DL 0.389      ;
    MQ LQU Q1*AQU AQU ;
    DL 1.439      ;
  ENDPROCEDURE ;

  {*********************************************************************}

PROCEDURE TRIPLET1 Qedge Qmid Sext;
    MQ LQT Qedge*AQT AQT ;
    DL 0.38          ;
    MQ LQT Qmid*AQT  AQT ;
    DL 0.24          ;
    MQ LQT Qmid*AQT  AQT ;
    DL 0.0685          ;
    MH 0.243 SEXT*brho*AQU^2 AQU ;
    DL 0.0685          ;
    MQ LQT Qedge*AQT AQT ;
  ENDPROCEDURE ;
```

```
{*****************************************************************}

PROCEDURE TRIPLET2 Qedge Qmid Sext;
  MQ LQT Qedge*AQT AQT ;
  DL 0.0685          ;
  MH 0.243 SEXT*brho*AQU^2 AQU ;
  DL 0.0685          ;
  MQ LQT Qmid*AQT  AQT ;
  DL 0.24          ;
  MQ LQT Qmid*AQT  AQT ;
  DL 0.38          ;
  MQ LQT Qedge*AQT AQT ;
ENDPROCEDURE ;

{*****************************************************************}

PROCEDURE HALFSTRAIGHT1A ;
  DL 4.546 ;
  TRIPLET1 GQT1 GQT2 MXL01;
  DL 6.457 ;
  TRIPLET1 GQT3 GQT4 MXL02;
  DL 1.41 ;
ENDPROCEDURE ;

{*****************************************************************}

PROCEDURE HALFSTRAIGHT1B ;
  DL 1.41 ;
  TRIPLET2 GQT3 GQT4 MXL03;
  DL 2;
{   PS 0.15; { EDDA }
}   DL 4.456 ;
  TRIPLET2 GQT1 GQT2 MXL04;
```

```
  DL 4.546 ;
ENDPROCEDURE ;

{*****************************************************************}

PROCEDURE HALFSTRAIGHT2A ;
  DL 2.547 ;
  TRIPLET1 GQT5 GQT6 MXL10 ;
  DL 2.488 ;
  { cavity }
  DL 3.968 ;
  TRIPLET1 GQT7 GQT8 MXL11 ;
  DL 2.112 ;
  DL 0.600 ; { toroid }
  DL 0.7 ;
ENDPROCEDURE ;

{*****************************************************************}
PROCEDURE HALFSTRAIGHT2B ;
  DL 0.7 ;
  DL 0.600 ; { toroid }
  DL 2.108 ;
  TRIPLET2 GQT7 GQT8 MXL12 ;
  DL 6.456 ;
  TRIPLET2 GQT5 GQT6 MXL13 ;
  DL 2.547 ;
ENDPROCEDURE ;

{*****************************************************************}

  PROCEDURE THERING ;

  { beginning of the ring, middle of target telescope }
  HALFSTRAIGHT1B ;
```

```
BCELL1 GQU1 GQU2 ALIGNX ALIGNY ALIGNROT ;
BCELL2 GQU3 GQU4 ALIGNX ALIGNY ALIGNROT;
BCELL3 GQU5 GQU6 ALIGNX ALIGNY ALIGNROT;

HALFSTRAIGHT2A ;
DL 1    ;
HALFSTRAIGHT2B ;
RF V1 0 fRF phiRF 1;

BCELL4 GQU5 GQU6 ALIGNX ALIGNY ALIGNROT;
BCELL5 GQU3 GQU4 ALIGNX ALIGNY ALIGNROT;
BCELL6 GQU1 GQU2 ALIGNX ALIGNY ALIGNROT;

HALFSTRAIGHT1A ;

DL 1    ;

{ end of the ring }
ENDPROCEDURE ;

[.....]
```

# Bibliography


[1] P. A. R. Ade and others (Planck Collaboration). Planck 2013 results. XVI. Cosmological parameters. *Astronomy & Astrophysics*, March 2013.

[2] C. L. Bennet et al. Nine-Year Wilkinson Microwave Anisotropy Probe (WMAP) Observations: Final Maps and Results. *arXiv:1212.5225v3 [astro-ph.CO]*, June 2013.

[3] A. G. Cohen, A. De Rújula, and S. L. Glashow. A Matter-Antimatter Universe? *The Astrophysical Journal*, 495:539–549, March 1998.

[4] A. D. Sakharov. Violation of CP invariance, C asymmetry, and baryon asymmetry of the universe. *Pis'ma Zh. Eksp. Teor. Fis.*, 5:32–35, 1967.

[5] J. H. Christenson, J. W. Cronin, V. L. Fitch, and R. Turlay. Evidence for the $2\pi$ decay of the $k_2^0$ meson. *Phys. Rev. Lett.*, 13:138–140, July 1964.

[6] B. Aubert and others (BABAR Collaboration). Study of CP-violating asymmetries in $b^0 \to \pi^+\pi^-, k^+\pi^-$ decays. *Physical Review D65*, 051502, 2002.

[7] E. M. Purcell and N. F. Ramsey. On the Possibility of Electric Dipole Moments for Elementary Particles and Nuclei. *Phys. Rev.*, 78:807–807, Jun 1950.

[8] J. H. Smith, E. M. Purcell, and N. F. Ramsey. Experimental Limit to the Electric Dipole Moment of the Neutron. *Physical Review*, 108:120–122, October 1957.

[9] P. Langacker. *The Standard Model and Beyond*. Series in High Energy Physics, Cosmology, and Gravitation. CRC Press, 2010.

[10] Jihn E. Kim and G. Carosi. Axions and the strong CP problem. *Rev. Mod. Phys.*, 82:557–601, Mar 2010.

[11] C. A. Baker et al. Improved Experimental Limit on the Electric Dipole Moment of the Neutron. *Phys. Rev. Lett.*, 97:131801, Sep 2006.

[12] D. Anastassopoulos et al. AGS Proposal: Search for a permanent electric dipole moment of the deuteron nucleus at the $10^{-29}$ $e \cdot cm$ level, April 2008. Available at http://www.bnl.gov/edm/.

[13] B. C. Regan et al. New Limit on the Electron Electric Dipole Moment. *Phys. Rev. Lett.*, 88:071805, Feb 2002.

[14] M. V. Romalis, W. C. Griffith, J. P. Jacobs, and E. N. Fortson. New Limit on the Permanent Electric Dipole Moment of $^{199}$Hg. *Phys. Rev. Lett.*, 86:2505–2508, Mar 2001.

[15] J. J. Hudson, B. E. Sauer, M. R. Tarbutt, and E. A. Hinds. Measurement of the Electron Electric Dipole Moment Using YbF Molecules. *Phys. Rev. Lett.*, 89:023003, Jun 2002.

[16] W. C. Griffith, M. D. Swallows, T. H. Loftus, M. V. Romalis, B. R. Heckel, and E. N. Fortson. Improved Limit on the Permanent Electric Dipole Moment of $^{199}$Hg. *Phys. Rev. Lett.*, 102:101601, Mar 2009.

[17] ACME Collaboration. Order of Magnitude Smaller Limit on the Electric Dipole Moment of the Electron. *ArXiv e-prints*, October 2013.

[18] B. Lee Roberts and W. Marciano. LEPTON DIPOLE MOMENTS, volume 20 of *Advanced Series on Directions in High Energy Physics - Vol. 20*. World Scientific, 2010.

[19] L. H. Thomas. The kinematics of an electron with an axis. *Philosophical Magazine*, 3:1–22, 1927.

[20] V. Bargmann, Louis Michel, and V. L. Telegdi. Precession of the Polarization of Particles Moving in a Homogeneous Electromagnetic Field. *Physical Review Letters*, 2:1–2, May 1959.

[21] The Storage Ring EDM Collaboration. A Proposal to Measure the Proton Electric Dipole Moment with $10^{-29}$ $e \cdot cm$ Sensitivity, March 2011.

[22] D. A. Edwards and M. J. Syphers. *An Introduction to the Physics of High Energy Accelerators*. Wiley Series in Beam Physics and Accelerator Technology. WILEY-VCH, 2004.

[23] G. Guidoboni. *Spin Coherence Time studies for a polarized deuteron beam at* COSY. PhD thesis, Università degli Studi di Ferrara, 2013.

[24] S. E. Darden. Polarized Spin-One Particles. *The American Journal of Physics*, 35, August 1967.

[25] D. Albers et al. A Precision Measurement of $pp$ Elastic Scattering Cross Sections at Intermediate Energies. *Eur. Phys. J. A*, 22:125 – 148, 2004.

[26] E. Stephenson. Run Plan Experiment 176.7: EDM Spin Coherence Time, August 2013. Introductive talk for the upcoming data taking time.

[27] Y. Satou et al. Three-body dN interaction in the analysis of the $^{12}C_{(\vec{d},d')}$ reaction at 270 $MeV$. *Physics Letters B*, 549(3–4):307 – 313, 2002.

[28] N. P. M. Brantjes et al. Correcting systematic errors in high-sensitivity deuteron polarization measurements. *Nuclear Instruments and Methods in Physics Research Section A: Accelerators, Spectrometers, Detectors and Associated Equipment*, 664(1):49 – 64, 2012.

[29] P. Benati et al. Synchrotron oscillation effects on an rf-solenoid spin resonance. *Physical Review Special Topics - Accelerators and Beams*, 15, 2012.

[30] M. Froissart and R. Stora. Depolarisation d'un faisceau de protons polarises dans un synchrotron. *Nuclear Instruments and Methods*, 7(3):297 – 305, 1960.

[31] M. Berz. *Modern Map Methods in Particle Beam Physics*. Academic Press, San Diego, 1999.

[32] M. Berz and K. Makino. COSY INFINITY 9.1 - Programmer's Manual. MSU Report MSUHEP 101214, Michigan State University, June 2011.

[33] M. Berz and K. Makino. COSY INFINITY 9.1 - Beam Physics Manual. MSU Report MSUHEP 060804, Michigan State University, June 2011.

[34] M. Berz. Computational aspects of optics design and simulation: COSY INFINITY. *Nuclear Instruments and Methods in Physics Research*, A298:473–479, 1990.

[35] H. Wiedemann. *Particle Accelerator Physics*. Springer-Verlag, San Diego, 3rd edition, 2007.

[36] J. Beringer and others (Particle Data Group). 2012 Review of Particle Physics. *Physical Review D*, 86, July 2012.

[37] E. Stephenson. *Note on Estimating Spin Coherence Time with COSY INFINITY*, October 2012.

[38] E. Stephenson. *Notes on converting spin tune changes into a spin coherence time*, December 2012.

[39] E. Stephenson. Extending the In-Plane Spin Coherence Time of a Polarized Deuteron Beam in a Storage Ring using Higher Order Fields, April 2013. COSY Program Advisory Committee.

[40] E. Stephenson. COSY run status, June 2012. Run status talk.

# Acknowledgements

Il mio primo ringraziamento è per il Prof. Paolo Lenisa che mi ha seguito e sostenuto durante il percorso di dottorato, dandomi anche l'opportunità di svolgere il mio lavoro ti tesi al Forschungszentrum di Jülich: un'esperienza impagabile sia dal punto di vista lavorativo che personale.

I would like to thank the JEDI collaborations, and in particular Prof. Andreas Lehrach, for the support offered during my PhD work. A special thanks to Prof. E. J. Stephenson and Dr. B. Lorentz for their constant help with the code.

Vorrei ringraziare tutto il gruppo di Ferrara, in particolar modo le mie super compagne d'ufficio Greta e Susy che, pur tra mille impegni, trovano sempre il tempo per un consiglio o un aiuto.

Grazie di cuore alla mia famiglia, che mi ha sempre sostenuto dandomi la possibilità di raggiungere questo importante traguardo.

A huge thanks to Zara, who always tries to see the best part of me and has supported me also in the most critical moments of my path. Thank you! I will always be grateful.

Finally, I would like to thank all my friends from all around the world: I met some of them in Germany, I have known some others for a lifetime, but all of them have contributed to make me who I am, and a thanks is the least I can do. Among them, a special mention for La Zhannà, whose friendship is invaluable, and Mr. Pol, to whom I will tell just one thing: Diamonds is waiting for us!